SYNTHESIS AND CHARACTERIZATION OF NANOCRYSTALLINE BINARY AND TERNARY INTERMETALLIC COMPOUNDS

A Dissertation

by

BRIAN M. LEONARD

Submitted to the Office of Graduate Studies of
Texas A&M University
in partial fulfillment of the requirements for the degree of

DOCTOR OF PHILOSOPHY

May 2008

Major Subject: Chemistry

SYNTHESIS AND CHARACTERIZATION OF NANOCRYSTALLINE BINARY AND TERNARY INTERMETALLIC COMPOUNDS

A Dissertation

by

BRIAN M. LEONARD

Submitted to the Office of Graduate Studies of
Texas A&M University
in partial fulfillment of the requirements for the degree of

DOCTOR OF PHILOSOPHY

Approved by:

Co-Chairs of Committee,	Raymond E. Schaak
	Kim R. Dunbar
Committee Members,	Timothy R. Hughbanks
	Donald G. Naugle
Head of Department,	David H. Russell

May 2008

Major Subject: Chemistry

ABSTRACT

Synthesis and Characterization of Nanocrystalline Binary and Ternary Intermetallic Compounds. (May 2008)

Brian M. Leonard, B.S., University of Nebraska at Kearney

Co-Chairs of Advisory Committee: Dr. Raymond E. Schaak
Dr. Kim R. Dunbar

Intermetallic compounds are among the most important solid-state materials because of their diverse physical properties and widespread use in numerous applications. The possibility of integrating intermetallics with emerging nano-technological applications has generated renewed interest in their synthesis. Current capabilities for synthesizing nanocrystalline materials are well-established for single metals and simple binary phases, but very few processes are capable of reliably producing intermetallic nanoparticles. In this dissertation, I describe several new approaches for synthesizing intermetallic nanocrystals.

The first approach involves reducing metal salts in aqueous solution using $NaBH_4$ and precipitating a composite of metal nanoparticles. This nanocomposite can then be annealed and rapidly converted to an intermetallic phase. Using this approach, I successfully synthesized several binary and ternary compounds including known magnetic and superconducting materials. The properties of these materials were found to be comparable or superior to materials synthesized using traditional techniques. The second approach, called the polyol process, utilizes high boiling point polyalcohol solvents to heat metal salts in solution and precipitate nanocrystalline powders. Using this

process, I was able to access several binary and ternary intermetallics, including two new phases: $AuCuSn_2$ and $AuNiSn_2$. These compounds were isolated as nanocrystals using low temperature solution synthesis techniques, which had not previously been applied to the synthesis of intermetallic compounds. Further investigation of the $AuCuSn_2$ reaction revealed that it proceeds through a unique four step pathway: (1) galvanic reduction of Au(III) to Au(0) nanoparticles with concurrent oxidation of Sn(II) to Sn(IV) (as a SnO_2 shell), (2) formation of NiAs-type AuSn along with Cu and Sn nanoparticles using $NaBH_4$ reduction, (3) aggregation and thermal interdiffusion to form a ternary alloy, and (4) nucleation of the ordered intermetallic compound $AuCuSn_2$. The proposed pathway was confirmed by forming $AuCuSn_2$ via reaction of AuSn nanoparticles with Cu nanoparticles formed ex-situ. Additional investigations into the reactivity and kinetics of chemical transformations involving metal nanoparticles have revealed the idea of orthogonal reactivity in multi-component nanoparticle systems, which would allow phase (or metal) specific reactions to take place sequentially within a system of multiple metal nanoparticles.

ACKNOWLEDGEMENTS

I would like to thank my research advisor, Dr. Raymond Schaak, for mentoring, teaching, guiding, and supporting me over the last four years. I would also like to thank my committee members, Dr. Dunbar, Dr. Hughbanks, and Dr. Naugle for their help and advice. Additionally I would like to thank other Texas A&M Chemistry faculty including Dr. Clearfield, Dr. D. Darensbourg, Dr. Gabbai, and Dr. Hall. Furthermore, I would like to thank Dr. Nattamai Bhuvanesh for sharing his expertise in powder diffraction and structure refinement.

I would also like to thank the members of the Schaak research group for their support. I would like to individually thank Dr. Rob Cable, Nam Hwan Chou, Dr. Mason Haneline, Dr. Lindsay Roy, Nathan Henderson, Farah Dawood, Zac Schaffer, Ting-Hao Phan, and Beth Anderson for their help, advice, and friendship.

I would like to thank my chemistry professors at the University of Nebraska at Kearney for their mentoring and teaching. In particular, I would like to thank Dr. Christopher Exstrom for his advice, support, and encouragement.

Finally, I would like to thank my family for all their love, support, and encouragement throughout the years. Without you, I never could have made it through this. Thank you!

NOMENCLATURE

CTAB	Cetyltrimethylamonium bromide
DSC	Differential scanning calorimetry
EDS	Energy dispersive x-ray spectroscopy
Fcc	Face centered cubic
Hcp	Hexagonal close packed
ICP-MS	Inductively coupled plasma – mass spectrometry
Oe	Oersted
PVP	Polyvinylpyrrolidone
SAED	Selected area electron diffraction
SEM	Scanning electron microscope
SQUID	Superconducting quantum interference device
TEG	Tetraethylene glycol
TEM	Transmission electron microscope
XRD	X-ray diffraction

TABLE OF CONTENTS

CHAPTER Page

LIST OF FIGURES

FIGURE Page

FIGURE Page

FIGURE Page

FIGURE Page

FIGURE Page

LIST OF TABLES

CHAPTER I

INTRODUCTION

1.1 Introduction to Nanomaterials

Inorganic nanocrystals are an important group of materials because of their diverse range of physical and chemical properties and their numerous potential applications. Metal nanoparticles have been show to have enhanced properties compared to their bulk counterparts, so the investigation into these materials is important not only for scientific study but also for integration into technologically important applications. These dimensionally confined materials often show size-dependent properties[1] and as such the controlled synthesis of these materials is crucial to their performance and implementation into devices. Several aspects of the particles, such as size,[1] morphology,[2] composition,[3] and crystal structure[4-6] all need to be accurately controlled in order to tune the desired properties. Obtaining such control is often a challenging task for even simple single metal systems, and typically the chemical reactions needed to access such nanocrystals are quite specific to the material they were originally targeting. For example, the seed mediated synthesis of gold nanorods can be accomplished by using Cetyltrimethylammonium bromide (CTAB) as a surface stabilizer and the formation process occurs under very specific temperatures and concentrations of Au seeds and ions.[7] Beyond a few other noble metals (Ag, Pd),[8] this chemistry is not usually

---

This dissertation follows the style and format of the *Journal of the American Chemical Society*.

successful and will either not form particles or will only result in spherical or randomly shaped particles. Most techniques developed for the synthesis of inorganic nanocrystals are not generally applicable to other phases or types of materials (even those that are chemically similar), so the conditions for each system need to be studied, and established on a case by case basis. If the reactions forming these materials could be better understood, it could be possible to create materials-general syntheses with the ability to control important aspects of the resulting particles including size, shape, composition, and functional properties.

The synthesis of microscale and nanoscale materials has been studied for decades but only recently have chemists begun to rigorously control key aspects of the particles, including size, shape, composition, and structure. Several approaches have been developed for the synthesis of inorganic nanomaterials and these can be generally divided into two categories: “top down” approaches where the materials are made by physically breaking down bulk pieces, and “bottom up” approaches where the materials are synthesized from molecular species that nucleate to form nanoparticles. Top down approaches generally consist of fracturing bulk pieces of the desired material and mechanically working them[9,10] into smaller nano-scale particles using techniques such as ball milling[11] and laser ablation.[12] While these techniques are useful, they are quite limited in controlling the morphology of the materials. Bottom up approaches, however, have been studied extensively and are readily adapted to controlling the size and morphology of the resulting materials. Some examples of these techniques include reduction of metal salt precursors in solution,[13] decomposition of organometallic

precursors,[14] the sol-gel method,[15,16] and solvothermal synthesis.[17,18] While several synthetic techniques have been developed for the synthesis of metals[2,19,20] and simple binary phases,[21-24] very few techniques allow for the solution-based synthesis of intermetallic nanomaterials.

1.2 Intermetallics

Intermetallics are an important class of materials with many useful properties and as such have been incorporated into numerous applications.[25] The properties of intrest for intermetallic compounds range from mechanical such as corrosion resistance[26] and structural rigidity[27] to electronic and magnetic such as ferromagnetic[4,5] and thermo-electric materials.[10,28,29] They are currently used in several common applications such as frames for eyeglasses and non-Freon based coolers and are also being developed for some of the most technologically advanced applications like high density information storage in computers.

By combining two or more metals homogeneously at the nanoscale, intermetallic and alloy nanoparticles increase the diversity of the materials available as nanocrystals and allow for more complex phases and properties to be investigated. Alloys consist of a solid solution of metals and as such have disordered arrangements of atoms within their periodic crystal structure. Intermetallic compounds can often have the same composition as alloys, but differ from their alloy counterparts in that they have an atomically ordered crystal structure. The atomic ordering of intermetallics usually gives rise to different crystal structures than the elements that comprise them and can also change the

properties of the material. For example, atomically disordered FePt alloy particles are superparamagnetic, but upon ordering the Fe and Pt atoms in alternating layers, FePt exhibits room temperature ferromagnetism with high coercivity and magnetoaniosotropy.[2,3] In order to study the properties of nanoscale intermetallics, new synthetic techniques need to be developed to readily synthesize these materials and offer some control over particle size, composition, and structure. The synthetic capabilities used to synthesize metal and alloy nanoparticles must be expanded to handle multimetallic compounds, which is a challenge that has been surmounted to very limited extent in the past.

Intermetallics are traditionally synthesized using high temperature reactions and lengthy annealing times. Some common synthetic techniques include arc melting and powder metallurgy, where the reactants are heated to high temperatures (>1000 °C) followed by days or weeks of annealing. Generally, it takes a significant amount of energy to mix the reacting metals homogenously on the atomic scale, and solid–solid diffusion is often the rate limiting step in the formation of intermetallic phases. Heating the reacting metals to high temperatures allows the metals to melt and intermix more rapidly. The lengthy annealing times are necessary for the reactants to become homogeneous and nucleate long range ordered intermetallic structures throughout the material. The high temperature reactions that are required for traditional solid-state syntheses, while important for generating many useful materials, have clear limitations. Under typical high temperature reaction conditions, it is difficult to piece together the interactions among the reactants, including the formation of important intermediates that

may be crucial for successfully forming a desired product. Furthermore, high-temperature reactions often preclude the formation of metastable and low-temperature phases that are not accessible under such conditions. Additionally, high temperature synthesis of these materials generally gives very limited control over morphology and particle size.

Some alternate techniques have been developed to synthesize bulk scale solid state materials at low temperatures and with reduced annealing times. Most of these methods try to overcome the diffusion problem that is inherent in solid state reactions by intimately mixing the starting materials. Examples of these techniques include co-precipitation of metal precursors,[30] sol-gel processing,[15,16] vacuum deposition,[31] and annealing elementally modulated thin films.[32-33] These techniques are quite practical and have been able to reduce both heating temperatures and annealing times. They have also resulted in the discovery of several new compounds[33] because the reaction products are influenced by kinetics rather than exclusively generating the thermodynamic product.

1.3 Solution Synthesis of Inorganic Nanoparticles

Several solution based approaches have been developed to synthesize metal nanoparticles.[3-5,13,14,19] These reactions typically use metal salts[13] or organometallic precursors[14] as reagents and thermally decompose or reduce them to form free zero-valent metal atoms in solution. The metal atoms then aggregate into small alloy and intermetallic particles whose growth, and therefore particle size and morphology, can be influenced by the presence of surface stabilizing agents. The composition of the

nanoparticles can often be controlled by altering the reagent concentrations. Additionally, several methods have also been developed which allow for exquisite control over particle size[2,34,35] and morphology.[36-40] Solution synthesis techniques also give solid state chemists new methods for studying the formation and reactivity of solids and can give insight into reaction pathways which can otherwise be difficult to elucidate. The low temperatures used in solution-based reactions also allows for the formation of metastable products that cannot be accessed or are difficult to form using traditional high temperature techniques.[41-43]

Using these solution based techniques, we can investigate the formation of intermetallic phases under low temperature conditions and begin to understand the interactions between metals in solution. This information is crucial to understanding the reactivity of metal nanoparticles and would allow us to expand the complexity of intermetallic phases accessible as nanocrystals. In time it should be possible to determine the reactivity of multiple metal nanoparticles in solution and use this knowledge to rationally synthesize target materials. The overall goal of this clearly would be to synthesize functional materials whose properties could be dialed in by composition and using previously studied methods, formed with specific shapes and sizes suitable for the intended application.

1.4 Experimental Work

The following chapters describe the development and investigation of solution chemistry methods for synthesizing intermetallic and related multi-metal nanoparticles.

The first approach, termed “Metallurgy in a Beaker,” utilizes metal nanoparticles as precursors to synthesize intermetallic nanocrystals.[44] This technique overcomes the diffusion limiting step associated with solid state reactions by using small metal particles with a large surface-to-volume ratio and aggregating them in solution to form a nanocomposite. This composite is then isoltated from solution and heated as a powder in an inert atmosphere, allowing the metals to diffuse into one another and form the atomically ordered intermetallic phase. This approach allows for the metals to become intimately mixed without high temperature heating and greatly reduces the heating time necessary to form the ordered phase. The technique was first demonstrated for the synthesis of AuCu and $AuCu_3$ by precipitating Au and Cu nanoparticles from aqueous metal salt solutions and subsequently annealing these powders to form ordered intermetallic nanocrystals.[45] In Chapter II, this approach is extended to several binary and ternary compounds including ferromagnetic and superconducting phases. These materials can also be processed using simple solution based techniques to form thin films, inverse colloidal crystal templates and free standing monoliths.

The second approach discussed here exploits the polyol process as a synthetic technique for the formation of intermetallic nanoparticles. The polyol process was originally developed years ago to precipitate elemental metal powders from solution by using high boiling and mildly reducing solvents to reduce metal salts in solution.[46,47] The powders produced using the polyol approach were generally micron sized and included single metal and bimetallic alloys of late transition metals. Several groups have since modified this process to more rigorously control particle size and shape and have

produced several important and useful materials.[36-40,48,49] We have developed modifications of this process utilizing surface stabilizing polymers and stronger reducing agents such as $NaBH_4$, which allows for a broader range of metals to be incorporated into nanoparticles using this technique and better control of the size and morphology of the resulting particles. Our group has shown that that this technique is useful in the direct synthesis of several known binary intermetallic phases including functional materials with magnetic, catalytic, and thermoelectric properties.[36,43,49] In Chapter III, we describe the synthesis of known ternary phases in the Au-Cu-Sn system and report the discovery of two new ternary intermetallic compounds: $AuCuSn_2$ and $AuNiSn_2$.[50] We also investigate the utility of this process in the exploratory synthesis of ternary systems facilitated by the rapid reaction time (minutes instead of hours or days) and high reactivity of the reagents at low temperatures.

In Chapter IV, we show that we can monitor the progress of these polyol reactions by taking aliquots at various times and temperatures and analyzing the products using a variety of complementary characterization techniques. In studying the synthesis of $AuCuSn_2$, we were able to discover a unique reaction pathway that proceeds through four distinct steps: (a) formation of Au nanoparticles at or near room temperature, mediated by a galvanic reaction between Au^{3+} and Sn^{2+} (forming Au^0 and Sn^{4+}, precipitated as SnO_2 that forms a shell around the nanoparticles), (b) formation of NiAs-type AuSn nanoparticles, along with Cu and Sn, upon addition of $NaBH_4$, (c) aggregation and thermal interdiffusion to form $AuCu_xSn_y$ alloy nanoparticles, and (d) nucleation of intermetallic $AuCuSn_2$, which has an ordered NiAs-derived

superstructure.[51] The reaction pathway was elucidated using multiple characterization techniques including UV-visible spectroscopy, X-ray and electron diffraction, transmission electron microscopy, and elemental analysis using microprobe and STEM capabilities. The proposed pathway was also tested and validated by starting the reaction with nanoparticles of a proposed key intermediate, AuSn, and reacting them with Cu and Sn nanoparticles.

In Chapter V, we further examine the formation of intermetallic nanoparticles in solution using the polyol method and discovered that products often form under distinct conditions of temperature and composition. After studying the formation of several binary phases, we compiled a set of reaction conditions under which specific phases will form in solution. Using these reaction conditions, we began to explore the possibility of orthogonal reactivity in metal nanoparticle systems.[52] By separating the conversion reactions by temperature, we have found that multiple binary intermetallics (PtPb and NiSb) can be formed in a one pot reaction by combining a mixture of single metal nanoparticles (Pt and Ni) and reacting each metal individually under distinct conditions identified from reactivity studies. In addition, we extend this to a mixture of three different metals and react each metal individually. Finally, we begin to study the conversion of materials containing multiple metals including lithographically patterned surfaces and multi-element segmented nanowires and demonstrate preliminary evidence that orthogonal reactivity is possible using these spatially confined nanostructured materials.

CHAPTER II

METALLURGY IN A BEAKER: NANOPARTICLE TOOLKIT FOR THE RAPID LOW-TEMPERATURE SOLUTION SYNTHESIS OF FUNCTIONAL MULTIMETALLIC SOLID-STATE MATERIALS*

2.1 Introduction

Intermetallic compounds and alloys are among the most important solid-state materials in modern science and technology. [53] They possess a surprisingly diverse range of physical and chemical properties, including ferromagnetism,[4,54] superconductivity,[55] shape-memory effects,[29,56] catalytic activity,[6,57,58] hydrogen storage,[59] structural hardness,[27] and corrosion resistance,[26] and thus find widespread use in many applications.[60] As for all solid-state materials, the synthesis of these multimetallic compounds is crucial for controlling their performance in advanced applications. The possibility of integrating the well-established properties of intermetallic compounds with emerging nanotechnological applications has generated a renewed interest in controlling their synthesis. Controlling the nanostructure and morphology of multimetallic materials is particularly important, as these are the critical factors that limit their utility in future applications.

Intermetallics and alloys are typically synthesized using traditional metallurgical

---

* Reprinted in part with permission from *J. Am. Chem. Soc., 127* Schaak, R. E.; Sra, A. K.; Leonard, B. M.; Cable, R. E.; Bauer, J. C.; Han, Y.-F.; Means, J.; Teizer, W.; Vasquez, Y.; Funck, E. S. "Metallurgy in a Beaker: Nanoparticle Toolkit for the Rapid Low-Temperature Solution Synthesis of Functional Multimetallic Solid-State Materials," 3506, Copyright 2005 by the American Chemical Society.

techniques, which include powder reactions and arc melting. Both of these strategies require high temperature heating (usually >1000 °C) and annealing for long periods of time (often days or weeks). While a few alternative approaches exist for controlling the nanostructure and morphology of multimetallic materials,[32,61-63] low-temperature solution based synthetic strategies are rare. This is in contrast to many other classes of materials, where well-established solution routes are ubiquitous, e.g., sol-gel synthesis of oxides[16] and spin coating of polymer and chalcogenide films.[64]

Sra and Schaak recently reported that, under appropriate conditions, binary mixtures of weakly stabilized Au and Cu nanoparticles aggregate to form binary nanocomposites, which can thermally transform into intermetallic nanocrystals at low temperatures.[44] An important consequence of this solution-based synthetic approach is that it can be scaled up to yield morphologically diverse intermetallic and alloy materials. Figure 2.1 illustrates the diverse morphological range of multimetallic materials with controlled shape, size, and dimensionality that can be readily accessed using solution-deposition techniques and nanoscale templating strategies. For example, a solution of nanocomposite precursors can be infiltrated into nanoscale templates, dried, and thermally converted into alloys and intermetallics while retaining the morphology of the template. Additionally, thin films and coatings of planar and non-planar surfaces can be created using common solution deposition techniques like evaporation and spin coating. Such flexibility in materials processing is unprecedented for intermetallics and alloys.

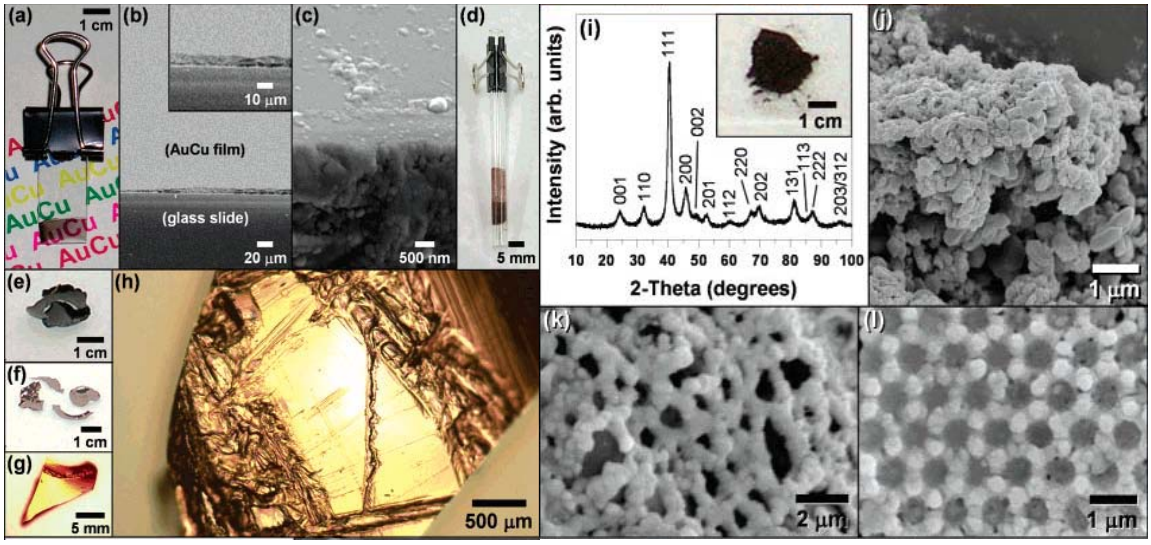

Figure 2.1 Morphologically diverse intermetallic AuCu nanomaterials: (a) photograph of an optically transparent intermetallic AuCu film formed by solvent evaporation and annealing at 300 °C; (b) cross-section SEM micrograph of an intermetallic AuCu film on a glass slide (showing an enlarged view in the inset); (c) high-magnification SEM micrograph of an edge of the film in (b), showing the nanoscale grains that comprise the film; (d) photograph of a 6 mm diameter glass rod coated with a film of intermetallic AuCu (the film appears darker at the bottom because it is thicker and was deposited from a solution with a higher concentration of nanocomposite precursor); (e) free-standing Au-Cu nanocomposite film prior to annealing; (f) free-standing intermetallic AuCu film after annealing at 300 °C for 30 min; (g) reflection-mode optical microscope image of a flat intermetallic AuCu free-standing film; (h) reflection-mode optical microscope image of a curved microetched intermetallic AuCu free-standing film; (i) photograph of intermetallic AuCu bulk powder (500 mg) synthesized by heating a large sample of nanocomposite powder to 300 °C for 60 min, and its corresponding powder XRD pattern; (j) SEM micrograph of sintered dense submicrometer powder of intermetallic AuCu; (k) intermetallic AuCu nanomesh; (l) intermetallic AuCu colloidal crystal replica formed by templating against polystyrene spheres.

Our subsequent work showed that this approach can be significantly expanded to include other bimetallic and trimetallic systems with a variety of compositions and accessible crystal structures. Accordingly, we describe here a generalized solution-based synthetic approach termed “metallurgy in a beaker” that uses metal nanoparticles as a

robust toolkit for synthesizing compositionally and structurally diverse intermetallics and alloys.

By using preformed nanoparticles of known metal ratios, multimetallic compounds of those ratios can be made by exploiting the nanoscale intermixing of the nanoparticles. This approach effectively separates the diffusion and nucleation steps, and eliminates solid-solid diffusion as the rate limiting step in bulk-scale solid-state synthesis. Furthermore, the materials made by this method are functional, yielding properties that match or are superior to similar materials made by traditional routes. In this work, we establish the viability of this new synthetic paradigm for producing bimetallic and trimetallic solid-state materials with functional properties.

2.2 Experimental Details

2.2.1 *Synthesis of Binary and Ternary Intermetallics and Alloys*

Cu-Pt nanocomposites were synthesized in a manner similar to that of our previous report.[44] Briefly, $Cu(C_2H_3O_2)_2 \cdot H_2O$ (26.7 mg, 0.134 mmol; Alfa Aesar, 98.0-102.0%), K_2PtCl_6 (40.11% Pt) (20.4 mg, 0.042 mmol; Alfa Aesar, 99.99%), and poly(vinylpyrrolidone) (PVP; MW = 40000, 114 mg) were added to 25 mL of distilled, deionized water (NANOpure, 18.2 MΩ). (Note that water was the only solvent used in the synthesis of these materials.) After the mixture was stirred for at least 30 min under Ar, 10 mL of 0.015 M $NaBH_4$ (Alfa Aesar, 98%) was added to form a mixture of Cu and Pt nanoparticles. After 3-6 h, the resulting nanocomposite was isolated in powder form by centrifugation (including several washing steps), and dried under ambient conditions.

The powder was then annealed at various temperatures (see Results section) under flowing Ar. FePt and $FePt_3$ were synthesized in the same way, using 18.4 mg (0.146 mmol) and 20.7 mg (0.0427 mmol) of $FeCl_2 \cdot xH_2O$ (99%) and K_2PtCl_6, respectively. The ternary phase Ag_2Pd_3S was synthesized as follows: PVP stabilized Ag_2S nanoparticles were synthesized according to ref 65 using $AgNO_3$ and $Na_2S \cdot 9H_2O$ (Alfa Aesar, 98.0-103.0%), washed, dried, and then added to a fresh aqueous solution of PVP-stabilized Pd nanoparticles synthesized according to ref 66. The final concentrations of Ag_2S and Pd used to form the nanocomposite were 18 and 1 mg/ mL, respectively. The resulting nanocomposite was isolated by centrifugation and annealed at 300 °C under Ar. Ag_3CuS_2 was synthesized using Ag_2S and Cu nanoparticles (similar to Ag_2Pd_3S) and the nanocomposite was annealed under Ar at 150 °C for 20 min.

2.2.2 *Characterization and Physical Property Measurements*

Powder X-ray diffraction (XRD) data were collected on a Bruker GADDS three circle X-ray diffractometer using Cu Kα radiation. Differential scanning calorimetry (DSC) data were collected on a TA Instruments Q600 SDT under an Ar purge. Inductively coupled plasma (ICP) elemental analysis results were obtained using a Perkin-Elmer DRCII ICP-MS. Transmission electron microscopy (TEM) images, selected area electron diffraction (SAED) patterns, and energy-dispersive X-ray analysis (EDS) were acquired using a JEOL JEM-2010 transmission electron microscope. Scanning electron microscopy (SEM) images were obtained at 15 kV using a JEOL JSM-6400 SEM. Optical microscope images were acquired on a Zeiss AxioSkop 2-MAT

operating in reflection mode. Magnetic susceptibility and magnetization measurements were carried out on a Quantum Design SQUID magnetometer MPMS-XL. Magnetization vs applied field data were collected in the 0-6.5 T range at 10 K. Low-temperature resistivity data characterizing the superconducting transition of Ag_2Pd_3S were acquired on a homebuilt dilution refrigerator, using a standard four-wire ac lock-in (PAR 124A) technique (f = 23 Hz) with an RMS excitation current of 0.5 mA. The temperature was measured using a factory-calibrated Ge resistor (Lake Shore Cryotronics GR-200A-100).

2.3 Binary Systems: Synthesis and Characterization

Figure 2.2 shows a schematic of the multistep reaction sequence that forms Cu_3Pt. Stoichiometric molar ratios of Pt and Cu metal salt precursors were reduced in solution by $NaBH_4$ in the presence of PVP to form nanoparticle mixtures, which were aged to form binary Pt-Cu nanocomposite precipitates with compositions that were closely related to the initial ratios of Pt and Cu that were present prior to reduction. The resulting powders were annealed under Ar to study their thermal transformation. Figure 2.3 shows powder XRD diffraction data for the Cu-Pt nano-composite heated to multiple temperatures forming first an alloy then the ordered intermetallic phase.

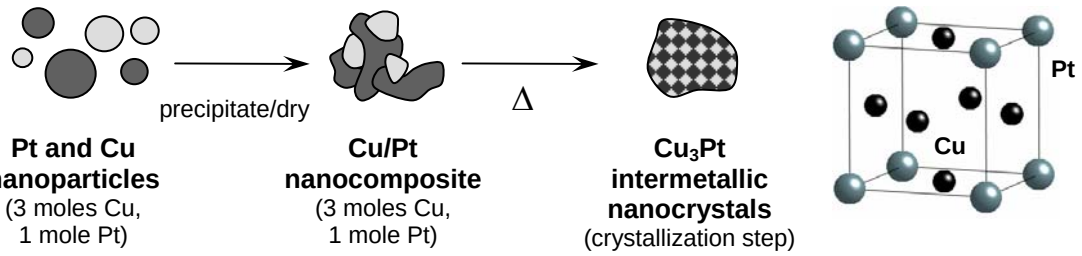

Figure 2.2 Idealized schematic of the multistep approach to the synthesis of atomically ordered Cu_3Pt nanocrystals from bimetallic nanoparticle aggregates. The crystal structure of Cu_3Pt is shown to illustrate the atomic ordering of the Cu and Pt atoms.

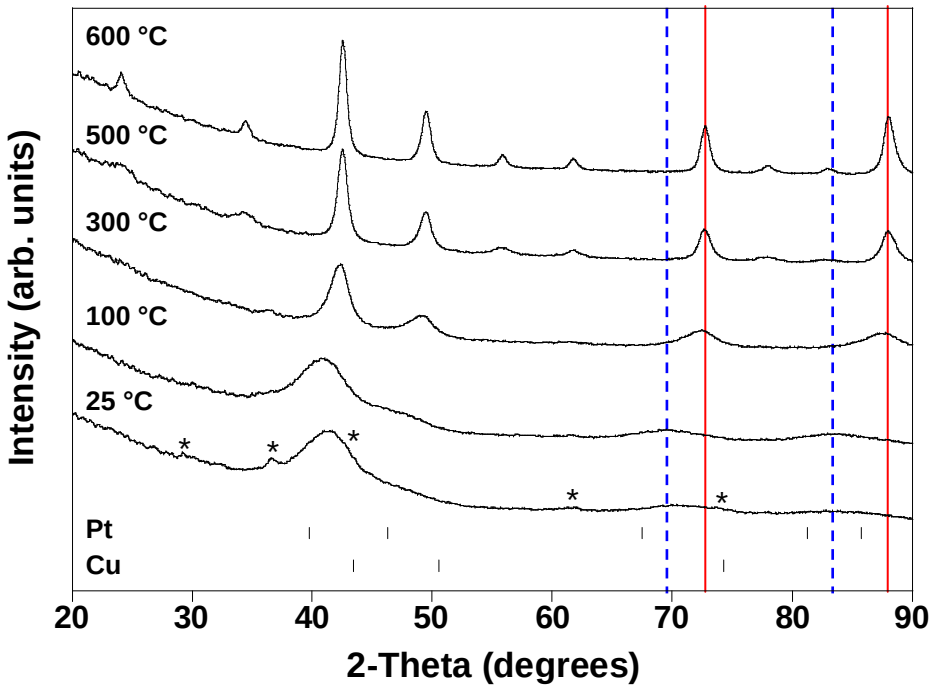

Figure 2.3 Powder XRD patterns for a Cu-Pt nanocomposite not heated and heated at 100, 300, 500, and 600 °C. Tick marks below the room temperature sample represent the allowed reflections for Cu and Pt metal. Reference lines for the alloy (blue) and ordered Cu_3Pt (red) are shown for comparison. Due to the high reactivity of Cu nanoparticles; some Cu oxidized prior to analysis by XRD and is seen as Cu_2O marked by (*).

XRD data showing the formation of atomically ordered Cu_3Pt (Figure 2.3) are demonstrative of the low-temperature diffusion afforded by the nanocomposite synthetic

route. At 20 °C, Pt is crystalline, and Cu is amorphous, and due to the high reactivity of Cu nanoparticles some oxidation occurred prior to analysis by XRD as seen in Figure 2.3 [Cu_2O is indicated by (*)]. Prior to heating, Cu and Pt nanoparticles appear to interdiffuse as the lattice constant shifts from a = 3.923 Å for platinum to a = 3.799 Å (for copper, a = 3.6078 Å). Using these values, the composition was estimated using Vegard's law,[67] which predicts the composition of an alloy by comparing its lattice constant with those of the single-metal end members. The composition of the precipitated powder is calculated to be 60% Pt after the Cu has diffused into the Pt particles upon reduction and subsequent aging. At 100 °C, a Cu-Pt alloy phase is still present with no noticeable shifting or changes in the lattice constants. By 300 °C, the diffraction pattern has shifted to lattice constants similar to that of the ordered Cu_3Pt phase indicating that the metals are nearly homogenous in composition. Further heating of the nanocomposite to 500 °C shows the ordered intermetallic phase, and heating to 600 °C increases the crystallinity of the product.

DSC data for our Cu_3Pt nanocomposite sample, with inherent nanoscale intermixing of Cu and Pt nanoparticles, is shown in Figure 2.4. For the Cu_3Pt sample, a broad exotherm centered near 300 °C is observed and corresponds to the interdiffusion and ordering of the Cu_3Pt solid solution into the intermetallic structure. At room temperature, the nanocomposite has already undergone some interdiffusion, but both DSC and XRD data confirm that the diffusion is not complete until ~300 °C and the ordered phase is not observed until 400 °C. No disordering transition for this phase is seen as Cu_3Pt is stable up to 1000 °C, which is consistent with the previous reports as

well as the equilibrium phase diagram.[68] XRD data confirm the assignments of the thermodynamic transitions discussed above, including diffusion and nucleation of the ordered phases and thermal stability of the ordered intermetallic phase.

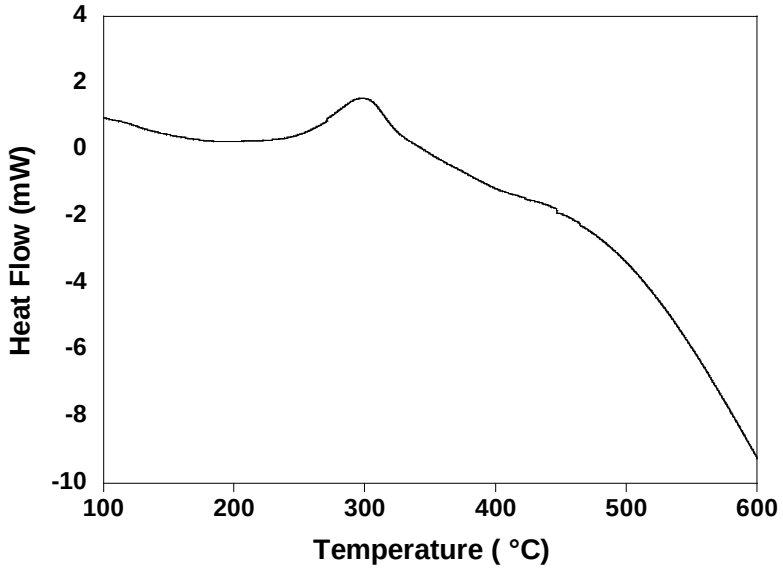

Figure 2.4 DSC trace for binary Cu-Pt nanocomposites with a 3:1 stoichiometry precipitated at from solution and heated under Ar. Positive output is exothermic.

In order to demonstrate the rapid nature of this synthetic technique, the nanocomposite was heated at 500 °C for various amounts of time and the diffraction patterns for the products are shown in Figure 2.5. After only 10 min of heating, the ordered intermetallic compound Cu_3Pt is formed, and further heating increases its crystallinity. The nanometer diffusion distances support low temperature diffusion without the high-temperature melting step that is necessary in traditional metallurgy. Likewise, the PVP confines the crystallites to nanoscale dimensions, allowing atomic ordering to occur rapidly without long-term annealing.

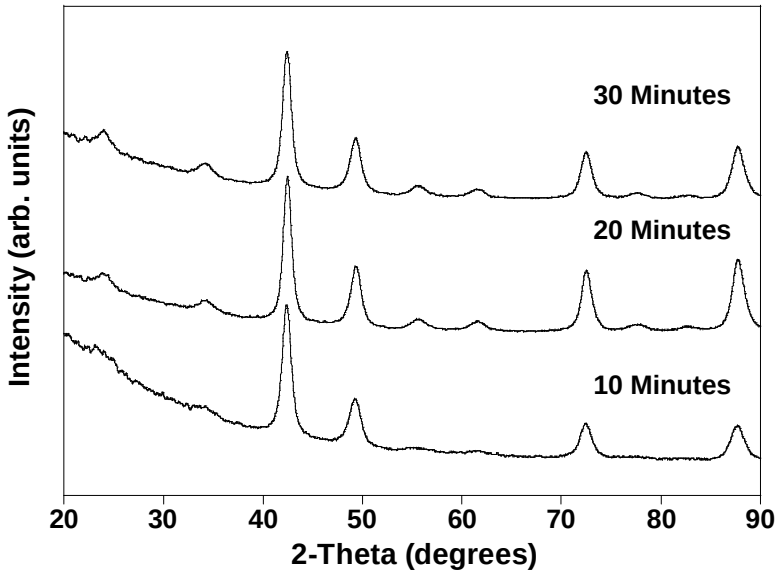

Figure 2.5 Powder XRD patterns showing the time-resolved transformation of Cu_3Pt nanocomposites into intermetallic Cu_3Pt at 500 °C. The listed heating times refer to the length of time the sample remained in the furnace after the furnace reached 500 °C.

The Fe-Pt system was also studied using the nanocomposite approach. FePt and $FePt_3$ are known magnetic materials with high corecivity that could have potential applications that include magnetic recording and data storage in computer hard-drives. Powders of both FePt and $FePt_3$ were synthesized using the nanoparticle precursors and annealing the nanocomposite under flowing Ar. In order to form FePt intermetallic particles, Fe and Pt precursor salts were dissolved in H_2O and purged under flowing Ar for 1h. Due to the highly reactive nature of Fe nanoparticles the solution was purged under a rapid flow of Ar for a longer time than other less reactive systems. Additionally the Fe-Pt system does not behave stoichiometrically. In order to access the 1:1 phase, a starting ratio of 3:1 Fe:Pt is required. Similarly, the $FePt_3$ phase is accessed by starting with a 1:1 ratio of Fe:Pt. Annealing the composite to 500° C forms the ordered phases

(Figure 2.6) for both materials and further heating increases the crystallinity of the particles. ICP analyses of the products indicate that the Fe-Pt systems have boron impurities (e.g., 0.5% B in $FePt_3$), which is consistent with known boron incorporation in nanoparticles prepared using borohydride reduction.[69]

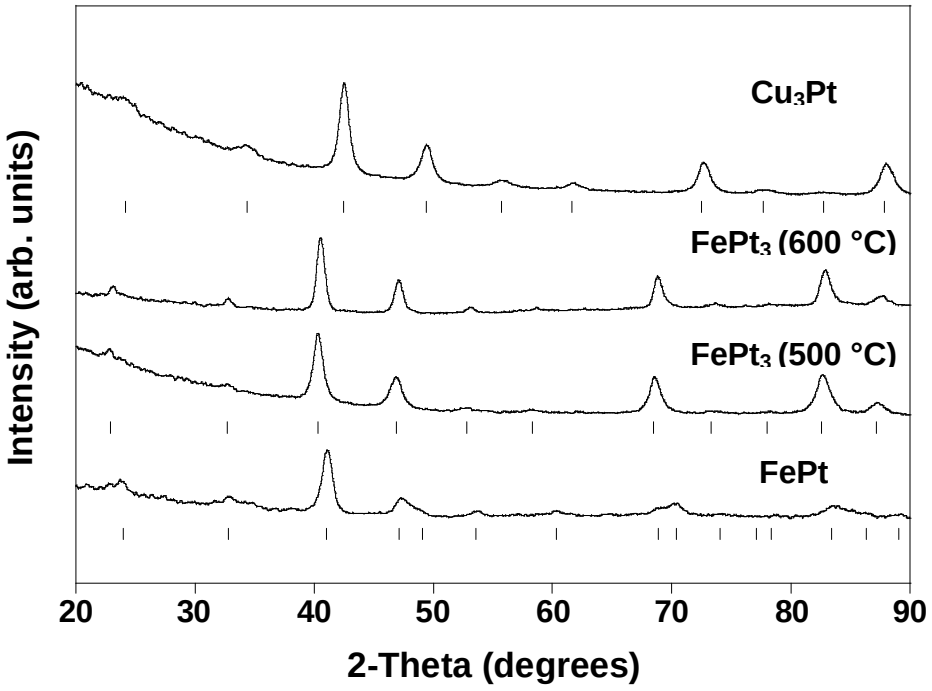

Figure 2.6 Powder XRD patterns for intermetallic AuCu-type FePt (600 °C), $AuCu_3$-type $FePt_3$ (500 °C and 600 °C), and $AuCu_3$-type Cu_3Pt (500 °C) synthesized from the corresponding binary nanocomposite precursors. Intermetallic Cu_3Pt forms by 400 °C, and the peaks that appear in the XRD pattern for the sample heated to 500 °C confirm the ordered structure.

2.4 Extension to Ternary Systems

Ternary phases are generally more complex than binary compounds in terms of synthesis, structures, and properties. Forming a nanocomposite of binary and single metal nanoparticles allows nanocomposites of ternary compositions to be accessed.

These ternary nanocomposites can be thermally processed to form ternary intermetallic phases, in analogy to the binary compounds discussed earlier. This greatly expands the complexity of compositions and structures that are accessible using a nanoparticle toolkit for solid-state synthesis. For proof-of-concept purposes, we chose the Ag-Pd-S system to demonstrate the formation of a ternary phase.[70-72] Nanocrystals of Ag_2S and Pd are easily synthesized according to literature methods,[65,66] and can serve as robust precursors to ternary Ag-Pd-S phases. Ag_2S nanocrystals were synthesized,[65] isolated by centrifugation, washed, and then added to a freshly prepared solution of PVP-stabilized Pd nanocrystals[66] in a 1:3 ratio of Ag_2S to Pd. The XRD patterns for powder samples of the Ag_2S and Pd nanoparticles are shown in Figure 2.7, and the corresponding TEM micrographs and SAED patterns are shown in parts a and b of Figure 2.8, respectively. Both Ag_2S and Pd nanocrystals are stable in solution, but when they are mixed together, a precipitate begins forming within minutes, and the resulting powder is easily isolated by centrifugation. The Ag_2S and Pd nanoparticles were mixed in a 1:3 ratio, since that stoichiometry (Ag_2Pd_3S) matches a known ternary phase that is superconducting at Tc = 1.13 K.[72] The XRD pattern for this Ag_2S-Pd nanocomposite at room temperature is shown in Figure 2.7, and the corresponding TEM micrograph is shown in Figure 2.8c. The XRD pattern has broad peaks that match those expected for Ag_2S and Pd, indicating that both of these phases are present in the nanocomposite. The peaks for Pd are shifted slightly to smaller angles in the Ag_2S-Pd nanocomposite, suggesting that some low-temperature interdiffusion between Ag and Pd is occurring (since the lattice constant for Ag is larger than that for Pd). The TEM micrograph of the Ag_2S-Pd nanocomposite in

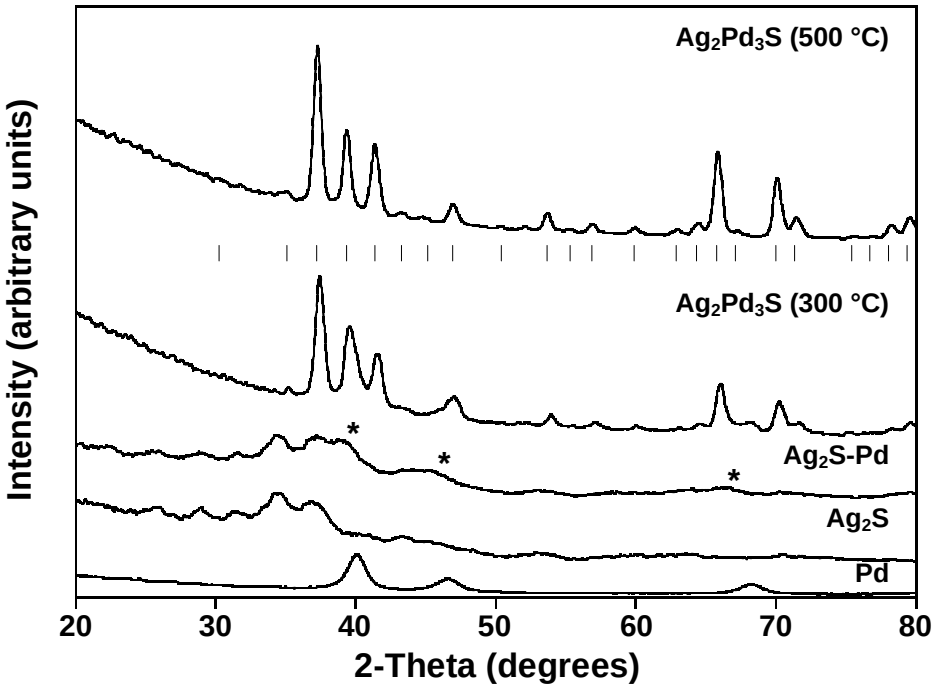

Figure 2.7 Powder XRD patterns for Pd nanoparticles, Ag_2S nanoparticles, the Ag_2S-Pd nanocomposite (1:3 stoichiometry) at room temperature, and the Ag_2S-Pd nanocomposite heated to 300 and 500 °C for 30 min, showing the formation of intermetallic Ag_2Pd_3S. The tick marks below the peaks for Ag_2Pd_3S (500 °C) represent the peak positions from PDF Card 27-1156 ($AgPd_2S$, which subsequent papers reported to be identical to the Ag_2Pd_3S superconductor). The asterisk in the Ag_2S-Pd room-temperature nanocomposite shows the peaks corresponding to Pd; the remaining peaks match Ag_2S.

Figure 2.8c initially appears to be a large aggregate of many smaller nanoparticles. Upon closer inspection, however, two distinct regions are discernible: a core region that contains a hexagonal superlattice of nearly monodisperse 5 nm nanoparticles, and a surrounding region that contains a random network of irregularly shaped 5-20 nm nanoparticles. Comparison with the TEM micrographs for Ag_2S and Pd nanoparticles in parts a and b of Figure 2.8, respectively, suggests that the hexagonal superlattice in the Ag_2S-Pd nanocomposite contains Ag_2S nanoparticles, and the surrounding region is

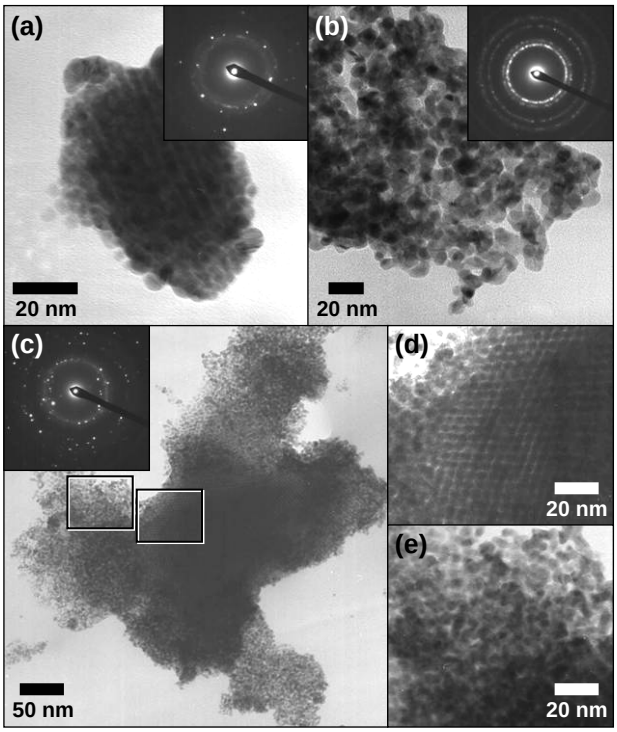

Figure 2.8 TEM micrographs and SAED patterns for (a) PVP stabilized Ag_2S nanoparticles, (b) PVP-stabilized Pd nanoparticles, and (c) the Ag_2SPd nanocomposite that forms at room temperature from the aggregation of Ag_2S and Pd nanoparticles. Panels d and e are enlarged regions from panel c, showing the Ag_2S and Pd regions of the nanocomposite.

made up of Pd nanoparticles. The SAED pattern for the entire aggregate in Figure 2.8c is complex, and can be indexed to a mixture of Ag_2S and Pd. Likewise, EDS analysis of the entire region in Figure 2.8c confirms that Ag, Pd, and S are present with an approximate overall composition of $Ag_{2.2}Pd_{2.9}S$, and bulk ICP analysis indicates an average composition of $Ag_2Pd_{3.3}S_x$ (the sulfur content was not determined by ICP). These data, combined with the XRD data in Figure 2.7, confirm that the aggregate in Figure 2.8c is a composite of Ag_2S and Pd nanoparticles. While this nanocomposite is clearly much larger and less homogeneously mixed than the Au-Cu nanocomposites

described earlier, the intermixing of Ag_2S and Pd is still homogeneous at the 50-200 nm scale, and this represents significantly better mixing than is attainable using traditional solid-state synthetic approaches. This nanoscale mixing, combined with the enhanced reactivity of nanoparticles relative to bulk powders, suggests that the Ag_2S-Pd nanocomposite may be easily converted into the ternary Ag_2Pd_3S phase upon rapid low-temperature heating. DSC data for the Ag_2S-Pd nanocomposite show a broad exotherm starting around 200 °C. Indeed, XRD data confirm that the nanocomposite begins converting to the ternary phase at this temperature. XRD patterns for the Ag_2S-Pd nanocomposite heated for 30 min at 300 and 500 °C are shown in Figure 2.7. Ag_2Pd_3S adopts the α-Mn structure,[72] which is distinct from any structures that exist in the constituent unary and binary systems. The XRD data show that the diffusion and nucleation steps are complete within 30 min of heating, yielding the desired ternary phase. This is in contrast to the standard procedure for synthesizing this material, which requires heating at 1000 °C for 2 h, followed by annealing at 550 °C for 3 days.[72]

Additional ternary systems were also tested using these methods and Ag_3CuS_2 can also be readily accessed using this approach. Figure 2.9 shows the powder XRD pattern, which shows the product of combining Ag_2S and Cu nanoparticles and annealing at 150 °C. As made with Cu and Ag_2S nanoparticles, the stoichiometry of this system is not correct and as such a small impurity of AgCuS is often seen in the product. These results establish that (a) the solution-based nanocomposite approach is applicable to ternary phases, (b) nanoparticle composites form between metals and semiconductors,

and (c) these metal-semiconductor nanocomposite precursors react similarly to the metal-metal binary composites to form ternary phases.

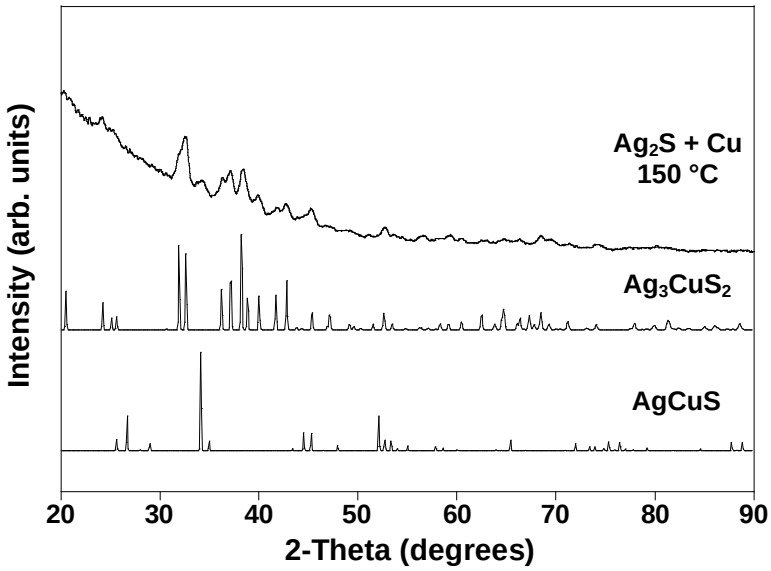

Figure 2.9 Powder XRD patterns for Ag_3CuS_2 made by precipitating Ag_2S and Cu nanoparticles then heating to 150 °C for 20 minutes. The bottom patterns represent the simulated patterns for AgCuS and Ag_3CuS_2.

2.5 Physical Properties

A synthetic strategy is viable if it produces new materials that have useful physical properties. Indeed, multimetallic solid-state materials made using the metallurgy in a beaker approach are functional, yielding a variety of important properties. Field-dependent magnetic measurements confirm that our $FePt_3$ sample is a room temperature ferromagnet, with a coercivity of 8000 Oe at 10 K (Figure 2.10a). This compares favorably to other Fe-Pt nanomaterials, considering that the coercivity is highly variable and depends on the annealing time and temperature and the Fe:Pt ratio.[4]

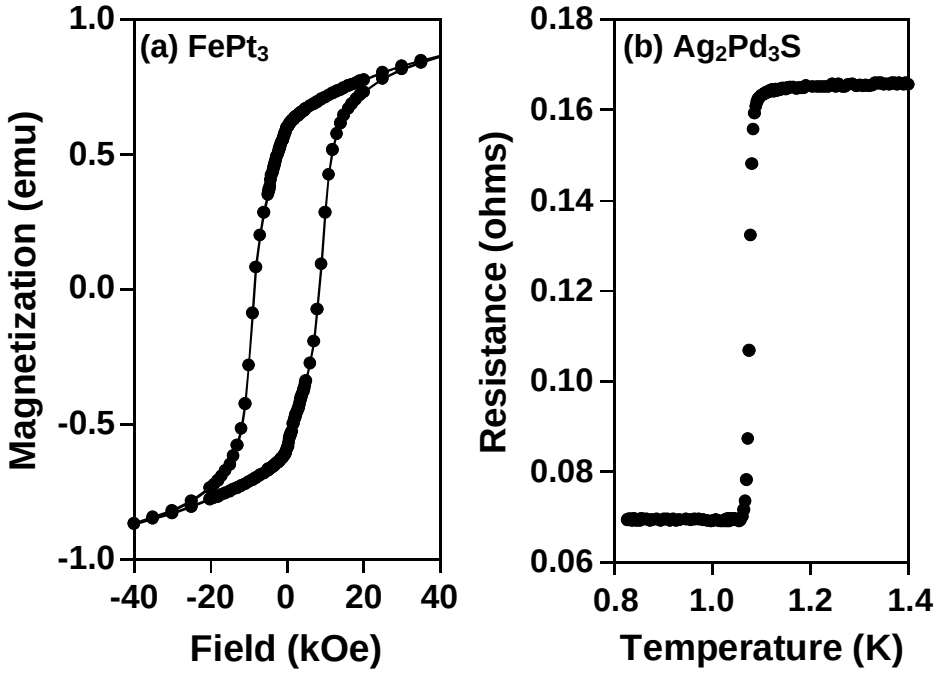

Figure 2.10 (a) Hysteresis loop at 10 K for an $FePt_3$ sample synthesized by heating an Fe-Pt nanocomposite to 600 °C for 60 min and (b) resistivity vs temperature from 0.83 to 1.40 K for a dense sample of superconducting Ag_2Pd_3S synthesized by heating a Ag_2S-Pd nanocomposite to 500 °C for 60 min.

Figure 2.10b shows a plot of resistance vs temperature for a piece of the Ag_2Pd_3S sample described in Figures 2.7 and 2.8. The data were acquired as a four-wire measurement, which included the resistance of two contacts to the sample. A sharp transition is seen near 1.10 K, where the slope reaches 8.0 Ω / K. For T < 1.10 K, the application of a magnetic field of H = 1.5 kOe restores the resistance to R = 0.165 Ω (not shown). These results indicate that our Ag_2Pd_3S sample is superconducting with Tc = 1.10 K. For the bulk material synthesized by a traditional solid-state reaction, Tc = 1.13 K.[72] (The resistance of the Ag_2Pd_3S sample below Tc is most likely due to contact resistance, but

may also result from the large number of grain boundaries that are inherent in the low-temperature sintering process.)

2.6 Summary

We have demonstrated that metal nanoparticles can be used as a robust solution-based toolkit for synthesizing intermetallic compounds and alloys within minutes at low temperatures. The strategy exploits the enhanced reactivity and nanoscale diffusion distances afforded by binary nanoparticle composites to eliminate the need for high-temperature heating and atomic-scale homogenization, which are necessary using traditional methods for solid-state synthesis. The composition of the product is related to the composition of the metal nanoparticle precursors, and multiple compounds in the same binary system can be readily accessed; e.g., FePt, and $FePt_3$ are both accessible in the Fe-Pt system. This approach is general with respect to composition, crystal structure, and morphology, and is successful for both binary and ternary phases. A significant benefit of the low-temperature solution process is that morphologically diverse nanomaterials of complex compositions and structures can be accessed including surface-confined thin films, free-standing films, nanomesh materials, inverse opals, and gram-scale bulk powders with dense submicrometer crystallites. As shown previously, this approach can also yield discrete solution-dispersible intermetallic nanocrystals in the Au-Cu system.[44] Such flexibility in materials synthesis and processing is unprecedented for intermetallics and alloys. This approach has several important implications for synthesizing new solid-state materials and for controlling critical aspects of materials

processing. The ability to synthesize multimetallic solids at low temperatures without arc-melting or high-temperature annealing shifts the rate-limiting step from solid-solid diffusion to nucleation, and thus has the potential to yield new metastable, non-equilibrium, and interfacially stabilized phases as bulk materials. Likewise, the solution-based precursors provide access to complex nanostructured materials and thin films that would otherwise be inaccessible or require high-temperature or vacuum deposition techniques. Thus, this approach could open the door to intermetallic and alloy coatings on a variety of planar and non-planar supports, flexible films on polymer substrates, high-surface-area materials for catalytic applications, and nanotemplated materials, such as inverse opals and possibly nanorods, for fundamental studies and devices that exploit nanoscale magnetic, electronic, and optical properties.

The materials synthesized using this metallurgy in a beaker strategy are inherently impure, since the synthesis relies on sacrificial polymers and other solution additives that are necessary for reducing the metal salts and inducing nanoparticle aggregation to form nanocomposites. However, we demonstrated that these materials can have properties that are comparable to or superior to those of materials synthesized through more traditional routes that generally have higher purities. Other alternative synthetic approaches yield highly pure materials, but require much more elaborate setups and are not as amenable to scaleup (e.g., thin films prepared by Johnson and co-workers using elementally modulated reactants).[32] Our materials, although not as pure as those made by other routes, are easy to synthesize and scale up and may be appropriate for applications where low-level impurities are tolerable. There is a tradeoff between

ultrapure materials and materials that are easy to process and simple to produce in large quantities with controllable compositions and morphologies. We believe that the approach described here could be a viable strategy for synthesizing complex nanostructured materials with useful, unique, and unanticipated properties.

CHAPTER III

LOW TEMPERATURE SYNTHESIS OF $AuCuSn_2$ AND $AuNiSn_2$: USING SOLUTION CHEMISTRY TO ACCESS TERNARY INTERMETALLIC COMPOUNDS AS NANOCRYSTALS*

3.1 Introduction

Ternary intermetallic compounds of the late transition metals possess a wide variety of physical properties, including superconductivity,[54,72] magnetoresistance,[73] and shape memory effects,[29,56] that are important for many scientific studies and technological applications. Traditionally, intermetallics are synthesized using high-temperature arc melting or powder metallurgy techniques, which require high temperatures to homogenize the constituent elements followed by lengthy annealing times at reduced temperatures. These reactions are typically limited by solid-solid diffusion which makes the high temperatures necessary. While these methods are quite successful, they generally yield thermodynamically stable structures and offer little control over nanostructure and morphology. A few alternative techniques have been exploited to synthesize new intermetallic phases at low temperatures,[32,61,74] and often these synthetic techniques have resulted in new solid-state materials. Robust low temperature methods that allow kinetic control over phase formation and reactivity of

---

* Reprinted in part with permission from *J. Am. Chem. Soc., 127* Leonard, B. M.; Bhuvanesh, N. S. P.; Schaak, R. E. "Low-Temperature Polyol Synthesis of $AuCuSn_2$ and $AuNiSn_2$: Using Solution Chemistry to Access Ternary Intermetallic Compounds as Nanocrystals," 7326, Copyright 2005 by the American Chemical Society.

intermetallic compounds as well as morphological control still remain quite rare.

Solution methods for synthesizing nanocrystalline intermetallics at low temperatures have also remained largely unexplored. In solution based nanocrystal synthesis, the solvent and surface stabilizing agents can play a key role in kinetically trapping phases that are not stable at high temperatures, providing access to nanocrystalline phases, such as α-Co[41] and wurtzite-type ZnS.[42] This suggests that low-temperature solution strategies, which were recently shown to yield known binary intermetallics,[44,45,75] may be attractive for synthesizing new or metastable intermetallics with more complex structures and compositions.

The polyol process was originally developed for the synthesis of transition metal powders as nanocrystals.[46-48] This technique uses high boiling polyalcohol solvents which act as a reducing agent at elevated temperatures. Our group[40,75,76] and others[36-39,46,47,48] have modified this process to yield nanocrystals of a variety of different elements,[40] alloys,[34,37-39,49] and intermetallics,[40,75,76] including several important technological materials. This technique eliminates the need for the high temperature melting that traditional solid state techniques require and greatly reduces the annealing time due to intimate mixing of nanoparticle reactants. Additionally, modifications of this process are known to produce size and shape controlled nanocrystals, which makes this process a useful approach to explore the formation of intermetallic nanocrystals.

Here, we show for the first time that low-temperature solution routes originally developed for the synthesis of nanocrystals[77] and nanocrystalline powders[45] can be exploited to access new ordered intermetallics with ternary compositions. While ternary

phase diagrams are difficult to map out, the Au-Cu-Sn system has been studied in detail. Intermetallics that form at the solder/metal interface are responsible for the brittleness and fracture of solder joints, and the Au-Cu-Sn system is among the most important for understanding interfacial phase formation in microelectronic devices.[78] Several intermetallic phases are known in the Au-Cu-Sn system including binary and ternary phases.[79,80] We were able to access several of these phases as seen in Figure 3.1, and we also discovered an unknown phase which did not match any of the known phases.

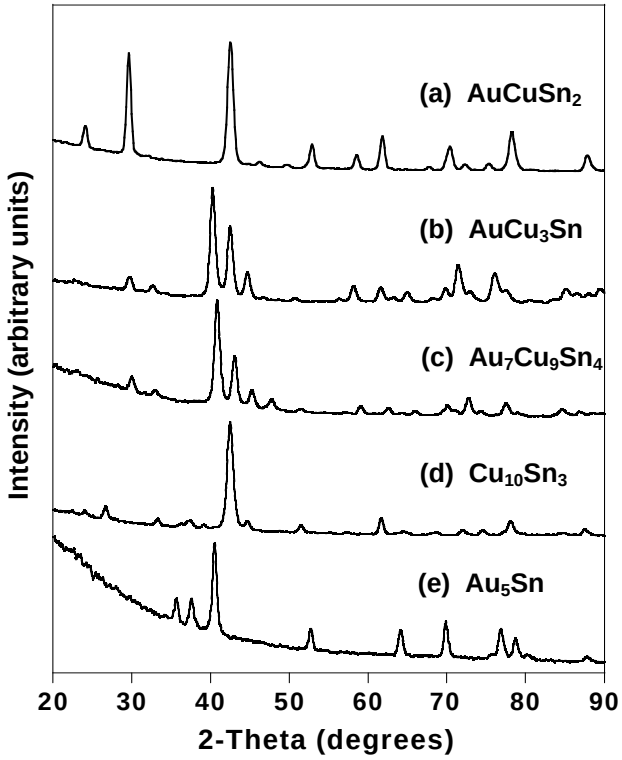

Figure 3.1 Powder XRD patterns for binary and ternary intermetallic phases in the Au-Cu-Sn system synthesized using low temperature solution techniques.

Here we report the discovery of a new ordered intermetallic compound, $AuCuSn_2$, that was not previously observed in bulk systems using traditional synthetic techniques.[80] Nanocrystalline $AuCuSn_2$ is stabilized using low-temperature solution chemistry. Additionally, we explored other ternary metal systems using this solution based approach and found that we can access another ordered intermetallic phases $AuNiSn_2$ as well as several ternary alloy phases with a similar NiAs-type structure. Au-M-Sn and Pt-M-Sn systems (M = Co, Ni, Cu) were chosen due to their solder applications and potential magnetic properties.

3.2 Experimental Details

3.2.1 *Synthesis of $AuCuSn_2$*

Nanoparticles of $AuCuSn_2$ were synthesized using a modified polyol process. $HAuCl_4 \cdot 3H_2O$ (69.5 mg, 0.1765 mmol), $Cu(C_2H_3O_2)_2 \cdot H_2O$ (43.2 mg, 0.2164 mmol), $SnCl_2$ (141.8 mg, 0.7479 mmol), and poly(vinyl pyrrolidone) (PVP, MW = 40,000; 356.3 mg) were sequentially dissolved in tetraethylene glycol (TEG) under sonication. This solution was stirred under Ar for 20-30 min and then heated to 70°C. A freshly prepared solution of $NaBH_4$ in TEG (0.4 M, 5 mL) was added to the stirring solution of metal salts and PVP at 70 °C. The solution was then heated to various temperatures between 120 – 220 °C for 10 min and cooled to room temperature. Nanocrystals of $AuCuSn_2$ were collected via centrifugation, washed several times with NANOpure water (18.2 MΩ) and ethanol, and dried under ambient conditions.

3.2.2 *Synthesis of Au-M-Sn Nanocrystals*

$AuNiSn_2$ nanocrystals were synthesized in a similar manner using $HAuCl_4 \cdot 3H_2O$ (69.9 mg, 0.1775 mmol), $Ni(C_2H_3O_2)_2 \cdot xH_2O$ (48.9 mg, 0.1964 mmol), $SnCl_2$ (143.7 mg, 0.7579 mmol), and PVP (360.2 mg). A freshly prepared solution of $NaBH_4$ in TEG (0.4 M, 5 mL) was added to the stirring solution of metal salts and PVP at 70 °C. The solution was heated to reflux (~310 °C) for 10 min. AuCoSn nanocrystals were synthesized under similar conditions using $Co(C_2H_3O_2)_2 \cdot xH_2O$ and heating in solution to 200 °C.

3.2.3 *Synthesis of M-Pt-Sn Nanocrystals*

Nanocrystals of Pt-M-Sn (M = Co, Ni, Cu) were synthesized similar to the Au based ternary nanocrystals. K_2PtCl_6 (45.1 mg, 0.093 mmol), and poly(vinyl pyrrolidone) (PVP, MW = 40,000; 134.1 mg) were sequentially dissolved in tetraethylene glycol (TEG) under sonication. This solution was stirred under Ar for 20-30 minutes and then heated to 180°C. $Cu(C_2H_3O_2)_2 \cdot H_2O$ (19.1 mg, 0.0957 mmol) and $SnCl_2$ (105.3 mg, 0.555 mmol) were dissolved separately in 3 ml TEG and added to the stirring Pt solution dropwise. A freshly prepared solution of $NaBH_4$ in TEG (0.4 M, 5 mL) was added to the stirring solution of metal salts and PVP at 180 °C. The solution was then heated to various temperatures and cooled to room temperature. Nanocrystals were collected via centrifugation, washed several times with NANOpure water (18.2 MΩ) and ethanol, and dried under ambient conditions.

3.2.4 *Characterization*

Powder X-ray diffraction (XRD) data were collected using a Bruker GADDS three-circle X-ray diffractometer using microdiffraction powder techniques. High resolution XRD data for structure refinement were collected on a Bruker D-8 Advance powder diffractometer. Both used Cu Kα sources. Simulated powder data were created using the CrystalDiffract software package. Rietveld refinement of the high-quality powder XRD data was carried out using TOPAS.

Transmission electron microscopy (TEM) images were colleted on a JEOL 2010 TEM. Samples were prepared by re-suspending the isolated and cleaned nanoparticles in ethanol (1 mg powder in 2 mL of ethanol) and dropping the solution on a carbon coated Ni grid. Composition analyses were carried out on a four spectrometer Cameca SX50 electron microprobe at an accelerating voltage of 15 kV at a beam current of 10 nA. All analyses were carried out after daily standardization using pure elements, and had an accuracy of +/- 1 to 2%. Differential scanning calorimetry (DSC) data were collected on a TA Instruments Q600 SDT under an Ar purge at a heating rate of 10 °C/min. Magnetic susceptibility measurements were obtained using a Quantum Design SQUID magnetometer MPMS-XL by cooling the sample from 300 – 5 K in a 10000 Oe field.

3.3 Synthesis and Structural Analysis of $AuCuSn_2$

$AuCuSn_2$ was synthesized by heating a nominally stoichiometric solution of $HAuCl_4 \cdot 3H_2O$, $Cu(C_2H_3O_2)_2$, $SnCl_2$, and poly(vinyl pyrrolidone) (PVP, MW = 40,000) in tetraethylene glycol (TEG, 20 mL) to 70 °C, then adding a freshly prepared solution

of dilute $NaBH_4$ and heating the solution to 120 – 200 °C for 10 min. The X-ray diffraction (XRD) patterns for $AuCuSn_2$ annealed in TEG at 120, 160, and 200 °C are shown in Figure 3.2. The patterns, which did not match any known phases in the Au-Cu-Sn ternary system or the constituent unary and binary systems, can be indexed to a hexagonal cell with a = 4.2287(1) Å and c = 5.2301(1) Å. Microprobe analysis indicated an average composition of $Au_{0.80(6)}Cu_{0.98(4)}Sn_{2.0(1)}$, which is close to a nominal composition of $AuCuSn_2$.

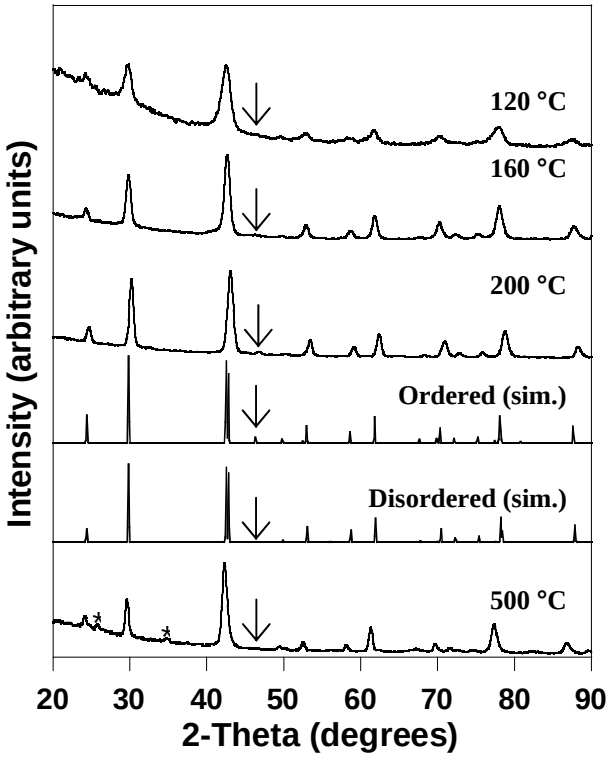

Figure 3.2 Powder XRD patterns for $AuCuSn_2$ synthesized in TEG at 120, 160, and 200 °C, simulated XRD data for ordered and disordered (NiAs-type) $AuCuSn_2$, and $AuCuSn_2$ powder heated to 500 °C under Ar. The arrows highlight a superlattice peak (see Figure 3.3 for others), and asterisks show a small amount of SnO_2 that crystallizes on heating.

Figure 3.2 shows a simulated powder XRD pattern for NiAs-type $AuCuSn_2$, with Au and Cu disordered over the Ni site. While the major reflections are in agreement, several smaller reflections in the experimental XRD data are not accounted for. As the Au and Cu atoms are allowed to order in alternating layers, superlattice peaks emerge, and the ordered NiAs superstructure matches all of the observed reflections. The structure was solved in the trigonal space group *P*312, and after imposing additional symmetries, the structure was transformed to the hexagonal space group *P*-6*m*2, where the structural model was refined using TOPAS.[81] The calculated diffraction pattern is in good agreement with the experimental data (Figure 3.3). The structure of $AuCuSn_2$ (Figure 3.4) consists of an ordered hcp array of Sn with Au and Cu in alternating layers

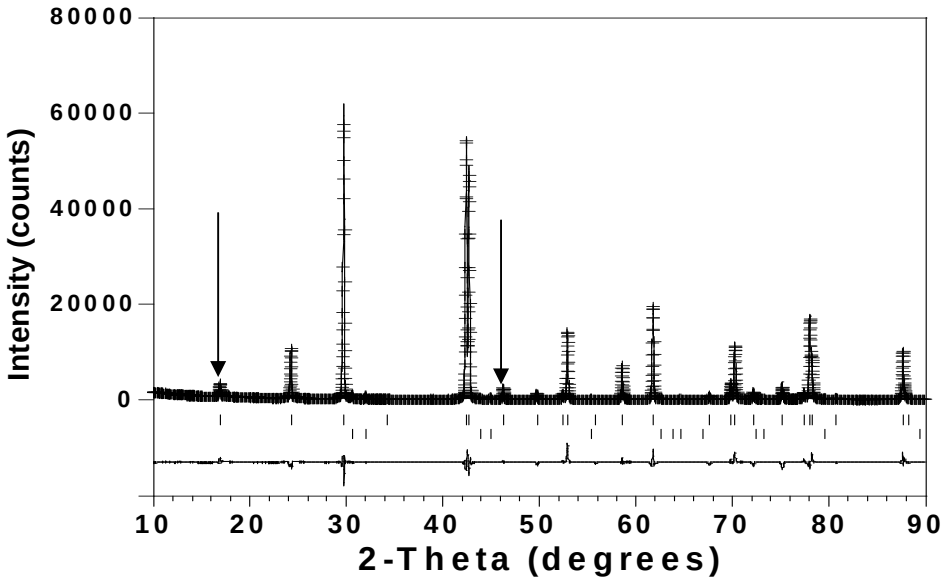

Figure 3.3 Rietveld structure refinement for $AuCuSn_2$ synthesized at 200 °C in TEG showing the calculated (top, solid line) and observed (top, crosses) XRD patterns. The difference curve (bottom, solid line) indicates the agreement between the observed and calculated patterns. The top and bottom sets of tick marks indicate the allowed Bragg reflections for ordered $AuCuSn_2$ and a Sn impurity, respectively.

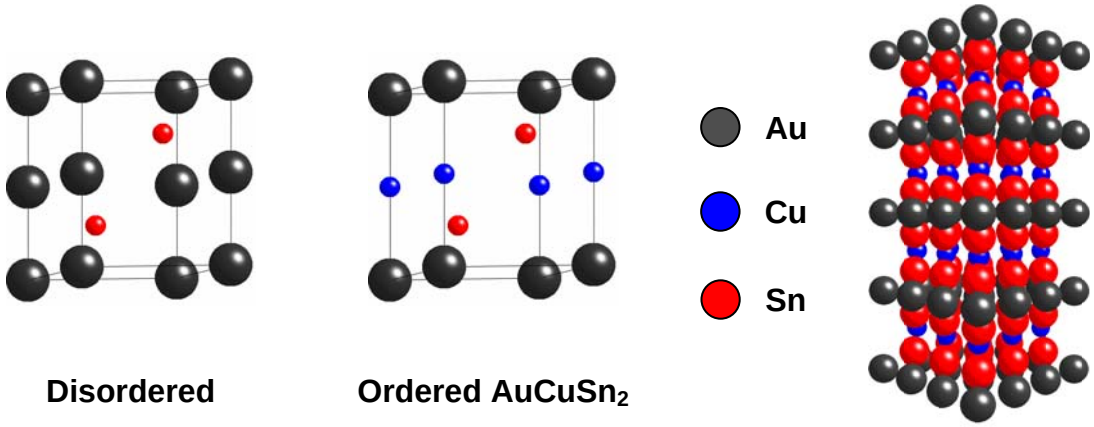

Figure 3.4 Structure of ordered $AuCuSn_2$ and unit cells for the ordered and disordered structures. (Au = gray, Cu = blue, Sn = red. Gray spheres in the disordered structure represent a mixture of Au and Cu.)

occupying the octahedral holes. Refinement of the atomic positions indicated only 10% disorder between the Au and Cu sites. Importantly, a previous study of the Au-Cu-Sn phase diagram under equilibrium conditions reported that $AuCuSn_2$ exists as a dis-ordered NiAs-type solid solution at 250 °C.[12] In contrast, we find that the ordered structure is stable at 250 °C when the polyol method is used, providing strong evidence that low temperature solution routes can stabilize structures that do not readily form using traditional synthetic techniques.

The differential scanning calorimetry (DSC) data in Figure 3.5 show two endotherms. The first, near 210 °C, corresponds to the melting of Sn. A small Sn impurity was included in the structure refinement shown in Figure 3.3, and magnetic susceptibility measurements (Figure 3.5) indicated a superconducting transition at 3.7 K, consistent with a small Sn impurity. The endotherm at 450 °C is evidence of an order/disorder phase transition, which is confirmed by powder XRD data for $AuCuSn_2$

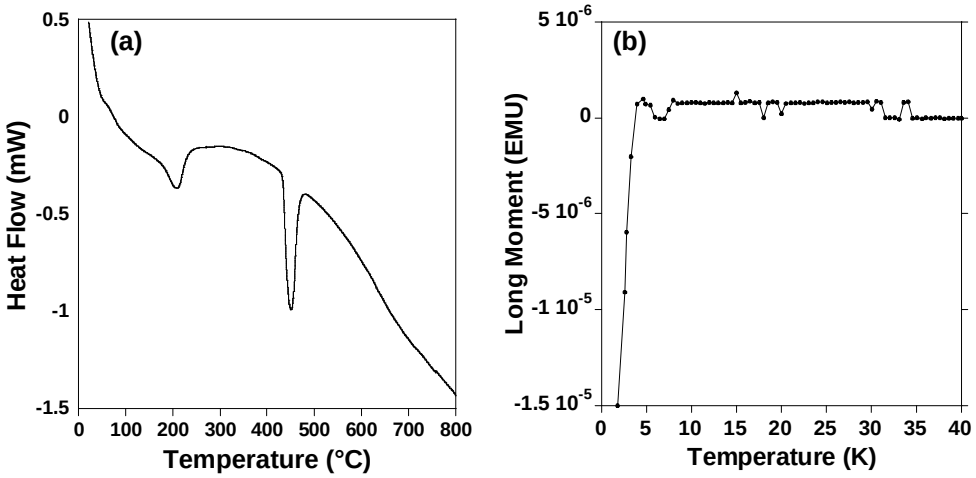

Figure 3.5 (a) DSC trace and (b) magnetic susceptibility measurements of $AuCuSn_2$ nanocrystals synthesized at 160 °C in TEG. The DSC trace shows two endotherms, the first near 210 °C is due to a Sn impurity melting and the second at 450 °C is evidence of and order/disorder transition. The magnetic susceptibility measurement shows a superconducting transition at 3.7 K consistent with a Sn impurity.

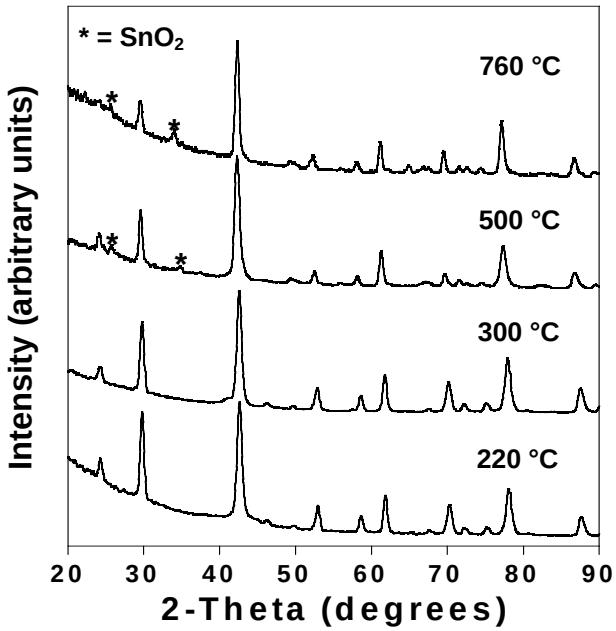

Figure 3.6 Powder XRD data for $AuCuSn_2$ heated under Ar to 220, 300, 500, and 760 °C. This data confirms the order/disorder transition seen in the DSC trace at 450 °C as the superlattice peaks disappear once the powder is heated above the transition. Asterisks show a small amount of SnO_2 that crystallizes on heating.

heated to 500 °C under Ar (Figure 3.6), showing the disappearance of the superlattice reflections. Figure 3.7 shows a transmission electron micrograph (TEM) of $AuCuSn_2$ synthesized at 160 °C, indicating that the new ordered phase exists as well-defined nanocrystals. The average crystallite size determined by analysis of TEM micrographs (ca. 180 nanocrystals) is 27 +/- 14 nm. No attempt was made at this point to control the size or dispersity of the nanocrystals, although we expect that standard synthetic modifications to the polyol process will allow such control in the future.

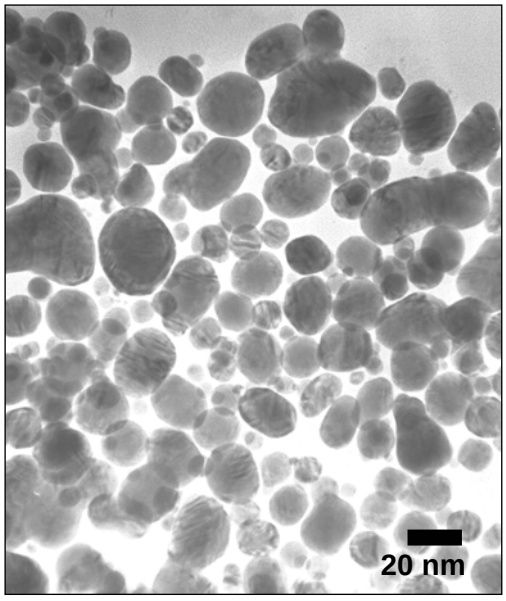

Figure 3.7 TEM micrograph of $AuCuSn_2$ nanocrystals synthesized at 160 °C in TEG and re-suspended in ethanol. This shows that the $AuCuSn_2$ forms as individual nanocrystals.

Recently, the structures of $AuCuSn_2$ and $AuNiSn_2$ were solved by single crystal X-ray analysis.[82] The crystals were synthesized using traditional solid state methods by heating Au, Sn, and Cu or Ni in a sealed tube at 1300 K and annealing for several days at

a reduced temperature. The corrected structures were solved in the space group *P*-3*m*1 in contrast to our report of *P*-6*m*2. While our structural model fit the powder data we were working with, single crystal data is much more conclusive in structure determination. The Laue classes 6/*mmm* and -3*m* are not distinguishable when using powder diffraction to refine the structure. Additionally, in terms of identifying positions of Au and Cu vs Sn (in alternating layers), Au and Cu together have 108 electrons, while two Sn atoms have 100 electrons. Therefore, the scattering power of these positions is similar and indistinguishable using laboratory X-ray methods.

3.4 Extension to Other Ternary Systems

3.4.1 *Synthesis of Au-M-Sn Ternary Nanocrystals*

Using the same solution method, ordered $AuNiSn_2$ can also be synthesized. Like $AuCuSn_2$, $AuNiSn_2$ is stabilized at low temperatures in solution and was not identified in previous studies of the ternary phase diagram.[83] Figure 3.8 shows the powder XRD pattern for nanocrystalline $AuNiSn_2$ and the simulated XRD data for the ordered and disordered structures based on the refined structural model for $AuCuSn_2$. Similar to the $AuCuSn_2$ structure, the Au and Ni atoms are allowed to order in alternating layers which give rise to superlattice peaks, and the ordered NiAs superstructure formed by this ordering matches all of the observed reflections in the $AuNiSn_2$ diffraction pattern. The peaks in $AuNiSn_2$ are much broader than that of the $AuCuSn_2$ as a result of smaller particle size. The lattice constants determined from the powder patterns and refined using Checkcell were found to be a = 4.093(1) Å and c = 5.301(1) Å.

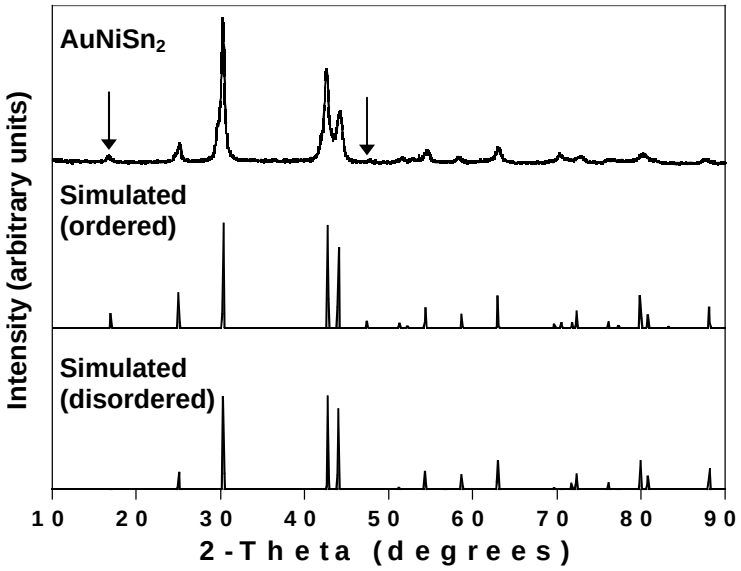

Figure 3.8 Observed and simulated (ordered and disordered) powder XRD patterns for $AuNiSn_2$, with a = 4.093(1) Å and c = 5.301(1) Å. Primary supperlattice reflections are marked with an arrow. The average particle size was estimated to be 12 nm using the Scherrer equation.

Under similar reaction conditions, AuCoSn alloy nanocrystals can also be formed. The powder XRD patterns (Figure 3.9) of the product look similar to those of $AuCuSn_2$ and $AuNiSn_2$ but lack the ordering peaks seen in both of those phases. Because ordering peaks are not present, we have to assume that the three metals are all disordered at each position in the unit cell. The lattice constant for AuCoSn (a= 4.174(8) Å, c= 5.364(7) Å) is shifted away from the AuSn (a= 4.3218 Å, c= 5.5230 Å) and Co_3Sn_2 (a= 4.162 Å, c= 5.233 Å) due to the incorporation of all three metal atoms in the crystal structure. Additionally, there are not any binary phases in the Au-Co system with a NiAs-type structure, so the diffraction pattern does not match any known phases in the Au-Co-Sn system.

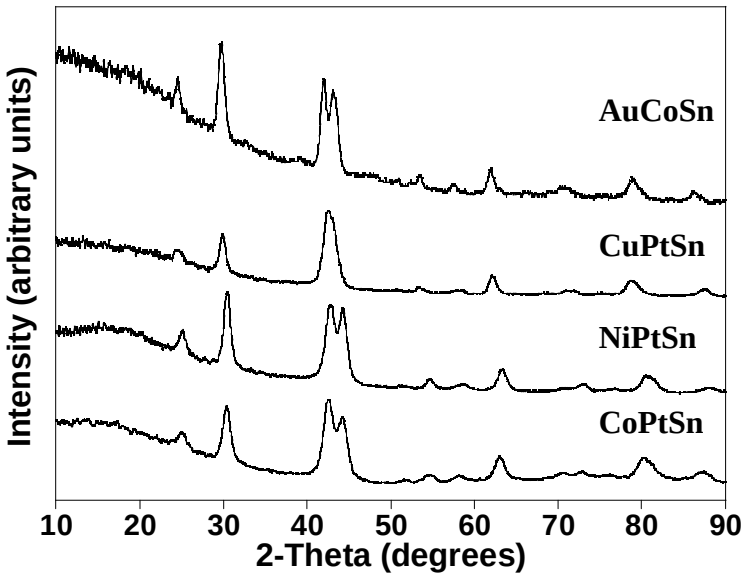

Figure 3.9 Powder XRD patterns for ternary alloys synthesized using the polyol process. Each of the ternary phases adopts the NiAs type structure but the lattice constants are all shifted off of the parent structure (AuSn or PtSn) due to incorporation of the third metal.

3.4.2 *Synthesis of M-Pt-Sn Ternary Nanocrystals*

The polyol process has allowed us to access ternary intermetallic nanocrystals and we extended this to also include Pt-based ternary phases. A series of compounds were attempted, building on the success seen in the Au-M-Sn system by substituting Pt for Au. Co, Ni, and Cu were each studied using reaction conditions similar to those used for $AuCuSn_2$. Powder XRD patterns show a NiAs type structure for each of the phases studied. A previous report listed lattice constants for Pt-M-Sn ternary alloys with a NiAs type structure including M=Cr, Mn, Fe, Co, and Ni.[84] No other structural information was given in the report and for most of these ternary systems this was the only data ever reported.

Using solution based techniques, we were able to access three ternary alloys in the Pt-M-Sn system all with NiAs type structures. No ordering peaks are present in the diffraction patterns, indicating that the metals are disordered within the NiAs structure. Lattice constants for each phase were determined from the powder patterns and refined using Checkcell: PtCuSn a= 4.149(2) Å, c= 5.2575, PtNiSn a= 4.086(7) Å, c=5.281(5) Å, PtCoSn a= 4.090(3) Å, c= 5.328(1). These values all differ significantly from those of the binary phases for each system due to incorporation of all three metals in the crystal structure.

TEM micrographs (Figure 3.10) for CuPtSn confirm the presence of nanocrystalline CuPtSn and electron diffraction confirms the NiAs-type structure. EDS

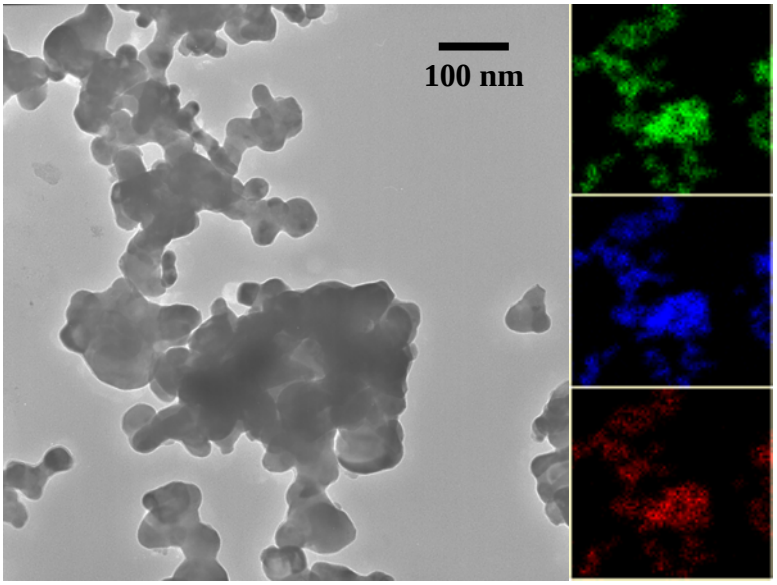

Figure 3.10 TEM micrograph of CuPtSn nanoparticles synthesized at 160 °C in TEG and re-suspended in ethanol. EDS mapping images show that each of the three metals are incorporated into all of the particles shown and the overall composition of the particles is $CuPt_{0.7}Sn_{0.97.}$

mapping shows that each metal is present in the particles and the sample has an average composition of $CuPt_{0.7}Sn_{0.97}$. Similarly TEM data for CoPtSn also show that nanocrystals are formed and EDS analysis of the particles confirms the presence of all three metals with an average composition of $Co_{0.7}Pt_{0.28}Sn$.

3.5 Summary

The discovery of a new family of ordered intermetallics as nanocrystals using low-temperature solution methods has several important implications. First, it shows that ternary intermetallic phases are accessible as nanocrystals, which has the potential to greatly expand the availability of complex multimetallic nanomaterials for future studies of size-dependent properties, intermetallic catalysis, and integration into nanotechnological devices. Second, it demonstrates that low-temperature solution methods that have been developed for nanocrystal synthesis are appropriate exploratory media for synthesizing new and possibly metastable intermetallics. Third, it opens the door to studying phase formation and stability of complex multimetallic solids at low temperatures, where reaction kinetics are typically too slow and impurities are unavoidable. Finally, the fact that we were able to discover new phases in well studied ternary systems attests to the ability of this solution-based synthetic method to stabilize new structures that are not accessible using traditional methods. We expect that other new binary, ternary, and perhaps quaternary intermetallic compounds will be accessible as nanocrystalline solids using this approach.

CHAPTER IV

MULTI-STEP SOLUTION-MEDIATED FORMATION OF $AuCuSn_2$: MECHANISTIC INSIGHTS FOR THE GUIDED DESIGN OF INTERMETALLIC SOLID-STATE MATERIALS AND COMPLEX MULTI-METAL NANOCRYSTALS*

4.1 Introduction

The ability to understand how solids form is critically important for rationally designing new materials, yet the elucidation of reaction pathways remains one of the most widely-recognized challenges in solid-state chemistry. Solid-solid diffusion is generally the rate limiting step in solid-state reactions, and as a result, high temperatures and long heating times are usually needed to drive the reactions to completion. Consequently, it is difficult to piece together the interactions among the reactants, including the formation of important intermediates that may be crucial for successfully forming a desired product. Furthermore, high-temperature reactions often preclude the formation of metastable and low-temperature phases that are not accessible under such conditions. The high temperature reactions that are required for traditional solid-state syntheses, while important for generating many useful materials, have clear limitations in terms of understanding reaction pathways and stabilizing low-temperature and meta-

---

* Reprinted in part with permission from *J. Am. Chem. Soc., 128* Leonard, B. M.; Schaak, R. E. "Multi-Step Solution-Mediated Formation of $AuCuSn_2$: Mechanistic Insights for the Guided Design of Intermetallic Solid-State Materials and Complex Multimetal Nanocrystals," 11475, Copyright 2006 by the American Chemical Society.

stable structures.

A few general strategies exist for understanding and controlling reaction pathways in solid-state systems, and these typically involve alternative low-temperature techniques. For example, Johnson and co-workers have used elementally modulated reactants as a platform for understanding and controlling reaction pathways in thin films,[32,85] and also for generating new solids that are inaccessible using traditional methods.[86] Topochemical strategies that modify the structures of framework solids in a stepwise and predictable manner can also be used to generate new solids via consideration of reaction pathways.[87] Understanding how low-temperature and metastable phases form could provide solid-state chemists with mechanistic guidelines for rationally designing new solids, in analogy to the retrosynthetic strategies routinely used by organic chemists.

The development of low-temperature solution routes to solid-state materials,[48,76,88,89] including strategies that yield colloidal and nanocrystalline solids, provides intriguing opportunities for studying solid-state formation mechanisms and accessing new structures. Along those lines, we[44,45,50,75] and others[17,90-92] have recently begun to explore the formation of nanocrystalline alloys and intermetallic compounds using low-temperature strategies that differ significantly from traditional high-temperature metallurgical techniques. Building on extensive work by many groups on the synthesis of metal nanoparticles using the polyol process,[37-39,46,47,76,90,93] we have been able to access a growing library of binary[75,76] and ternary[50] intermetallic compounds using modifications of this approach. The polyol process provides a low-

temperature medium for precipitating reduced multi-metal compounds as nanoparticles, and like most successful strategies for low-temperature solid-state synthesis, avoids solid-solid diffusion as the rate limiting step. As anticipated from the low-temperature nature of the technique, the polyol process can also be used to generate metal and multi-metal nanocrystals with new structures, including ε-Co[41] and Au*M*Sn_2 (*M* = Cu, Ni).[50]

$AuCuSn_2$ is a new ordered ternary intermetallic compound that was discovered during our initial attempts to synthesize ternary metal nanocrystals using the polyol process.[50] The Au-Cu-Sn system has been studied in detail under bulk-scale equilibrium conditions because of its importance in solder applications,[78-80] and when this work was published the ordered polymorph of $AuCuSn_2$ had only been isolated as nanocrystals using a low-temperature solution route.[50] (A subsequent report demonstrated that $AuCuSn_2$ could be accessed as single crystals using a high temperature route.[82]) We discovered that $AuCuSn_2$ can only be synthesized in solution using an unusual multi-step process;[50] more common one-step polyol reactions do not yield the new intermetallic phase (Figure 4.1).

Importantly, we have been able to probe the formation mechanism by taking aliquots from the solution at various stages of the reaction and studying the crystalline and non-crystalline products, as well as the species that remain in solution. The result, presented here, is a detailed understanding of an unusual multi-step reaction pathway that yields nanocrystals of a new intermetallic compound. In addition to elucidating a solid-state reaction pathway and providing a new way of thinking about the synthesis of

intermetallic compounds, this work also has important implications for controlling the synthesis of complex nanocrystals.

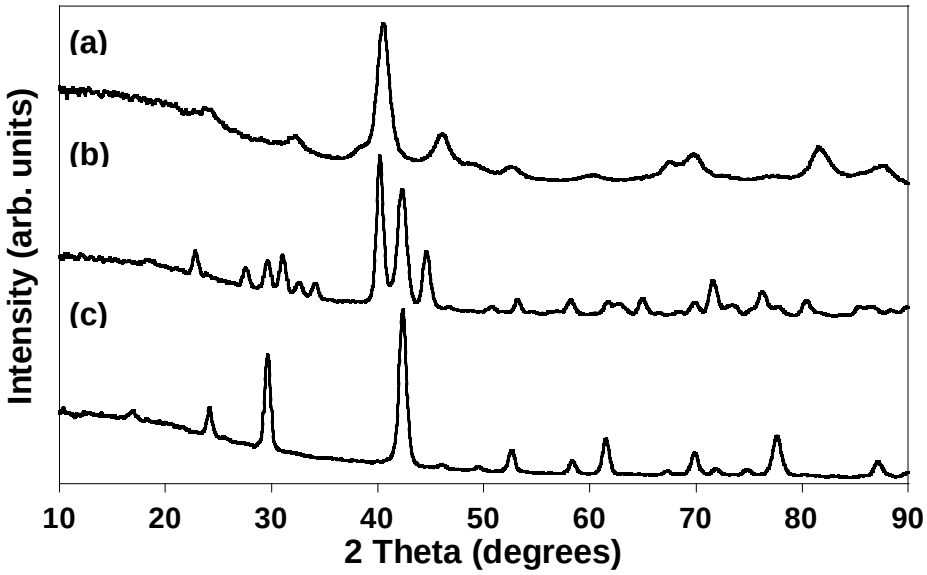

Figure 4.1 Powder XRD patterns for the products isolated from various modifications to the polyol process, in all cases heated to ~ 200 ºC: (a) a straight polyol reaction using only TEG as the reducing agent, (b) a modified polyol reaction that was reduced with $NaBH_4$ at room temperature prior to heating, and (c) the successful multi-step reaction that generated $AuCuSn_2$ (heat to 70 ºC, then reduce with $NaBH_4$ and continue heating). In the straight polyol reaction of Au^{3+}, Cu^{2+}, and Sn^{2+}, no $NaBH_4$ is added, so the solvent acts as the only reducing agent. In this case, intermetallic AuCu is formed as the only crystalline product. If the metal salts are co-reduced with $NaBH_4$ at room temperature, the Au^{3+} is reduced at the same time as the Cu^{2+} and Sn^{2+} salts and this leads to the formation of multiple phases, including $AuCu_3Sn$ and AuCuSn; ordered $AuCuSn_2$ is not observed. $AuCuSn_2$ can only be isolated when using the multi-step reaction in which the solution is reduced with $NaBH_4$ at 70 °C and subsequently heated.

4.2 Experimental Details

4.2.1 *Materials*

All chemicals were purchased from Alfa Aesar and were used as received without further processing or purification: $HAuCl_4 \cdot 3H_2O$ (99.99%), $Cu(C_2H_3O_2)_2 \cdot 2H_2O$

(98.0-102.0%), $SnCl_2$ (anhydrous, 99+% min), poly(vinyl pyrrolidone) (PVP, MW = 40,000), $NaBH_4$ (98%), and tetraethylene glycol (TEG, 99+%).

4.2.2 *Synthesis of $AuCuSn_2$*

$AuCuSn_2$ was synthesized using a modified polyol process similar to our previous report.[10] Briefly, PVP (175.0 mg), $Cu(C_2H_3O_2)_2 \cdot 2H_2O$ (21.8 mg, 0.1089 mmol), $SnCl_2$ (70.2 mg, 0.3703 mmol, 4-fold excess), and $HAuCl_4 \cdot 3H_2O$ (35.0 mg, 0.0887 mmol) were dissolved sequentially in 20 mL of TEG with sonication. This solution was stirred vigorously under bubbling Ar for fifteen minutes. The solution was then heated to 70° C, and a freshly prepared solution of $NaBH_4$ (35 mg in 2-3 mL TEG) was added dropwise to the solution while stirring. After the metals were reduced (within 5 min), the solution was further heated to 120 – 200 ºC. Aliquots were extracted during the reaction in order to characterize the species present at each step. Powders were collected by centrifugation and washed several times with ethanol. Acetonitrile was also used occasionally as a co-solvent to aid in precipitating all of the nanocrystalline powder from solution.

4.2.2 *Characterization*

Powder X-ray diffraction (XRD) data were collected on a Bruker GADDS three-circle X-ray diffractometer using Cu Kα radiation. Transmission electron microscopy (TEM) images, selected area electron diffraction (SAED) patterns, and energy-dispersive X-ray analysis (EDS) were collected using a JEOL JEM-2010 TEM. Elemental mapping images were acquired using a semi-STEM (STEM = scanning transmission

electron microscopy) attachment. Samples were prepared by sonicating the isolated nanocrystalline powders in ethanol and dropping a small volume onto a carbon-coated nickel grid or by dropping the reaction solution directly onto the grid. Optical spectroscopy measurements were taken on a Jasco V-530 UV-Visible spectrometer. Solid-state composition analysis was carried out on a four spectrometer Cameca SX50 electron microprobe.

4.3 Reaction Pathway for the Formation of $AuCuSn_2$

Figure 4.2 shows a schematic of the proposed multi-step reaction pathway that was derived from the detailed studies that follow. Initially, the metal salt precursors and polymer stabilizer are dissolved in a high-boiling glycol solvent. Next, the polyol solvent is heated to 70 ºC. This facilitates reduction of the Au^{3+} to Au^0 nanoparticles and concomitant oxidation of some of the Sn^{2+} to Sn^{4+}, which precipitates as SnO_2 nanocrystals that ultimately anneal to form a shell around the Au-containing nanoparticles. Next, $NaBH_4$ is added, which is a strong reducing agent that immediately reduces the remaining Sn^{2+} to Sn^0 and converts the Cu^{2+} to Cu^0. In this step, the Au nanoparticles appear to quickly react with the Sn to form nanocrystals of intermetallic AuSn. With further heating, the Cu^0 nanoparticles begin to aggregate and interdiffuse into the intermetallic AuSn nanocrystals, along with the remaining Sn. $AuCuSn_2$ nanocrystals form once the reaction is allowed to proceed to completion, either by controlling reaction temperature or time.

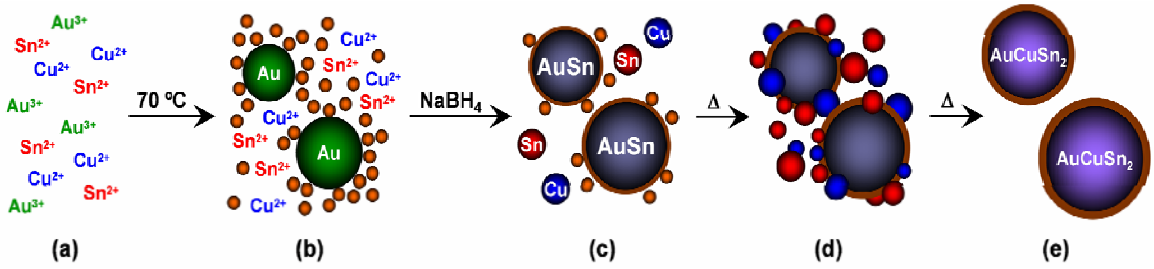

Figure 4.2 Schematic of the proposed multi-step reaction pathway for the formation of $AuCuSn_2$ nanocrystals: (a) metal salt reagents (with PVP in TEG), (b) formation of Au and SnO_2 nanoparticles (the small orange spheres represent SnO_2, resulting from a galvanic reaction between Au^{3+} and Sn^{2+} that forms Au^0 and Sn^{4+}, which precipitates as SnO_2), (c) formation of NiAs-type AuSn nanoparticles, along with Sn and Cu, (d) aggregation and thermal interdiffusion to form $AuCu_xSn_y$ alloy nanoparticles, and (e) nucleation of intermetallic $AuCuSn_2$. In (c), (d), and (e), the orange-colored shell on the AuSn, $AuCu_xSn_y$, and $AuCuSn_2$ nanoparticles represents the SnO_2 coating that forms from annealing the SnO_2 nanoparticles in solution, and it persists throughout the entire reaction.

4.3.1 *Step 1: Formation of Au Nanoparticles*

After dissolving the metal salts and polymer stabilizer in TEG, the solution has a pale yellow color (Figure 4.3a). Upon heating to 70 ºC, the solution containing Au^{3+}, Cu^{2+}, Sn^{2+}, and PVP develops an intense purple color (Figure 4.3a), which suggests the formation of metal nanoparticles that have a visible surface plasmon resonance (SPR) peak. This is confirmed by UV-Visible spectroscopy (Figure 4.3a). Interestingly, when a solution containing only Au^{3+} and PVP is heated to 70 ºC in TEG, no visible reaction occurs. However, when reduced with $NaBH_4$, the solution turns wine red and exhibits a SPR peak centered around 515 nm (Figure 4.3a), which is consistent with the well-known SPR peak of spherical Au nanoparticles.[94] The optical data suggests subtle but important differences between the Au-Cu-Sn sample (purple) and the pure Au sample

(red), and these differences are probed and understood by utilizing several complementary techniques that are described below.

The powder XRD pattern for the solid product isolated from the purple Au-Cu-Sn solution by solvent-induced precipitation and centrifugation, yielding a clear colorless solvent, shows only nanocrystalline Au (Figure 4.3b). However, electron microprobe analysis of the solid product shows the presence of both Au and Sn in a

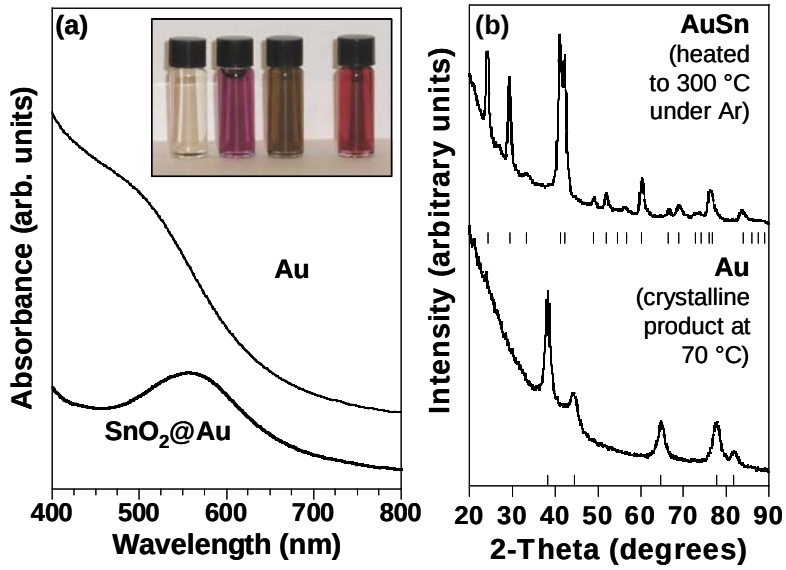

Figure 4.3 (a) Visible absorption spectra showing that the SPR band for the red-colored solution of Au nanoparticles is centered near 520 nm and the SPR band for the purple-colored Au-Cu-Sn solution heated to 70 °C is centered at 555 nm. The SPR peak for the Au-Cu-Sn solution is red-shifted relative to that of Au due to the presence of SnO_2 nanoparticles in solution, which interact with the surface of the Au nanoparticles. The inset shows a photograph of (i) the metal salts (Au^{3+}, Cu^{2+}, Sn^{2+}) dissolved in solution, (ii) the purple-colored solution after heating to 70 °C, (iii) the heated solution reduced by $NaBH_4$, and (iv) a control (red-colored) solution of Au nanoparticles formed by $NaBH_4$ reduction. (b) Powder XRD patterns for the solid product precipitated from the Au-Cu-Sn reaction solution heated to 70 °C (bottom) and the same powder annealed at 300 °C in a tube furnace under Ar (top), showing the formation of intermetallic AuSn from the Au-Sn nanocomposite. Tick marks below each pattern represent the allowed Bragg reflections for Au (bottom) and NiAs-type AuSn (top).

1.00:0.96 ratio. The Cu content of this sample is below the detection limit of the instrument, which indicates that Au and Sn are incorporated into the product, but Cu is not.

Careful analysis by TEM reveals several additional details. The TEM micrograph in Figure 4.4, prepared by dropping the purple-colored Au-Cu-Sn solution directly onto a TEM grid, shows high-contrast nanoparticles that range in size from 5 to

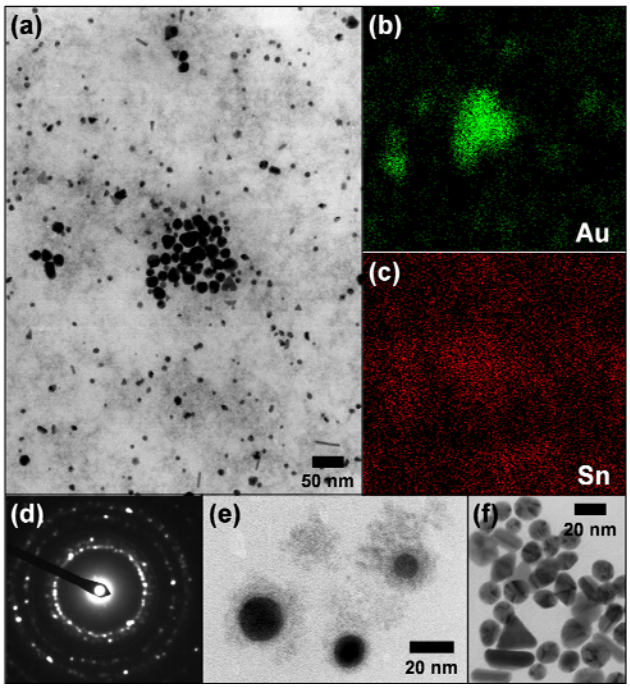

Figure 4.4 (a) TEM micrograph for the Au-Cu-Sn reaction solution heated to 70 °C, showing the presence of Au (larger, high contrast) and SnO_2 (small, medium contrast) nanoparticles. Panels (b) and (c) show semi-STEM elemental mapping data for the TEM micrograph in panel (a), showing that Au is present in the high contrast areas (b) and Sn is present in the areas of medium contrast (c). (The lowest contrast regions represent the background.) The SAED pattern in (d) shows an fcc pattern matching that of Au. The TEM micrograph in (e) shows a close-up of Au nanoparticles surrounded by smaller SnO_2 particles (facilitated by solution-phase annealing), and the micrograph in (f) shows Au nanoparticles that were isolated without a SnO_2 coating by using low speed centrifugation.

20 nm. The SAED pattern (Figure 4.4d) shows an fcc pattern that is consistent with that expected for Au, and also agrees with the XRD data shown in Figure 4.3b. However, a significant amount of diffuse contrast surrounding the Au nanoparticles implies that other smaller nanoparticles are present in the solid product. Qualitative EDS analysis shows that both Au and Sn are present, consistent with the electron microprobe data. Elemental mapping of the TEM micrograph in Figure 4.4a shows that Au is only present in the high-contrast regions (Figure 4.4b), while Sn is also present in the regions of diffuse contrast that surround the Au particles (Figure 4.4c). This indicates that the Au nanoparticles are loosely surrounded by smaller Sn-containing nanoparticles.

Interestingly, if the TEG solution containing Au^{3+}, Sn^{2+}, and Cu^{2+} is *not* heated, it also turns purple over a short period of time (Figure 4.5). The same color change occurs when no Cu is present. Considering the standard reduction potentials of Au^{3+}/Au [E^o = 1.498 eV *vs*. standard hydrogen electrode (SHE)] and Sn^{4+}/Sn^{2+} (E^o = 0.151 eV *vs*. SHE), we hypothesize that a spontaneous galvanic reaction occurs, in which Au^{3+} is reduced to Au^0 as Sn^{2+} is oxidized to Sn^{4+}, precipitated as SnO_2 (since the reaction is not performed under rigorously air-free conditions).

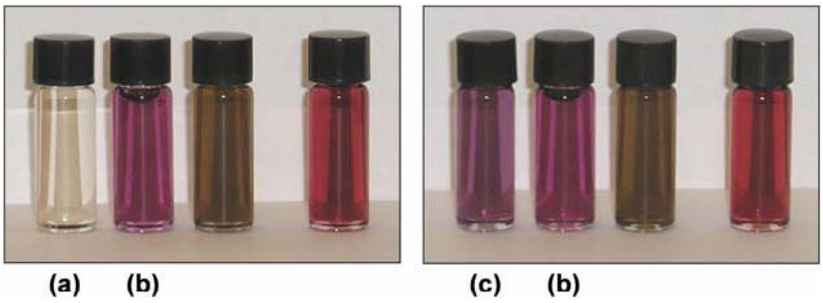

Figure 4.5 Left: the dissolved metal salt solution (a) has a clear pale yellow color, and once this solution is heated to 70 °C, it develops a purple color (b). (The photograph on the left, shown for comparison to the one on the right, is the same as the one shown in the inset to Figure 4.3.) Right: shown in (c), after 15 minutes at room temperature without heating, the metal salt solution that was shown in (a) develops the same purple color as (b) [e.g. compare (a), which is immediately after the metal salts are dissolved in TEG, and (c), the metal salt solution after reacting at room temperature for 15 min, to (b), which is the Au-Cu-Sn solution heated to 70 ºC]. This is thought to be the same galvanic reaction, albeit somewhat slower, that occurs upon heating the solution. Au and SnO_2 nanoparticles form from this reaction.

Furthermore, a higher-magnification TEM image confirms the presence of 2-3 nm SnO_2 particles (Figure 4.6). Apparently, Au and SnO_2 nanoparticles are mixed in solution, and they form a nanoscale composite when the solution is dropped onto a TEM grid (Figure 4.4a). Importantly, when this solid composite product is annealed under Ar at 300 ºC, the XRD pattern matches that of intermetallic AuSn (Figure 4.3b), which is further evidence that the Au and Sn are mixed in a 1:1 ratio in the solid product and in solution. We speculate that the SnO_2 remains unreactive and does not participate in the subsequent steps. However, its presence (the result of a galvanic reaction between Sn^{2+} and Au^{3+}) is the result of a critical reaction that helps to reduce the Au^{3+} to Au^0 at a much lower temperature than would normally occur in a standard polyol reaction.

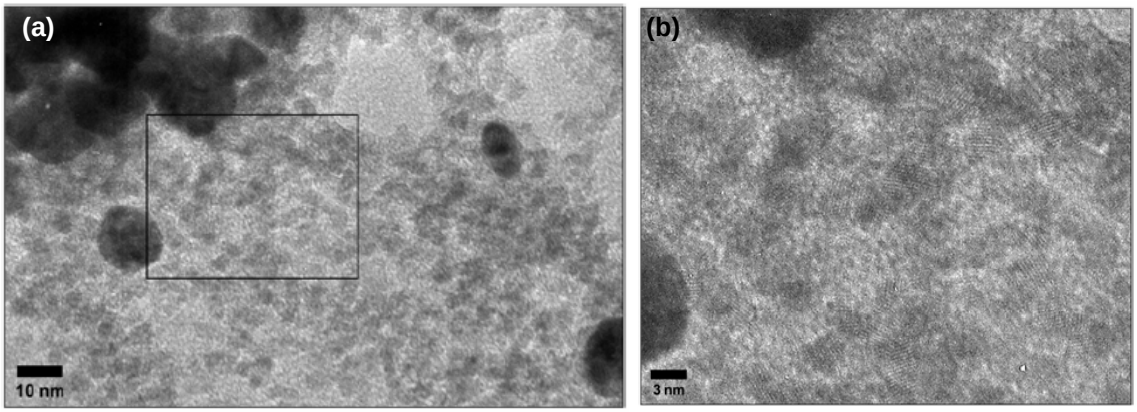

Figure 4.6 High-resolution TEM micrographs (close-up of the same sample shown in Figure 4.4a of the manuscript) for the Au-Cu-Sn reaction solution heated to 70 °C, showing the presence of Au (large high-contrast) and SnO_2 (smaller medium-contrast) nanoparticles. The bottom micrograph is an enlargement from above, showing the SnO_2 nanoparticles.

Furthermore, the fact that Au and SnO_2 nanoparticles can be generated at room temperature implies that the polyol solvent is not the reducing agent. Rather, this further supports the hypothesis that a galvanic reaction is responsible for the formation of Au nanoparticle seeds.

Returning to the UV-Visible spectroscopy data shown in Figure 4.3a, the red shift in the SPR peak for the Au-Cu-Sn sample relative to that of the Au sample, making the Au-Cu-Sn solution purple instead of red, can be explained by the nanostructure of the sample. The Au nanoparticles are surrounded by smaller SnO_2 nanoparticles in a pseudo core-shell composite arrangement. Mulvaney and co-workers have studied this in detail, observing a red shift of the SPR band as Au nanoparticles are coated by a SnO_2 shell; the shift in the SPR peak is related to the thickness of the SnO_2 coating.[95] In their system, the SnO_2@Au nanoparticle solution is purple instead of red,[95] which matches

what we observe. Indeed, after solution-phase annealing of our SnO_2/Au nanoparticle mixture, core-shell SnO_2@Au aggregates are clearly observed (Figure 4.4e). However, if a low centrifugation speed is used prior to annealing, the constituent Au nanoparticles can be removed without the SnO_2 coating (Figure 4.4f), implying that the core-shell structure is dynamic in solution rather than fully passivating the surface. Furthermore, at the intermediate centrifugation speeds typically used, the SnO_2 that is attached to the Au nanoparticles can be isolated along with the Au, but some remains in solution because of its small size. Thus, the amount of SnO_2 present in the centrifuged sample is less than the total amount of SnO_2 present in the system. While a complete galvanic reaction between Sn^{2+} and Au^{3+} would require 1.5 moles of Sn^{2+} for every mole of Au^{3+}, the centrifuged sample does not isolate all of the SnO_2. Consequently, the electron microprobe data that shows a 1.00:0.96 ratio of Au:Sn for the centrifuged sample is reasonable, based on this analysis.

Taken together, the UV-Vis, XRD, TEM, and electron microprobe data are consistent with the initial formation of Au nanoparticles via a galvanic reaction between Au^{3+} and Sn^{2+}, which ultimately forms SnO_2 nanoparticles. Also, the data imply that Cu is does not participate in the initial reaction.

4.3.2 *Step 2: Formation of AuSn Nanoparticles*

When the reaction solution turns purple (e.g. reaches 70 ºC or is allowed to react at room temperature), a solution of $NaBH_4$ is added dropwise and the Au-Cu-Sn solution immediately turns dark brown (Figure 4.3a), which implies reduction of other species in

solution. In control experiments, Cu^{2+} and Sn^{2+} can both be reduced to Cu^0 and Sn^0 nanoparticles, respectively, under these conditions (70 ºC in TEG upon addition of $NaBH_4$). The powder XRD pattern of the precipitate from this reaction, isolated by centrifugation, shows exclusively the formation of intermetallic NiAs-type AuSn (Figure 4.7a). Indeed, electron microprobe analysis of the centrifuged product finds a Au:Sn:Cu ratio of 1.00 : 1.32 : 0.15, which is consistent with the presence of nanocrystalline AuSn, some of the SnO_2 generated in the first step (specifically, the approximate fraction of the total SnO_2 that is incorporated into a core-shell structure as described below), and very little Cu or extra Sn. Indeed, after centrifuging all of the solid products, the supernatant retains a brown color, which is consistent with the presence of small nanoparticles of Cu and Sn that remain in solution. No well-defined SPR band is observed by UV-Visible spectroscopy, but this is not unexpected, since Cu nanoparticles smaller than 4 nm do not show a distinct SPR peak[96] and the SPR band for Sn nanoparticles is primarily in the UV.[97] Taken together, these data imply that the Cu remains in solution and does not appreciably incorporate into the AuSn product, and that reduced Sn nanoparticles are also present in solution.

TEM micrographs of the AuSn nanoparticles are shown in Figure 4.7c. The nanoparticles, which are mostly ~ 20 nm but range in size from 5 to 40 nm, are generally single-crystal AuSn and have a clearly defined core-shell structure (Figure 4.7d) that results from solution-phase annealing of the SnO_2 nanoparticles onto the AuSn surface. (Our previous work with the $FeSn_2$ system showed analogous SnO_2 shells on most Sn-based nanoparticles synthesized using a similar polyol-based approach.[40,76]) SAED

(Figure 4.7b) shows the hexagonal NiAs structure expected for the AuSn core. Furthermore, XPS analysis (not shown) shows the presence of primarily oxidized Sn on the surface with very little signal from Au or Cu, consistent with a thin coating of SnO_2 on the majority of the particles. Based on these data, we propose that the core is intermetallic AuSn and the shell is amorphous SnO_2.

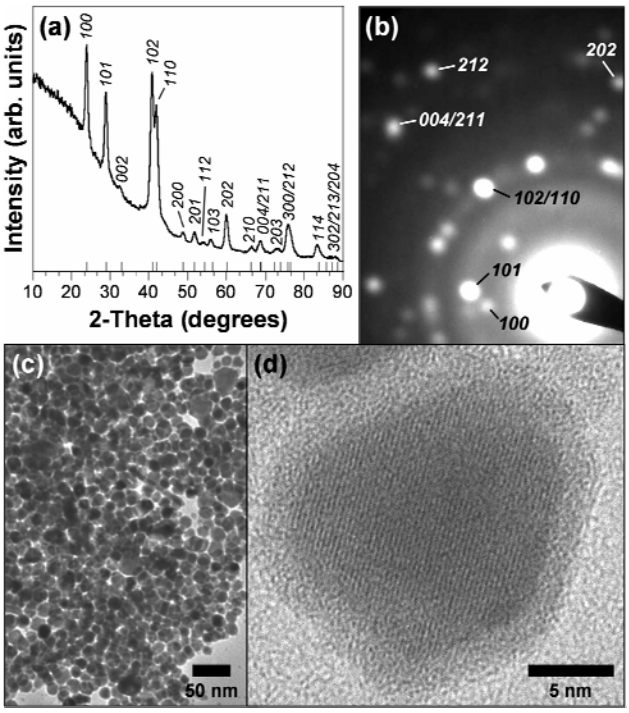

Figure 4.7 (a) Powder XRD and (b) SAED pattern of the solid product isolated after heating to 70 °C and reducing by $NaBH_4$. Tick marks below the XRD pattern in (a) represent the allowed Bragg reflections for NiAs-type AuSn. The TEM micrograph in (c) shows the morphology of the AuSn nanocrystals, and panel (d) shows a representative single AuSn nanocrystal, which has a single-crystal core and a 1 – 2 nm SnO_2 shell.

This step in the reaction pathway is surprising but important, and it is significant for several reasons. First, intermetallic AuSn forms very quickly at 70 ºC, which is a

lower temperature than is required to crystallize most other related intermetallics we have synthesized using similar methods.[50,75,76] Second, the fact that Au forms first and then converts to AuSn when $NaBH_4$ is added implies that the Au nanoparticles are highly reactive with the reduced Sn, and that the presence of Au seeds may catalyze the nucleation of intermetallic AuSn. Finally, AuSn crystallizes in the NiAs structure, which is the structure from which ordered $AuCuSn_2$ is derived. The NiAs-type AuSn intermediate may provide a structural template for the formation of ordered $AuCuSn_2$. Taken together, the data presented above are consistent with the formation of a core-shell SnO_2@AuSn intermediate with small Cu and Sn nanoparticles present in solution.

4.3.3 *Step 3: Interdiffusion to Form an $AuCu_xSn_y$ Alloy*

At this point in the reaction (at 70 ºC and after $NaBH_4$ is added), the solution appears to contain a mixture of SnO_2@AuSn, Cu, and Sn nanoparticles. As a control experiment, we confirmed that SnO_2 nanoparticles dispersed in TEG with $NaBH_4$ do *not* convert to Sn^0 at temperatures up to 300 ºC. Thus, we conclude that the SnO_2 nanoparticles do not react or incorporate into the product, so they remain inert in solution. The remainder of the Sn necessary to convert AuSn into $AuCuSn_2$ comes from the Sn^{2+} that is reduced to Sn^0 by $NaBH_4$. This conclusion is also consistent with the large 4-fold excess of Sn^{2+} that is used to form $AuCuSn_2$. Per mole of $AuCuSn_2$, 1.5 moles of Sn are required to reduce all of the Au^{3+} to Au^0, concomitantly oxidizing Sn^{2+} to Sn^{4+}. An additional mole of Sn is required to reduce and react with the Au nanoparticles to form AuSn. Another mole of Sn (along with one mole of Cu) is

required to form $AuCuSn_2$ from AuSn. Thus, 3.5 moles of Sn are required based on our proposed mechanism, and 4.0 moles are routinely used. Experimentally, we found that $AuCuSn_2$ will not form with less than 3.6 moles of Sn, which agrees well with the proposed mechanism and the amount of Sn it requires.

As heating continues in the presence of reduced Sn and Cu, the particles continue to interact and react, which is similar to the reaction of Au with Sn to form AuSn. The result is the evolving formation of $AuCu_xSn_y$ alloy nanoparticles, which have variable composition that changes with time (Figure 4.8) and temperature (Figure 4.9a) as the reaction progresses. Continual incorporation of Sn and Cu into the alloy nanoparticles is likely facilitated by the enhanced diffusivity and reactivity inherent in nanoparticle

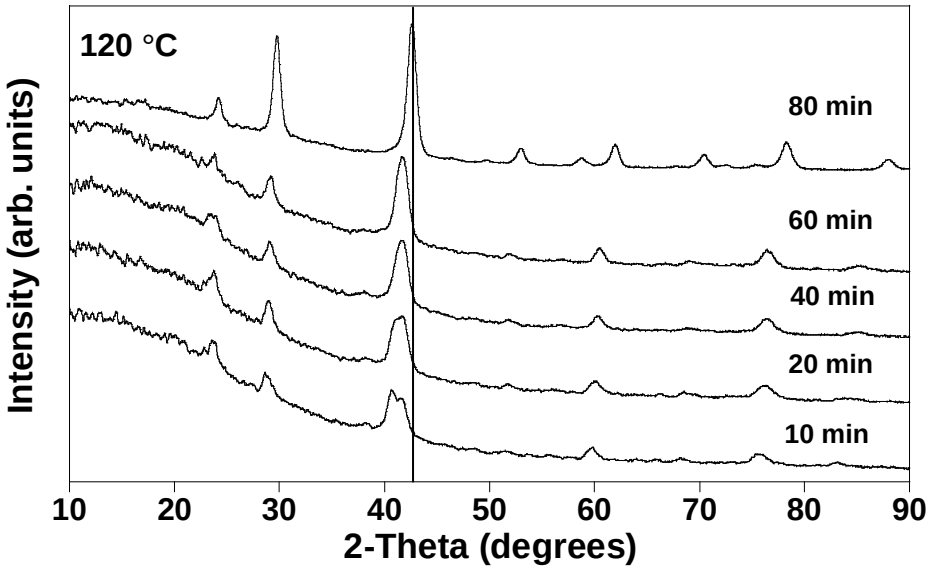

Figure 4.8 Powder XRD data for $AuCu_xSn_y$ nanoparticles heated to 120 °C, then held there for various lengths of time. After 80 min of heating at 120 °C, the characteristic superlattice peaks of ordered $AuCuSn_2$ can be seen. Time-dependent interdiffusion is also evident from the peak shifting.

systems.[98] The thermal interdiffusion of Cu and Sn into AuSn can be monitored using powder XRD of the solid products that are isolated from aliquots taken at different temperatures (Figure 4.9a). At 130 °C, the lattice constants are a = 4.29 Å and c = 5.34 Å, and the unit cell becomes progressively smaller as the temperature is increased to 160 °C (a = 4.24 Å, c = 5.25 Å) and 190 °C (a = 4.23 Å, c = 5.23 Å). This is consistent with the diffusion of Cu into the structure, since Cu is smaller than both Au and Sn. (It is worth noting that the lattice constants of the $AuCu_xSn_y$ alloy at 190 °C agree with those of ordered $AuCuSn_2$, implying that diffusion is nearly complete by this point and that the composition is close to $AuCuSn_2$.)

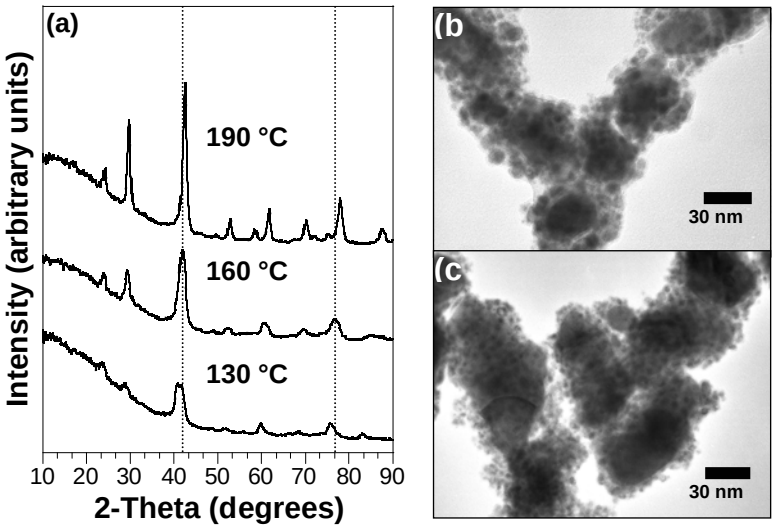

Figure 4.9 (a) Powder XRD patterns for the products isolated as a function of increasing temperature. The progressive shift of the lattice constants highlights the diffusion of Cu and Sn into the AuSn nanoparticles. TEM micrographs of the aliquots taken at (b) 85 °C and (c) 120 °C show larger AuSn particles that are surrounded by smaller particles, which are likely Cu, Sn, and Cu_xSn_y.

TEM micrographs of the Au-Cu-Sn particles in the 85 – 120 ºC range show larger 30 – 40 nm particles surrounded by smaller particles that are typically 5 – 10 nm in diameter (Figure 4.9b,c). EDS mapping confirms that Au, Cu, and Sn are present in the clusters of particles (Figure 4.10). Thus, based on the available data, we hypothesize that the smaller particles on the periphery of the larger ones are Cu, Sn, or Cu-Sn alloys, and that they continually interdiffuse and incorporate into the larger particles as a function of time and temperature, consistent with the available data.

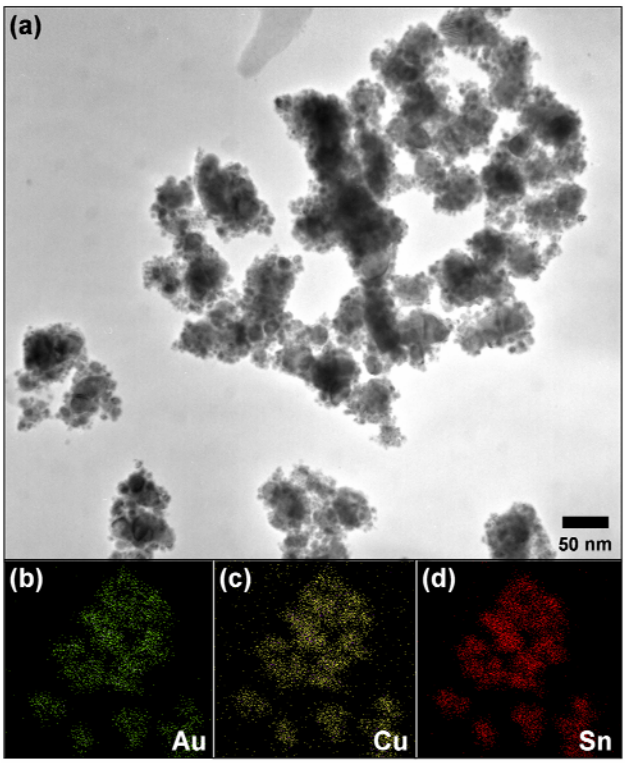

Figure 4.10 (a) TEM micrograph of the product isolated at 85°C, and semi-STEM elemental mapping data that shows the presence of (b) Au, (c) Cu, and (d) Sn in each of the aggregates.

4.3.4 *Step 4: Formation of Intermetallic $AuCuSn_2$*

As the solution continues heating, diffusion continues until the stoichiometry reaches $AuCuSn_2$, and the ordered ternary structure forms. The XRD pattern in Figure 4.11a shows the characteristic superlattice peaks of the ordered $AuCuSn_2$ structure, which appear above 190 ºC. Ordered $AuCuSn_2$ can also be accessed at temperatures as low as 120 ºC, if the solution is heated at this temperature for at least 1 h (Figure 4.8). Importantly, the $AuCuSn_2$ nanocrystals have a core-shell structure (Figure 4.11b), which implies that the SnO_2 coating does indeed persist throughout the reaction, as shown schematically in Figure 4.2.

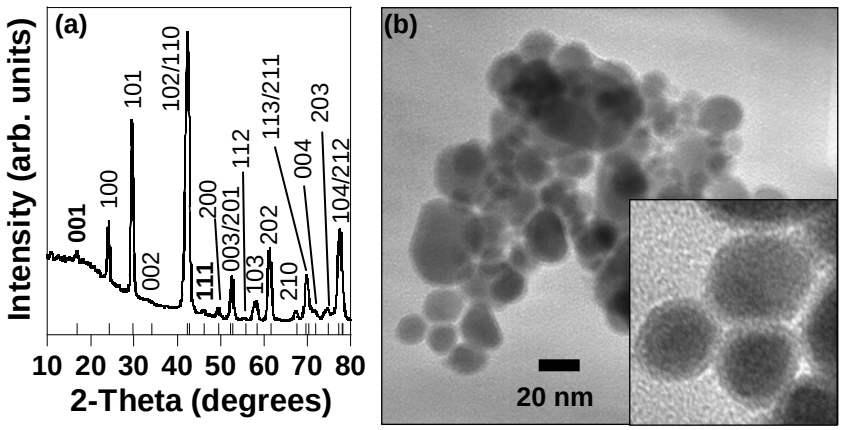

Figure 4.11 (a) Powder XRD pattern of intermetallic $AuCuSn_2$ isolated at 190 °C. Tick marks below the pattern show the positions of the allowed Bragg reflections, and the reflections in boldface type highlight the most prominent superlattice peaks of $AuCuSn_2$ (see ref. 50 for details). A TEM micrograph of the $AuCuSn_2$ powder isolated at 190 °C is shown in (b). The inset in (b) reveals that the core-shell structure is still present on the final product.

4.4 Testing and Confirming the Reaction Pathway

The results above, characterizing each of the steps involved in the formation of ordered $AuCuSn_2$ nanocrystals, provide compelling evidence that $AuCuSn_2$ forms by (a) nucleating Au nanoparticles from Au^{3+} via a galvanic reaction with Sn^{2+}, (b) reacting the Au nanoparticles with Sn to form intermetallic AuSn nanocrystals, (c) incorporating the additional Sn and Cu into the AuSn nanocrystals via solution-mediated interdiffusion, and (d) nucleation of the ordered $AuCuSn_2$ structure when the 1:1:2 stoichiometry has been reached. If this is indeed the correct reaction pathway, it should be possible to begin the reaction at any of the intermediate steps, and drive the reaction to completion, e.g. formation of ordered $AuCuSn_2$. Accordingly, Figure 4.12 shows that ordered $AuCuSn_2$ can be formed by first synthesizing AuSn nanocrystals (in the presence of excess Sn as discussed earlier), then thermally reacting them in solution with Cu nanoparticles that are formed ex-situ.

In this alternate scenario, $HAuCl_4$ and $SnCl_2$ are dissolved in TEG with PVP as a surface stabilizing agent. This solution is heated to 70 ºC to form a purple solution similar to that formed when all three metal salts were present. As expected from the reaction pathway, the XRD pattern for the solid product isolated from this solution by centrifugation matches that of nanocrystalline Au. Furthermore, TEM micrographs show a mixture of Au and SnO_2 nanoparticles that look similar to the product isolated from the original three-component system (Figure 4.13).

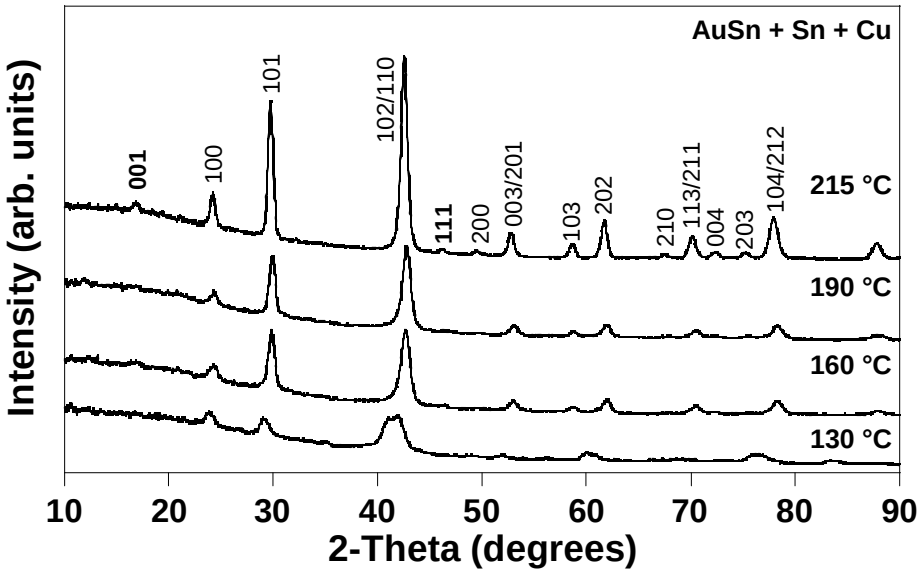

Figure 4.12 Powder XRD patterns for the products isolated from the reaction of a physical mixture of AuSn (along with excess Sn) with a solution of Cu nanoparticles that were formed ex-situ. The patterns show temperature-dependent changes in lattice constants that are similar to those seen in the original reaction that began with all of the metal salts in solution. Intermetallic $AuCuSn_2$ is formed by 215 °C, and the reflections in boldface type highlight the most prominent superlattice peaks of $AuCuSn_2$.

This unambiguously establishes that Cu is not implicated in the first step of the reaction. When $NaBH_4$ is added, AuSn nanoparticles are formed, again without any Cu present in the solution. In a separate vial, a solution of $Cu(C_2H_3O_2)$ and PVP in TEG are reduced with $NaBH_4$, forming a brown solution of Cu nanoparticles. This solution is then added to the solution of AuSn nanoparticles (containing excess Sn) and heated to 215 ºC. Both the XRD pattern (Figure 4.12) and the SAED pattern (Figure 4.13a) for the product of this reaction match that of the ordered ternary $AuCuSn_2$ structure, which forms after the Cu nanoparticles react with the AuSn nanoparticles. Furthermore, the progression of XRD patterns from 130 – 215 °C in Figure 4.12 shows the same evidence for interdiffusion (e.g. progressive evolution of the lattice constants) as the original sample.

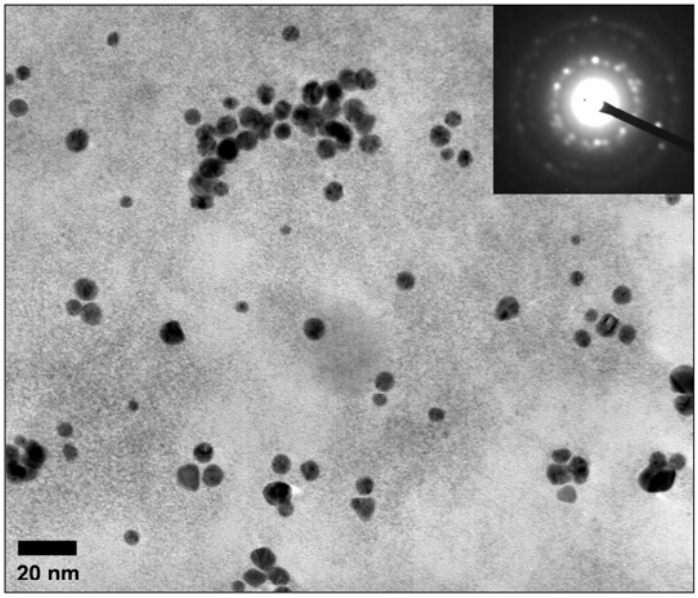

Figure 4.13 TEM micrograph of the purple-colored solution formed from a TEG solution of Au^{3+} and Sn^{2+} without any Cu present. The image shows that both Au and SnO_2 nanoparticles are present, which is similar to the images taken of the reaction solution which contained Cu as a starting material. The inset shows a fcc SAED pattern, which matches that expected for Au.

Finally, the $AuCuSn_2$ nanoparticles made by this method also contain a SnO_2 shell, consistent with the proposed reaction pathway (Figure 4.14). Taken together, these results prove that $AuCuSn_2$ can be made directly from a physical mixture of AuSn and Cu nanoparticles (in the presence of excess Sn), and provide compelling evidence that the reaction pathway described in Figure 4.2 is reliable.

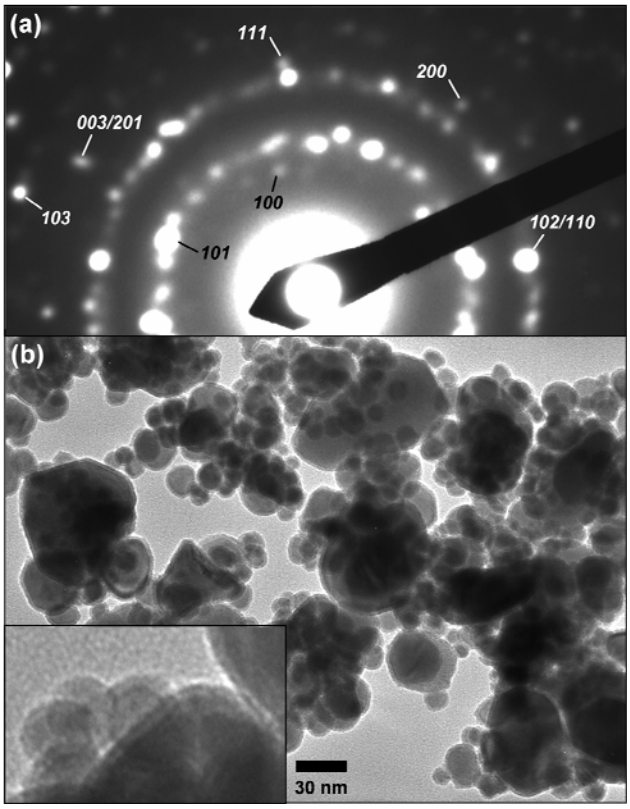

Figure 4.14 (a) SAED pattern and (b) TEM micrograph of the intermetallic $AuCuSn_2$ powder isolated at 215°C from the reaction of AuSn with Sn and Cu.

4.5 Applicability to Other Systems

While our proposed multi-step reaction pathway is clearly applicable to the formation of $AuCuSn_2$, it is important to consider its generality for other systems. As a first step toward this goal, we studied the formation of $AuNiSn_2$. While $AuNiSn_2$ is structurally identical to $AuCuSn_2$,[50] the synthesis, stability, and reactivity of metal nanoparticles can often be different for each element,[99] so it is worthwhile to compare the Ni and Cu systems. Like $AuCuSn_2$, ordered $AuNiSn_2$ appears to only form from a careful multi-step reaction sequence that is analogous to the one shown in Figure 4.2.

After dissolving appropriate amounts of $HAuCl_4 \cdot 3H_2O$, $Ni(C_2H_3O_2) \cdot xH_2O$, and $SnCl_2$ in TEG, the color of the solution changes from yellow to red-brown as the temperature is increased to 85 °C. Powder XRD data for the solid product isolated from this reaction shows the presence of nanocrystalline Au (Figure 4.15), consistent with the first step of the mechanism required to form $AuCuSn_2$. After adding $NaBH_4$, the color changes to black, and the XRD pattern is consistent with that expected for AuSn, although the particles are significantly smaller than those observed for the $AuCuSn_2$ system. As the temperature is further increased, the XRD peaks sharpen and shift systematically with temperature (Figure 4.15), suggesting diffusion to form disordered $AuNi_xSn_y$ nanoparticles. Finally, by 210 °C, the characteristic superlattice peaks are clearly evident (Figure 4.15), indicating the formation of ordered $AuNiSn_2$.

The isolation of intermediates that are similar to those obtained for the $AuCuSn_2$ system imply that the reaction pathway of $AuNiSn_2$ is also similar, which gives an indication of its generality to other new, yet related, systems. We are currently in the process of testing this reaction pathway with other systems, and preliminary evidence suggests that it will indeed result in the formation of new nanocrystalline alloys and intermetallic compounds, including in systems that are structurally and compositionally distinct from the $AuMSn_2$ phases. Thus, we reasonably anticipate that this reaction pathway will be applicable to other systems. However, even if this particular reaction pathway turns out not to be overly general, it still provides important new insights into how nanoparticles combine in solution, in a controllable manner, to form derivative compounds with more complex structures and compositions. As such, it provides guide-

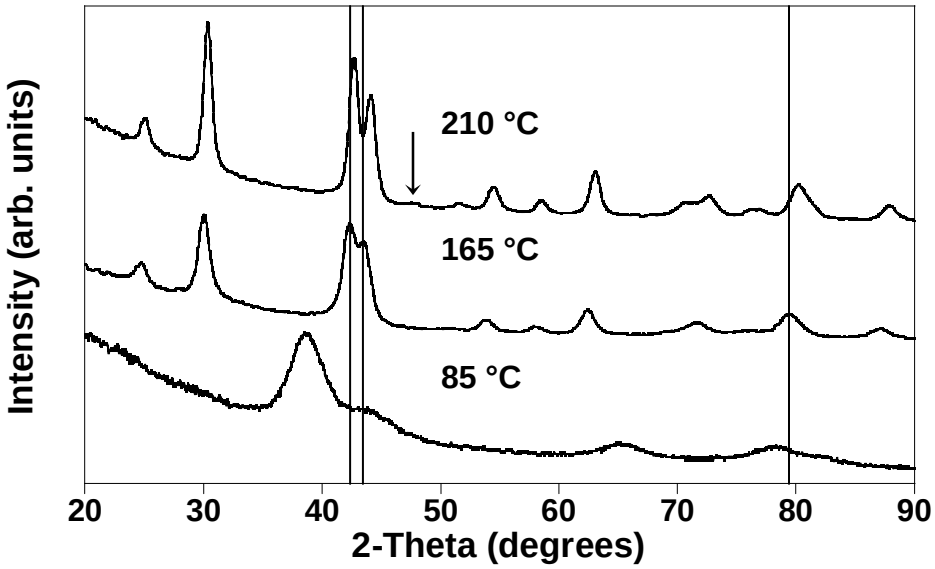

Figure 4.15 Powder XRD patterns for the products isolated as a function of increasing temperature for the Au-Ni-Sn system. The bottom pattern shows Au nanoparticles isolated at 85° C, the middle pattern shows $AuNi_xSn_y$ isolated at 165° C, and the top pattern shows ordered $AuNiSn_2$ isolated at 210° C (the arrow highlights one of the key superlattice peaks). The dashed lines highlight the peak shifting that occurs with heating, indicative of interdiffusion.

lines for systematically modifying the structures and compositions, and thus the properties, of nanocrystalline intermetallic compounds.

4.6 Summary

In this chapter, we identified and tested a plausible multi-step reaction pathway that results in the formation of a new ternary intermetallic compound, $AuCuSn_2$, as nanocrystalline particles. Our experiments identified four key reaction steps: (a) formation of a mixture of Au and SnO_2 nanoparticles mediated by a spontaneous galvanic reaction between Au^{3+} and Sn^{2+}, (b) formation of SnO_2-coated AuSn nanoparticles, along with small particles of Cu and Sn, upon $NaBH_4$ reduction, (c)

temperature-controlled interdiffusion to form $AuCu_xSn_y$ nanoparticles, and (d) nucleation of the ordered ternary structure of $AuCuSn_2$, which retains a coating of SnO_2. Consistent with this mechanism, $AuCuSn_2$ can also be formed by starting with the AuSn intermediate and reacting it with Cu and Sn.

Elucidation of the reaction pathway that is required to form $AuCuSn_2$ has several important implications. First, it provides a rare look at the steps involved in the formation of a new solid-state compound, and these mechanistic insights could provide valuable tools for the guided design of other new intermetallic solids. In particular, the formation of NiAs-type AuSn as an intermediate is important, and may help to template the formation of $AuCuSn_2$, which is an ordered variant of the NiAs structure. Second, it demonstrates a novel strategy for studying mechanistic details of solid-state phase formation at the nanometer scale by combining data from multiple complementary techniques, including microscopy, spectroscopy, and diffraction. While the approach and tools are quite different from those necessary to elucidate molecular reaction mechanisms, the result is analogous – a systematic piece-by-piece look at the interactions of small building blocks to form a larger structure – and has similar implications in terms of applying the mechanism to other systems. Third, the reaction pathway provides a strategy for fine-tuning the composition and structure of multi-metal nanocrystals in a more systematic and controllable manner than is routinely achievable using one-pot reactions. Indeed, the ability to react metal and intermetallic nanoparticles in solution to form derivative phases could open up new doors for the guided design of compositionally and structurally complex nanocrystals, and preliminary evidence with

other systems suggests that it can. Fourth, there are several strategies for controlling the shape and size of single-metal nanocrystals,[37-39,93,100] but analogous achievements for multi-metal systems remain rare. Since the formation of $AuCuSn_2$ begins with the nucleation of Au nanoparticles, it may be possible to control nanocrystal size and shape of this ternary intermetallic (or other complex phases) by starting with pre-made Au nanocrystals that have the appropriate morphological characteristics.

Finally, this study effectively merges what were thought to be two distinct strategies for synthesizing alloys and intermetallic compounds using low-temperature "metallurgy in a beaker" techniques. In one approach, metal nanoparticles are mixed in known ratios in solution to form nanocomposites, which precipitate and are heated as dry powders to form alloys and intermetallics of pre-determined compositions.[8,9] In this case, the rapid low-temperature reactivity is attributed to the nanoscale diffusion distances afforded by the self-assembled precursors that form in solution, which mimic the mixing achieved by the high temperature melting step usually required in traditional metallurgical synthesis. In the other approach, alloy and intermetallic nanocrystals are formed using modifications of the polyol process, which traditionally uses the polyol solvent as the reducing agent, but in some cases can also utilize stronger reducing agents (e.g. $NaBH_4$).[50,75,76] The multi-step reaction pathway presented here provides compelling evidence that a nanocomposite forms in solution and transforms into alloy and intermetallic nanocrystals via solution-mediated reactions. Essentially, the two approaches are the same – both involve the formation and interdiffusion of nanoscale composites of two or more distinct phases. The approaches appear to differ only in the

method used to interdiffuse the components, e.g. dry powder processing *vs*. solution annealing. A similar mechanism may be implicated in the formation of other multi-metal nanocrystals formed by reacting metal salt precursors in high-boiling solvents, and may turn out to be general for the formation of many multi-metal nanocrystals using low-temperature solution routes.

CHAPTER V

TOWARD ORTHOGONAL CHEMISTRY FOR THE SELECTIVE AND STEPWISE MODIFICATION OF NANO-CRYSTALLINE METALS: ONE-POT MULTI-COMPONENT SYNTHESIS OF INTERMETALLIC NANOPARTICLES

5.1 Introduction

Inorganic nanocrystals comprise a chemically diverse class of dimensionally-confined materials that can have interesting size dependent physical properties and applications that include catalysis, nanoelectronics, magnetic data storage, and thermoelectric refrigeration. The controlled synthesis of inorganic nanocrystals is an important pre-requisite to realizing these important applications. In particular, the development of reliable and materials-general strategies for synthesizing nanocrystals with simultaneously controlled compositions, crystal structures, sizes, and shapes is necessary for accessing, enhancing, and tuning the properties of these materials. Looking ahead toward future advances in the applications of nanoscale materials, it is clear that synthetic methods must support spatial organization of chemically disparate nanoscale components and also be compatible with diverse classes of solids for optimal flexibility of design. For example, multi-segment nanowires with pre-designed arrangements of multiple metal components can have important magnetic[101] and optical properties[102], as well as bioanalytical capabilities[102,103] and the ability to undergo chemically and magnetically induced motion[104]. Likewise, periodic and aperiodic nanocomposites of two or more functionally distinct types of nanocrystals can produce metamaterials with

collective properties that differ from those anticipated based on a linear addition of their components as demonstrated for exchange-coupled magnets and nanoscale catalytic systems[105].

To date, most of the multi-component materials that have been made in a controlled manner primarily include only a handful of relatively simple metal, oxide, and chalcogenide components (e.g. Au, Ag, Pt, CdS, PbS, ZnO, and Fe_xO_y), although a few examples exist that use more complex building blocks[106]. More advanced applications will require access to a larger repertoire of more complex solids that require simultaneous synthetic control over elemental composition, stoichiometry, size, and shape. For example, some of the most common and simple devices used today involve materials far more complex than those that have been synthetically mastered at the nanoscale, including magnetoresistive elements (CoFeB, CoFeZr, PtMn), superconducting sensors (Nb, Pb_9Au, Pb_9In, $YBa_2Cu_3O_7$), and permanent magnets ($Nd_2Fe_{14}B$, $SmCo_5$, Gd). Robust methods appropriate for the on-demand and by-design synthesis of elaborate multi-component nanoscale systems need to be developed to meet the above-mentioned stringent challenges while being materials general, so that when a particular spatial combination of nanoscale materials is needed, it can be generated quickly using reliable and proven methods.

While challenging for nanoscale solid-state systems, meeting such requirements is straightforward for molecular systems. For example, designing and synthesizing a tripeptide with any desired sequences of amino acids is almost trivial. In contrast, designing the nanoscale equivalent – a three segment nanorod incorporating components

outside of the dozen or so metals routinely incorporated – can be a daunting challenge, with few exceptions. One can assemble molecules into almost countless arrangements, including derivative molecules, macromolecules, natural products, and polymers, using well-established and ever-growing libraries of chemical transformations. To accomplish this, one part of a multi-functional molecule can be modified using chemical reactions that are selective to that functionality in the presence of others, for example a ketone can be protected by formation of a hemiacetal while an ester group on the same molecule is reduced to an alcohol. The basis for this is orthogonal reactivity – the idea that different functionalities react differently (e.g. one reacts and the others do not) under the same conditions, and different conditions are required for all components to react. Put another way, in a one pot reaction, conditions can be found to selectively react one component of a molecule while leaving the others untouched, then go back and react another component.

The ability to perform similar orthogonal reactions on nanoscale solid-state systems would be powerful. For example, it is straightforward to synthesize a variety of three segment metal nanowires (eg. Au-Ag-Au). However, general methods for synthesizing three segment nanowires that incorporate multi-element components (e.g. intermetallics, phosphides, oxides, etc.) are not yet established. Such nanostructures remain challenging targets that must be approached on a case by case basis. Other classes of heterostructured nanoscale materials, including nanoparticle dimers and trimers, capped nanorods, and core-shell nanocrystals, are also limited in the complexity of solids that can be incorporated into them. It is therefore desirable to develop robust

synthetic strategies that bridge the gap between current synthetic capabilities that are mature, e.g. those used to make nanostructures of noble metals, and those that are extremely challenging, e.g. similar capabilities for intermetallics and other multi-element nanoscale solids.

Toward that goal, we describe here a first step toward applying the idea of orthogonal reactivity to metal nanoparticle systems. The concept exploits the idea of "conversion chemistry" that is being developed by several groups for the chemical transformation of one type of nanoparticle into another. For example, shape-controlled single-metal nanoparticles that are straightforward to synthesize can be converted into derivative nanoparticles of metal sulfides,[107] metal oxides,[108] metal phosphides,[109] and intermetallic compounds,[40] often with the ability of the final multi-element product to retain the shape defined by the single-metal nanoparticle template. Notable examples of this include the conversion of spherical cobalt nanocrystals to hollow spherical Co_3S_4 nanocrystals by reaction with sulfur,[107] the conversion of Se nanowires to Ag_2Se nanowires by reaction with $AgNO_3$,[110] the reversible conversion of CdSe nanocrystals and tetrapods to Ag_2Se by cation exchange reaction,[98] the conversion of spherical Ni nanoparticles to hollow spherical Ni_2P by reaction with trioctylphosphine (TOP),[109] the conversion of β – Sn nanocubes to hollow cube-derived nanostructures of $FeSn_2$ by the reaction of $FeCl_3$ under reducing conditions,[40] and the conversion of various intermetallic nanocrystals into derivative intermetallics[14,51] and oxides.[111]

To accomplish these chemical transformations of nanoparticles, appropriate conditions must be found to facilitate the reactions. In some cases, reactions can occur at

room temperature, e.g. the reaction of cobalt with sulfur to form Co_3S_4.[107] In other cases, higher temperatures (>350 °C) are needed, e.g. the reaction of cobalt nanoparticles with TOP to form CoP.[109] Other examples at intermediate temperatures are also known. When these synthetic conditions are collectively analyzed, it becomes evident that for a given metal, reactions occur with different reactants at different temperatures, but often under otherwise similar conditions (e.g. solvent, atmosphere, reaction time), as mentioned for the cobalt system above. Likewise, under identical reaction conditions, some metals will react with a reagent and others will not. For example, if Ni and Co nanoparticles are reacted with TOP at 300 °C, Ni will form Ni_2P, but Co will not react. Only after heating above 350 °C will the Co react to form CoP.[109]

These are simple examples of orthogonal reactivity, a metal nanoparticle analogy to orthogonal reactions used extensively in organic chemistry. If this idea could be expanded and generalized to many different types of metal systems and reagents, it would be possible to develop a robust toolbox of orthogonal chemical transformations for selectively converting one metal into a derivative compound in the presence of other metals and/or reagents. If such chemistry were then compatible with chemical transformations of segmented nanowires and heterostructured nanoparticles, truly selective orthogonal conversions could be carried out to generate exceptionally complex multi-component nanostructures in an on-demand and by-design manner. Since the products of many of these chemical transformations maintain the morphology of the metal nanoparticle precursors, often involving single-crystal transformations,[40] it is reasonable to anticipate the successful application of these ideas to heterostructured

nanoscale systems without destroying the morphology, providing that interfacial stability can be retained either directly or by incorporating adhesion layers between components.

In this chapter, we establish the concept of orthogonal chemistry for metal nanoparticle systems based on the idea of converting metal nanoparticle precursors into derivative multi-element intermetallics nanoparticles. We define the conditions under which an extensive library of chemical transformations occur and demonstrate that multiple reactions can be carried out in a one pot reaction, which is central to the idea of orthogonal reactivity. We demonstrate true orthogonal reactivity in a two component system by showing that Ni and Pt nanoparticles can react sequentially with Pb and Sb reagents in the same one-pot reaction to selectively form PtPb and NiSb without generating PtSb, NiPb, or other cross reaction products. Additionally, we explore orthogonal reactivity in a three component system, and begin to investigate these reactions on lithographically patterned surfaces with multiple metal features. Finally, we identify general guidelines for carrying out such reactions, and discuss limitations to the approach and possible strategies for overcoming them, including issues that must be addressed to apply such chemical transformations to heterostructuted nanomaterials. In addition to establishing and studying the concept of orthogonal reactivity in metal nanoparticle systems, we also report the formation of several intermetallic compounds that are accessible but have not been previously reported as polyol-derived nanocrystals (RhSb, RhBi, PbBi, PdSb, Pd_5Pb_3), further expanding the library of intermetallics accessible using low-temperature solution routes.

5.2 Experimental Details

5.2.1 *Materials*

The following metal reagents were used: Sulfur powder, Na_2PdCl_4, $RhCl_3$, $SnCl_2$ (anhydrous, 99% min.), $Cu(C_2H_3O_2)_2 \cdot H_2O$, $HAuCl_4 \cdot 3H_2O$ (99.99%), $AgNO_3$ (99.9+%), K_2PtCl_6 (40.11% Pt), $Ni(C_2H_3O_2)_2 \cdot xH_2O$ (99+%), $SbCl_3$ (99.9%), $Pb(C_2H_3O_2)_2 \cdot 3H_2O$, and $Bi(NO_3)_3 \cdot 5H_2O$ (Mallinckrodt Chemical Works). Sodium borohidride ($NaBH_4$) was used as a reducing agent. Poly(vinyl pyrrolidone) (PVP, MW = 40,000) was used as a surface stabilizer, and the solvent for all reactions was tetraethyleneglycol (TEG, 99+%). All chemicals were purchased from Alfa Aesar unless otherwise noted.

5.2.2 *Synthesis*

The single metal nanoparticles were prepared by a modified polyol process in which a metal salt and a surface stabilizer, PVP, were dissolved in TEG followed by heating and reduction with $NaBH_4$. For example, $Ni(C_2H_3O_2)_2 \cdot xH_2O$ (76.5 mg, 0.425 mmol) and PVP (252 mg) were dissolved in 30 mL of TEG by sonication, then the solution was stirred vigorously while bubbling argon through the solution for 30 min. The metal salt solution was then heated to 180 °C and reduced with a freshly prepared $NaBH_4$ solution (0.5 M, 2 ml). The reaction solution was maintained at this temperature for 10 minutes then cooled to room temperature.

The single metal nanoparticle precursors were individually reacted with a variety of metal salts and $NaBH_4$ followed by heating to determine at what temperature the binary intermetallic phase would form. For example, a freshly prepared solution of Ni

nanoparticles was stirred under bubbling argon for 30 min, then a solution of $SbCl_3$ (0.235 M) was added. This solution was stirred for 1-2 minutes then reduced with $NaBH_4$ (0.5 M, 2ml). The solution was then heated and aliquots were taken at several temperatures. The aliquots were then centrifuged and washed with ethanol and acetonitrile. The resulting powders were analyzed by powder XRD to determine the phase formation and the temperature at which each phase formed.

The binary and ternary orthogonal reactions were performed by mixing equal molar ratios of pre-formed metal nanoparticles and stirring the solution under bubbling argon for 30 minutes. A metal salt dissolved in TEG was added to the reaction solution and reduced with $NaBH_4$. The solution was then heated to the temperature determined by the test reactions to form the first intermetallic phase. A second metal salt was then added to the solution, reduced with $NaBH_4$, and heated to a second temperature to form the second intermetallic phase. In the case of the ternary precursor mixture, the process was repeated a third time. The nanocrystalline products were precipitated from solution by centrifugation and were washed with ethanol. Acetonitrile was also added to some reaction solutions to aid in precipitation of the nanocrystalline product.

5.2.3 *Characterization*

Powder X-ray diffraction (XRD) data were collected using Cu Kα radiation on a Bruker GADDS three-circle X-ray diffractometer and a Huber Guinier G670 Image Plate Camera with a Rigaku RU200H rotating anode X-ray generator. Transmission electron microscopy (TEM) images, selected area electron diffraction (SAED) patterns,

and energy-dispersive X-ray analysis (EDS) were collected using a JEOL JEM-2010 TEM. Samples were prepared by sonicating the nanocrystalline intermetallic powders in ethanol and dropping a small volume onto a carbon-coated nickel or copper grid. Scanning electron microscopy (SEM) images were obtained at 20 kV using a JOEL JSM-6400 SEM.

5.3 Results and Discussion

5.3.1 *Idea of Orthogonal Reactivity on Metal Nanoparticles*

We discovered that metal nanoparticles can be used as reactive precursors in the synthesis of binary intermetallic compounds and that the reaction conditions (temperature and concentration) play a crucial role in the formation of these intermetallic phases. To explore the reactivity of the metal nanoparticles, we prepared several solutions of single metal nanoparticles and began reacting them with metal salt solutions. After determining the conditions necessary for the formation of several intermetallic phases, we compiled a table of reaction conditions that allow the formation of binary intermetallics from single metal nanoparticles. With this library of binary phases available, we began to study orthogonal reactivity in systems with multiple metal nanoparticles. Initially we began mixing two different metal precursors (Ag and Ni) and reacted these with metal salts ($SbCl_3$ and $SnCl_2$) to produce two different binary intermetallics (Ag_4Sn, and NiSb). From there we went on to explore the reactivity of other binary and ternary mixed metal systems.

5.3.2 *Synthesis of Metal Nanoparticles*

The synthesis of each of the single metal starting materials was simplified to create particles with a general size range which aided in the resulting characterization of the nanocrystalline products. For the metal systems discussed here, shape and size were not rigorously controlled, but for future studies it should be possible to control the morphology of the precursor particles, and often the shape of the single metal nanoparticles will hold through the reaction giving shape controlled binary inter-metallics. For Ni, Pt, Cu, Rh, and Pd nanoparticles, the metal salt was dissolved in TEG by sonication and rapid stirring. The solution was then stirred under argon for 30 minutes to purge the solution of oxygen followed by heating to 100 - 190 °C to remove water from the solution and to ensure the metal salts were completely dissolved. $NaBH_4$ solution was then added dropwise to the stirring solution causing a distinct color change (usually black). The metal nanoparticle solution was then heated to the final temperature, which generally determined the size of the particles that formed. Reactions that were heated to higher temperatures typically resulted in larger particles and a greater degree of aggregation. Au nanoparticles were synthesized similar to the above mentioned metal nanoparticles except that the $NaBH_4$ was added at room temperature and the solution was heated to 100 °C for 15 minutes to allow for particle growth. Ag was synthesized by dissolving $AgNO_3$ and PVP in TEG followed by stirring under argon for 20 minutes to dissolve the reagents. Special care was taken to keep light out of the Ag solution as $AgNO_3$ is known to undergo photo-decomposition.[112] The Ag solution was then slowly heated to 150 °C and held there 10 minutes until the desired product was obtained.

Figure 5.1 shows the X-ray diffraction patterns of some representative single metal starting materials.

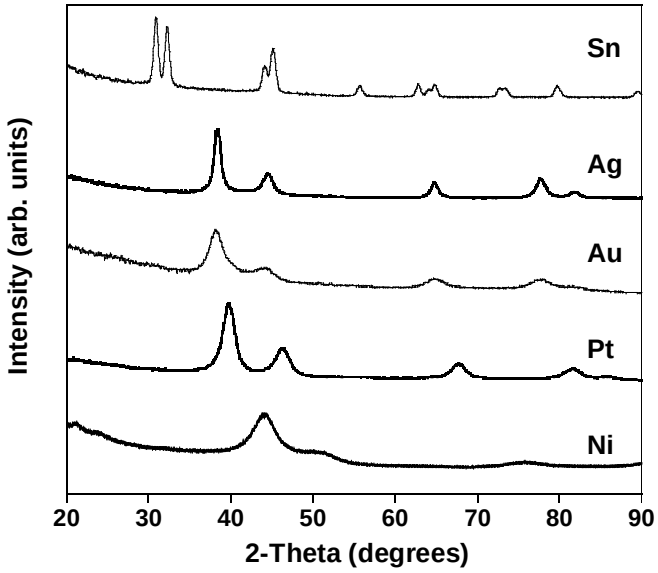

Figure 5.1 Powder XRD patterns for the single metal precursor particles as synthesized. Sn, Ag, Au, Pt, and Ni samples are shown as representative samples of the starting precursor nanoparticles.

5.3.3 *Building a Library of Chemical Transformations*

In order to build up a library of chemical transformations, each solution of metal nanoparticles was tested with a variety of metal salts to determine the reactivity of each system at different temperatures. The binary systems were chosen because of potential applications (Li-ion batteries, nanoelectronics) and physical properties (superconducting, semiconducting, catalytic activity and thermoelectric properties). For example, the Pt-M binary systems are known to be catalytically active and often show immunity toward CO poisoning.[6]

The test reactions were carried out using the as-made single metal nanoparticles and adding a stoichiometric amount of metal salt solution. The solution was then stirred under argon and reduced at room temperature, using a freshly prepared solution of $NaBH_4$. The solution was then heated and aliquots were taken at multiple temperatures to follow phase formation. The aliquots were then centrifuged and washed and the resulting powder was analyzed by powder XRD. Analyzing the powder diffraction patterns, we can determine the binary phase that forms and the lowest temperature at which it forms cleanly. Figure 5.2 shows the XRD data for Ni nanoparticles reacted with a $SnCl_2$ solution and heated. Upon reduction of the $SnCl_2$, an amorphous material is

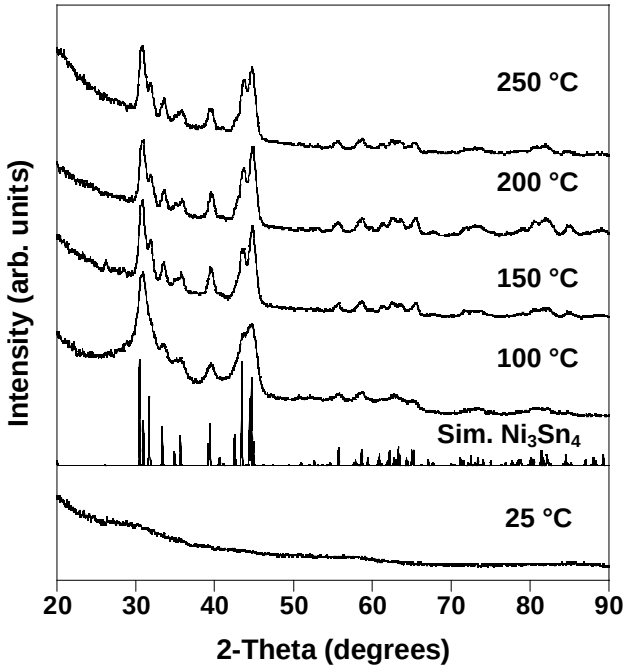

Figure 5.2 Powder XRD patterns for aliquots taken from the reaction of Ni nanoparticles reacted with $SnCl_2$. The Ni/$SnCl_2$ solution was reduced at room temperature and then heated to 250 °C. The simulated pattern below the 100 °C pattern shows the allowed reflections for Ni_3Sn_4.

formed, but after heating to only 100° C the binary phase Ni_3Sn_4 is observed and further heating enhances the crystallinity of the sample. Several metal ions were reacted in a similar way with each starting metal nanoparticle solution, and the results for these reactions are compiled into Table 5.1.

Table 5.1 Details for the Synthesis of Binary Intermetallics Using Metal Nanoparticle Precursors

Metal NP	$Bi(NO_3)_2$	$Pb(C_2H_3O_2)_2$	$SbCl_3$	$SnCl_2$	S
Ni	NiBi (220 °C)	N.R.[1]	NiSb (25 °C)	Ni_3Sn_4 (100 °C)	
Cu	N.R.	N.R.	CuSb (250 °C)	Cu_6Sn_5 (120 °C)	Cu_2S
Rh	RhBi (200 °C)	UNK.	RhSb (180 °C)	UNK.*	
Pd	β-PdBi (240 °C)	Pd_5Pb_3 (120 °C)	Pd_8Sb_3 (200 °C)	$PdSn_2$ (200 °C)	
Ag	N.R.	N.R.	N.R.	Ag_4Sn (175 °C)	Ag_2S (25 °C)
Pt	PtBi (230 °C)	PtPb (150 °C)	PtSb (200 °C)	PtSn (200 °C)	PtS_2
Au	N.R.	N.R.	N.R.	AuSn (25 °C)	N.R.[2]
Sn	N.R.	N.R.	SnSb (150 °C)	Sn	SnS

$NaBH_4$ solution was added after the metal salt solution for each of the reactions
[1] N.R. means no reaction was observed by powder X-ray diffraction for the precipitated powder
[2] Reactions between Au and S will block the surface of Au prohibiting further reactions but no Au-S phases form
* Reactions of Rh nanoparticles with $SnCl_2$ and $Pb(C_2H_3O_2)_2$ both produced mixed phase products that could not be identified

Table 5.1 shows the conditions necessary for synthesizing binary intermetallics from single metal nanoparticle precursors. The metal nanoparticle precursors were reacted with a metal salt solution in approximately 1:1 ratio. Most of the reactions listed are completed once the final temperature is reached (immediate reactions) with no annealing step required. The reactions with sulfur deviated from this procedure in that the reactions were carried out both at room temperature for various lengths of time, and

at elevated temperatures. Additionally, the reactions using $SnCl_2$ as a reagent typically do not react stoichiometrically and as a result either more $SnCl_2$ solution was required to obtain the 1:1 product or the product formed would be Sn deficient compared to the starting ratio.

In addition to determining the reaction conditions for the conversion of metal nanoparticles, we also explored Pd and Rh binary systems and report the formation of several intermetallic compounds (RhSb, RhBi, PbBi, PdSb, Pd_5Pb_3) that are accessible as polyol derived nanocrystals. These compounds are known in bulk systems but have not been previously reported as nanocrystals. This further expands the library of intermetallic phases accessible as nanocrystals and further emphasizes that the polyol technique is a quick and viable route to synthesize intermetallics as nanocrystals.

5.3.2 *Synthesis of Binary Intermetallics from a Two Component Mixture of Metal Nanoparticles*

Upon inspection of Table 5.1, it becomes apparent that multiple reactions are possible with the same metal salt by just changing the temperature of the reaction. For example, most of the metal nanoparticles tested will react with Sn but at quite different temperatures, i.e. Ni_3Sn_4 forms at 100 °C but Ag_4Sn will not form until 175 °C. Thus, using the temperature of phase formation, it should be possible to react one type of metal nanoparticle while leaving another metal in the same solution unreacted, i.e. orthogonal reactivity. Along those lines several systems starting with two different types of metal nanoparticles were tested.

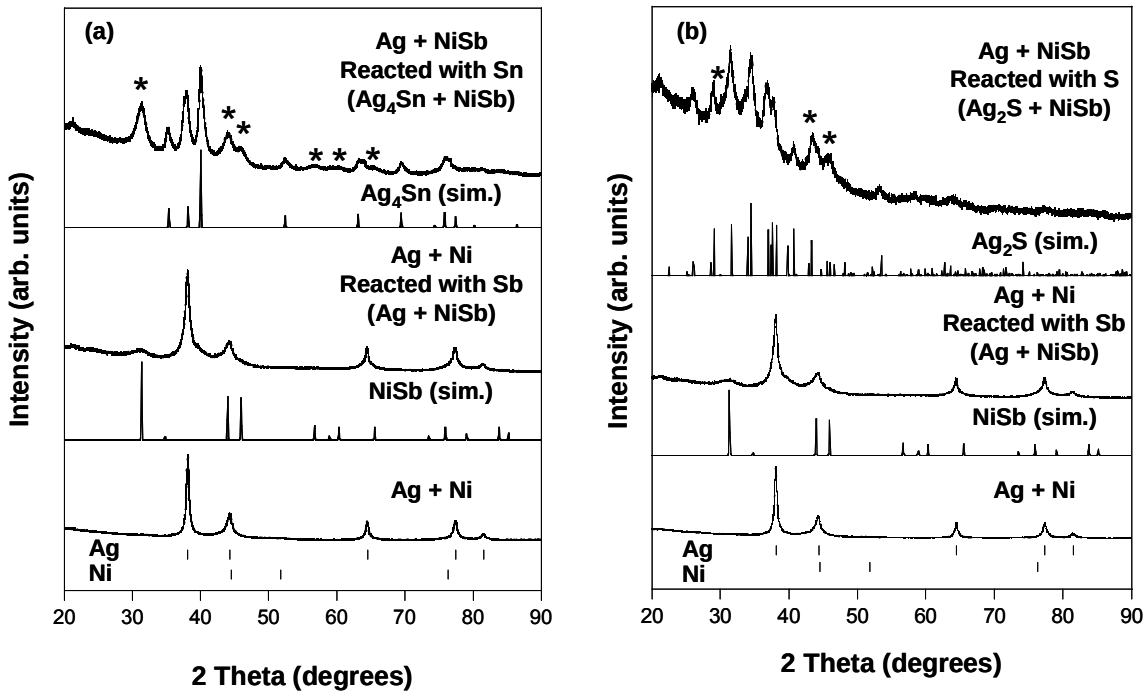

Figure 5.3 (a) Powder XRD patterns for a mixture of Ag and Ni nanoparticles followed by reacting the Ni particles first with $SbCl_3$ to form NiSb and then reacting the Ag nanoparticles with $SnCl_2$ to form Ag_4Sn. During the second conversion reaction NiSb further crystallizes due to the additional heat (marked with *). (b) A reaction of the same mixture but this time reacted with S powder forming a final mixture of NiSb (marked with *) and Ag_2S. Tick marks below the pattern for the mixture of Ag and Ni show the allowed reflections for each metal, and simulated patterns for NiSb, Ag_4Sn, and Ag_2S are below their respective experimental powder patterns.

Figure 5.3 shows the powder XRD patterns for a system of Ag and Ni nanoparticles reacted with solutions of $SbCl_3$ and $SnCl_2$. The bottom pattern shows the diffraction pattern for an equimolar mixture of Ag and Ni nanoparticles. The reflections for the Ni nanoparticles are difficult to see because they are overlapping with the Ag reflections, and are very weak in comparison to the Ag peaks due to the smaller size of the particles (~3-4nm) compared to the Ag particles (~20 nm). $SbCl_3$ was added to this nanoparticle mixture, reduced with $NaBH_4$, and heated to 100 °C to form NiSb while

leaving Ag unreacted. A simulated diffraction pattern for NiSb is shown below the experimental pattern for this first reaction. The major reflections for NiSb can be seen as broad peaks at 31.5°, 44°, and 46° 2-theta, and the Ag reflections remain unchanged. The reaction solution was then treated with $SnCl_2$ and heated to 175 °C to form Ag_4Sn. During the second reaction, NiSb further crystallizes due to the continued heat, and the diffraction pattern for the product of the second reaction shows two separate distinct intermetallic phases, NiSb and Ag_4Sn, synthesized in a one pot reaction with no evidence of any side products or cross reactions. Similarly, Ag and Ni can also be reacted to form NiSb and Ag_2S using sulfur powder as the sulfur source and reacting at room temperature for 4 hours. Figure 5.4 shows TEM micrographs for the Ag-Ni binary mixture after the reaction with (a) $SbCl_3$ and (b) $SnCl_2$. In the first image, a large (~25nm) Ag particle can be seen surrounded by an aggregate of NiSb particles. Electron

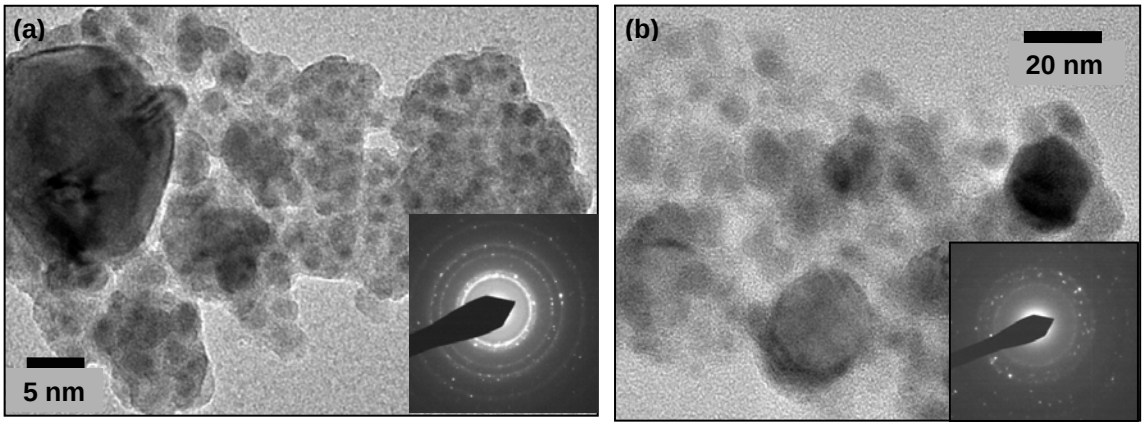

Figure 5.4 (a) TEM micrographs of a mixture of Ag and Ni nanoparticles after a reaction with $SbCl_3$. The image shows a large Ag particle surrounded by an aggregate of NiSb particles. Electron diffraction (insert) shows an fcc pattern consistent with that of Ag. (b) Image of the same solution reacted with $SbCl_3$ and $SnCl_2$. The image shows larger Ag_4Sn particles with NiSb particles aggregated around them.

diffraction shows a face centered cubic pattern consistent with that of Ag. After the second reaction, Ag is converted to Ag_4Sn and the Ag particles grow due to the incorporation of Sn. Electron diffraction shows an Mg-type pattern consistent with that of Ag_4Sn.

Figure 5.5 shows the powder XRD data for another binary mixture of metal nanoparticles, Ni and Pt, reacted with $Pb(C_2H_3O_2)_2$ and $SbCl_3$. The reflections for both Ni and Pt can be observed in the pattern for the as-made mixture. The mixture was first

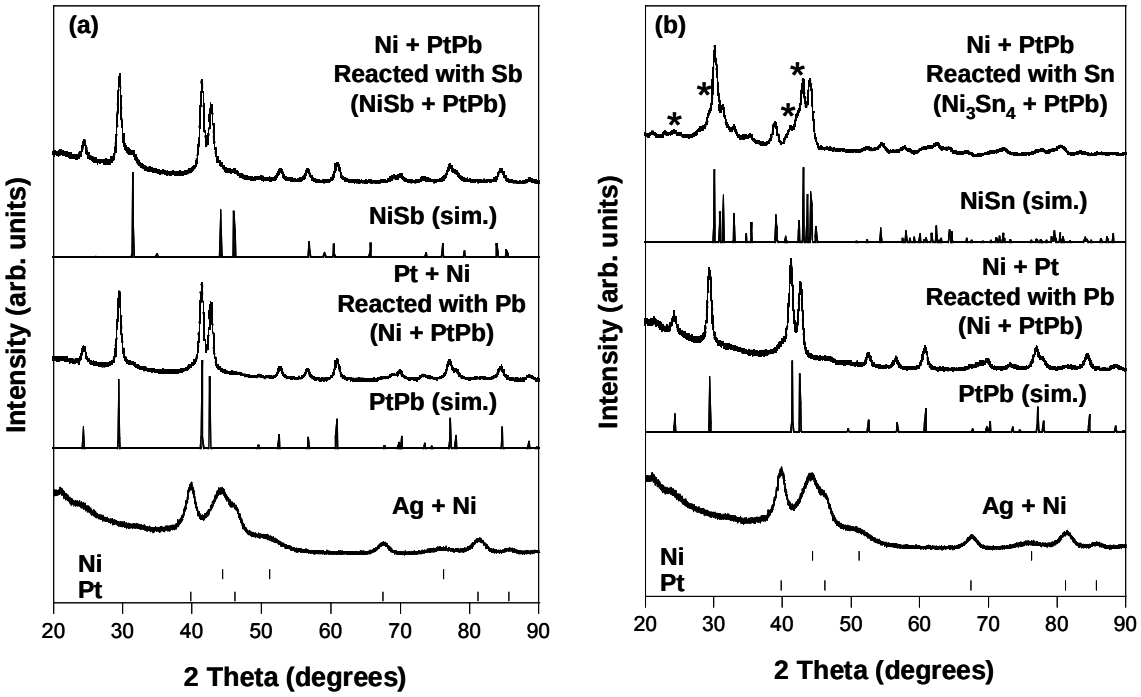

Figure 5.5 (a) Powder XRD patterns for a mixture of Pt and Ni nanoparticles followed by reacting the Pt particles first with $Pb(C_2H_3O_2)_2$ to form PtPb followed by reacting the Ni nanoparticles with $SbCl_3$ to form NiSb. (b) A reaction of the same mixture but this time reacted with $SnCl_2$ forming a final mixture of Ni_3Sn_4 and PtPb (marked with *). Tick marks below the pattern for the mixture of Pt and Ni show the allowed reflections for each metal, and simulated patterns for NiSb, PtPb, and Ni_3Sn_4 are below their respective experimental powder patterns.

reacted with $Pb(C_2H_3O_2)_2$ and $NaBH_4$ at room temperature, and then heated to 150 °C. The reflections for PtPb can be seen in the diffraction pattern for the product of this first reaction. The mixture was then reacted with $SbCl_3$ and $NaBH_4$ and heated to 100 °C to form NiSb. The experimental diffraction pattern shows both intermetallic phases present in the final product with the peaks for NiSb seen as broad peaks at 31.5°, 44°, and 46° 2-theta. Additionally, the Pt-Ni mixture can be reacted with $Pb(C_2H_3O_2)_2$ and $SnCl_2$ to form Ni_3Sn_4 and PtPb. Figure 5.5 illustrates TEM micrographs for the Pt-Ni binary mixture showing (a) a mixture of Ni and Pt nanoparticles prior to reaction, and (b) after the reaction with $Pb(C_2H_3O_2)_2$. Prior to reaction, most of the Pt nanoparticles (darker contrast) are smaller (3-5nm) and round. After the reaction with $Pb(C_2H_3O_2)_2$, the Pt particles grow significantly and form larger clusters of PtPb. Ni can be seen as the

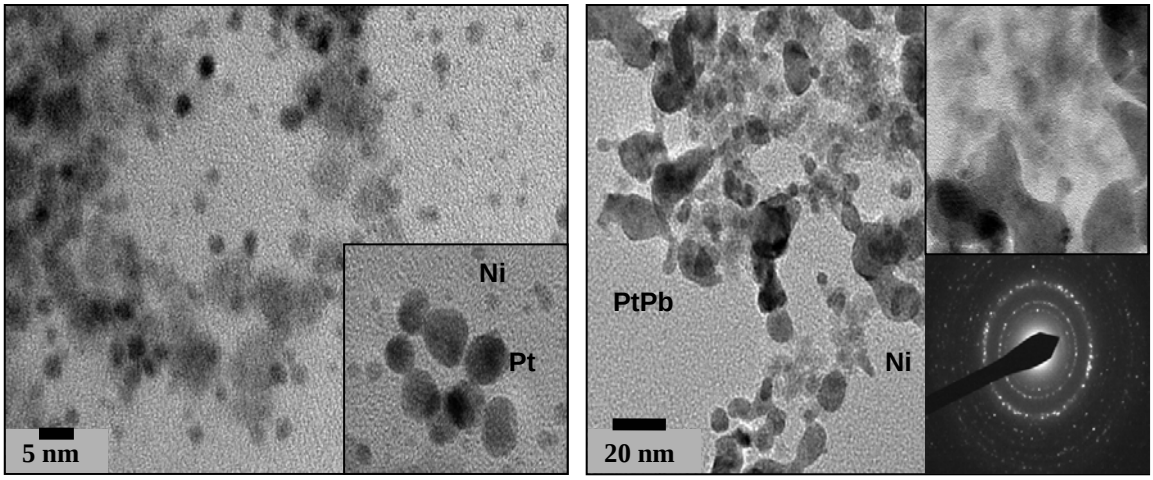

Figure 5.6 (a) TEM micrographs of a mixture of Pt and Ni nanoparticles as-made. The particles that are darker in contrast are Pt while the smaller lighter colored particles are Ni. The inset shows a close up of a group of Pt particles. (b) Image of the same solution reacted with $Pb(C_2H_3O_2)_2$ to form PtPb. The image shows larger PtPb particles with Ni particles dispersed around them. The insert shows a high resolution image of Ni particles surrounded by PtPb. The other inset shows the electron diffraction pattern for PtPb.

lighter contrast areas and the inset picture in Figure 5.6 b highlights one of these areas. After the reaction with $SnCl_2$, the particles further aggregated and characterization became quite difficult.

The data presented here demonstrate that both of the metal nanoparticle precursors can be reacted individually to form two binary intermetallic phases without noticeably generating any cross reaction side products.

5.3.3 *Synthesis of binary intermetallics from a ternary mixture of single metal nanoparticles*

Building off of the success of the binary mixtures, we explored the possibility of expanding the reaction system to three types of starting metal nanoparticles. The system attempted utilizes Ag, Ni, and Pt nanoparticles and involves the reaction of these with three metal salt solutions in a one pot reaction.

Because the system mixes three different types of starting metal nanoparticles, the complexity of the reaction quickly escalates. To simplify things, each single metal precursor was tested by reacting it with each of the metal salts used to transform all three metal starting materials into intermetallic phases. Figure 5.6 shows the powder XRD pattern for the products of each metal precursor material reacted with $Pb(C_2H_3O_2)_2$, $SbCl_3$, and S. For Ag, no interaction is seen for the first two reactions but when the solution is treated with S powder, the Ag nanoparticles are converted to Ag_2S. Similarly the Ni nanoparticles remain unaffected after the first reaction with Pb, but Ni does react

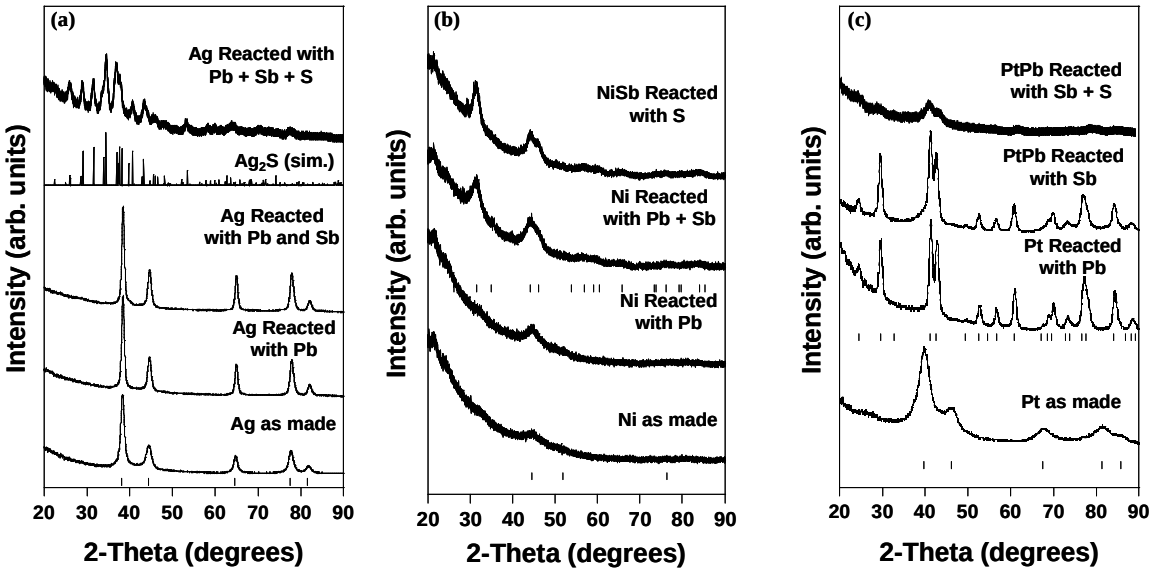

Figure 5.7 (a) Powder XRD patterns for Ag nanoparticles as synthesized, reacted first with $Pb(C_2H_3O_2)_2$, followed by reaction with $SbCl_3$, and finally with S powder to form Ag_2S. (b) Nickel nanoparticles reacted under the same conditions and with the same reagents as the Ag nanoparticles showing a reaction with the $SbCl_3$ to form NiSb, which is stable after the S reaction. (c) Platinum nanoparticles reacted under the same conditions first forming PtPb then staying unreacted during the $SbCl_3$ reaction. After the reaction with S, the PtPb appears to lose crystallinity or degrade. The peaks are still present but not as sharp. Tick marks for Ag, Ni, NiSb, Pt, PtPb, and a simulated pattern for Ag_2S showing the allowed reflections are below their respective experimental powder pattern.

with the $SbCl_3$ in the second step to form NiSb. NiSb is also shown to be stable after treating the reaction solution with S powder. Pt nanoparticles react in the first step to form PtPb, and remain unreacted after the subsequent reaction with Sb. Upon reaction with S powder, the PtPb appears to degrade or lose crystallinity. The peaks can still be observed, but are not as sharp as they were after the $Pb(C_2H_3O_2)_2$ and $SbCl_3$ reactions. This suggests that there are possible interactions between PtPb and S.

Figure 5.8 shows the powder XRD data for the mixture of Ag, Pt, and Ni nanoparticles and the subsequent reactions with $Pb(C_2H_3O_2)_2$, $SbCl_3$, and S. Initially all

three metals can be observed by powder XRD as three fcc patterns with different lattice constants. The peaks for Ni are more difficult to see due to the smaller size of the particles (~3-5nm) and overlapping peaks from the Ag pattern. After treating the ternary metal nanoparticle mixture with $Pb(C_2H_3O_2)_2$ and $NaBH_4$, the solution was heated to 150 °C for one minute then cooled to room temperature. The resulting diffraction pattern

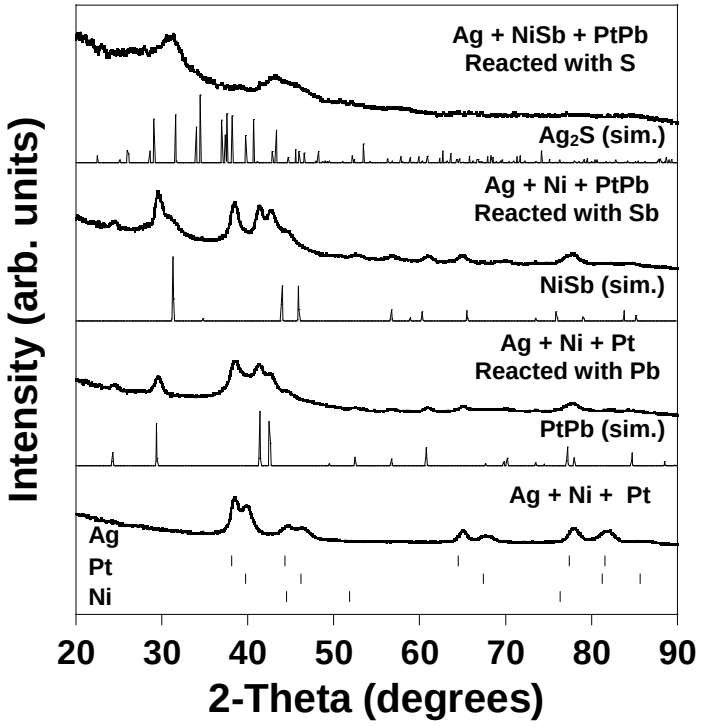

Figure 5.8 Powder XRD patterns for a mixture of Ag, Ni, and Pt nanoparticles reacted first with $Pb(C_2H_3O_2)_2$ forming PtPb, followed by reaction with $SbCl_3$ to form NiSb, and finally reaction with S powder to form Ag_2S. The reaction with S powder partially decomposes the PtPb so the final product looks like NiSb and Ag_2S. Tick marks for Ag, Pt, and Ni are located below the experimental data for the mixture of as-synthesized nanoparticles. Simulated patterns for Ag_2S, NiSb, and PtPb are below their respective experimental powder patterns.

shows peaks for Ag, Ni, and intermetallic PtPb. The reaction solution was then treated with $SbCl_3$ and $NaBH_4$, and heated to 100 °C. The XRD pattern for the product of this second reaction shows PtPb, NiSb, and Ag patterns. The pattern for NiSb has broad peaks due to the small particle size and the strongest reflections are seen at 31.5°, 44°, and 46° 2-theta.

The final reaction with sulfur powder converts Ag nanocrystals to Ag_2S at room temperature after 4h. The diffraction pattern shows the disappearance of the Ag (111) reflection indicating that the S has reacted with the Ag nanoparticles. The peaks for the PtPb phase again are diminished but still evident and the peaks for NiSb are still present. Ag_2S has a monoclinic structure and as a result the intensity of the major reflections is much less than that of the other higher symmetry phases present.

Investigation of this ternary system with TEM revealed that aggregation causes problems with the characterization of the product. Once the system has been reacted with multiple metal salts and heated, varying degrees of aggregation occur. Generally the more the reaction mixture is heated, the greater the degree of aggregation, which makes characterizing quite difficult. In the ternary mixed-metal system, there are six different metals in solution forming binary intermetallic particles and keeping these particles separated becomes quite difficult. Further research is required to optimize the conditions necessary for the successful conversion and characterization of a ternary mixed metal system. Some attempts were made to reduce this inherent aggregation by adding larger amounts of surface stabilizers and changing the concentrations of the reactants but produced limited success.

One way to avoid the problem of aggregation is spatially separating the metals on a surface using lithographically patterned metal features. A surface with Cu and Pt patterns was reacted with $Pb(C_2H_3O_2)_2$ and heated to 150 °C to form PtPb then reacted with $SnCl_2$ and heated to 150 °C to form Cu_6Sn_5. The sample was analyzed by SEM and EDS elemental analysis (Figure 5.9), and showed that Pb preferentially reacted with the Pt features, and no Pb is seen in the region where the Cu feature is located. EDS mapping also shows that Sn is everywhere on the surface and did not preferentially react anywhere. Another way to spatially separate the reacting metals is by using a multi-

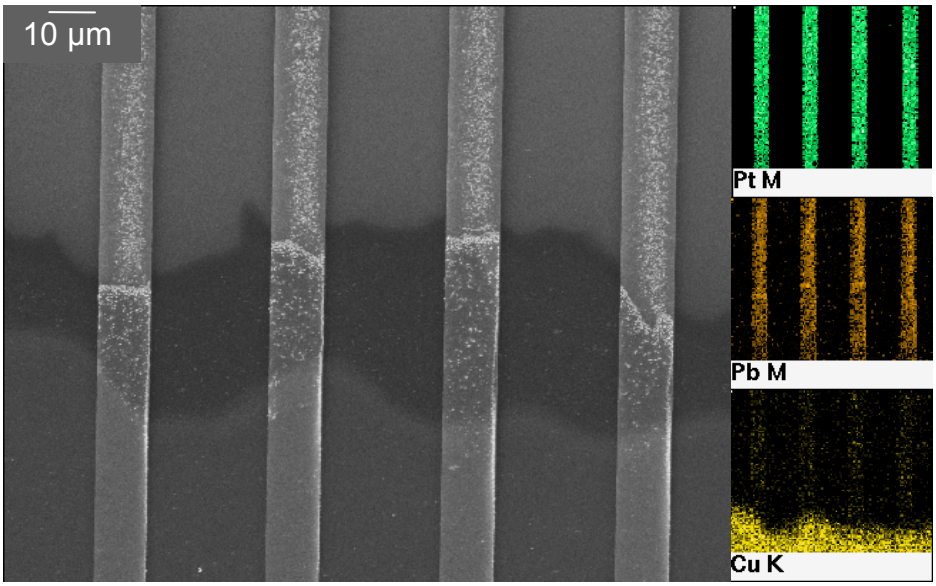

Figure 5.9 SEM image and EDS elemental mapping for a lithographically patterned surface of Cu and Pt features reacted sequentially with $Pb(C_2H_3O_2)_2$, and $SnCl_2$. The lead atoms react with the platinum and EDS shows Pb only where the Pt features are located. The Cu stays unreacted and EDS shows no Pb in the area of Cu. The reaction with $SnCl_2$ was not as selective and Sn was observed throughout the sample.

segmented nanowires and preliminary evidence suggests that a wire consisting of Au and Ag can be reacted to form Ag_2S with little interaction between the S and Au. While further optimization is necessary, these are examples of conversion reactions that take place in the presence of other metals without noticeable interactions.

5.4 Guidelines, limitations, and strategies for overcoming these limitations

While studying orthogonal reactivity of metal nanoparticles, we have discovered that there are certain guidelines and limitations to mixed metal reactions. The order in which the reactions are carried out is an important consideration. As in organic reactions, certain metal precursors are highly reactive and it is necessary to tie up these highly reactive nanoparticles with the first reaction to prevent future cross reactions. Once the particles have been converted to a stable binary phase, other metals in solution can be reacted to form additional mixed metal phases. This is similar to multi-step organic reactions where certain functional groups must be modified prior to the addition and reaction of other functionalities when building complex molecules.

Potential cross products can also be avoided by planning the reactions a certain way. An example of this involves the use of sulfur as a reactant. Because sulfur is reactive with multiple metals, its use in the initial reactions is not recommended. It will not selectively react with only one metal, but after stable binary phases are made it is possible to use this as a reagent to create a single metal sulfide phase in the presence of compounds without interactions. Additionally it was observed that Au treated with S would not undergo further reactions. The S acts as a protecting group for the Au

particles, blocking the surface so that no further reactions can occur. This could potentially be used to facilitate protection-deprotection chemistry on metal nanoparticles.

As discussed earlier, aggregation of the nanoparticle mixture is also a limiting factor in the synthesis of multi-phase products. Binary mixtures of single metal nanoparticles can be selectively converted to produce two intermetallic compounds with limited aggregation. As the system becomes more complex the degree of aggregation increases. Ongoing research is exploring ways to avoid this including spatially separating the reacting metals via lithographically patterned surfaces and multi-segmented nanowires.

Certain metal precursors are too reactive to be used in a solution of multiple metal nanoparticles. For example, Sn nanoparticles cannot be used as a starting material in a system which contains other metals which react with Sn. We attempted using Pt and Sn nanoparticles as starting materials in a binary mixture then reacting the Sn with Fe to make $FeSn_2$ and Pt with Pb to make PtPb. Upon heating of the reaction solution, Pt reacts with the Sn starting material instead of Pb ions. This is primarily due to the close proximity of the Pt and Sn nanoparticle reactants and the high reactivity of Sn nanoparticles. If the metals were spatially separated, this would not be a problem but in our proof of concept reactions the metals are free to interact and react.

5.5 Conclusions

In this chapter, we have established the concept of orthogonal chemistry for metal nanoparticles using conversion chemistry to synthesize multi-element intermetallic nanoparticles. We have established reaction conditions by which an extensive library of multi-element intermetallic compounds can be synthesized from single metal nanoparticles. These conditions can then be used to selectively react specific metal nanoparticles in solution. By exploiting differences in phase formation temperatures, we are able to individually react metal nanoparticles in a multi-metal mixture to produce multiple binary intermetallic products in a one pot reaction. This concept was demonstrated by reacting mixtures of Pt and Ni metal nanoparticles in solution to form PtPb and NiSb. The ability to deliberately synthesize multiple mixed metal intermetallic phases in a one-pot reaction is unprecedented for nanoparticle synthesis and has several important implications. First it extends the ability of the polyol systems by allowing multiple mixed metal nanoparticles to be synthesized in a single pot reaction. Previous reports have used these methods to synthesize a wide variety of compounds in a controlled manner but few techniques are able to make multiple phases cleanly from a one pot reaction. Most synthetic preps that produce nanocrystalline products are quite specific to the phase that is being studied and will not easily work for reactions with similar metals or producing similar products. However, the polyol process has now been shown to produce multiple types of intermetallic phases from a single type of metal nanoparticles. Additionally, a diverse range of starting metal nanoparticles were tested and several similar reactions occur with a given metal salt, varying only in temperature

necessary to form the intermetallic phase. Secondly this process allows the formation of chemically diverse materials to be prepared in the same solution. For example, we synthesized intermetallic and sulfide phases in the same solution. With further optimization, this process should be capable of synthesizing a broad variety of materials including alloys, intermetallics, oxides, sulphides, and phosphides. This has potential applications in many fields including composite materials and microelectronics where multiple diverse functional materials are needed.

While there are some limitations to this synthetic technique, we have demonstrated that orthogonal reactivity is possible in mixed metal nanoparticle starting materials. In time, it is should be possible to develop a robust toolbox of orthogonal chemical conversions for the transformation of one metal into a derivative compound in the presence of other metals. This has powerful implications toward the synthesis of chemically complex heterostructures and multi-metal materials. Preliminary evidence has shown that multi-segmented mixed metal nanowires and lithographically patterned surfaces can be selectively reacted to produce multimetallic phases while leaving other metals unreacted. Building off of these results it should be possible to create exceptionally complex multi-component nanostructures. Additionally, it has been demonstrated previously that the morphology of single metal precursors can be preserved in similar conversion reactions,[40] and it is reasonable to expect that these ideas could be applied to multi-metal systems.

Other ideas commonly used in organic synthesis could also be applied to these mixed metal systems like the protection-deprotection of a reactive species. In much the

same way a protecting group is added to prevent the reaction of a certain functional group in organic reactions, metal nanoparticles could be reacted in such a way that a second element reversibly binds to the starting material and can be removed once other reactions have been completed. We believe that this approach has powerful implications toward the synthesis of complex structures and further research will open the doors to rational design of heterostructured materials where multiple phases can be produced routinely in a controlled systematic way.

CHAPTER VI

GENERAL CONCLUSIONS

This dissertation has presented the development of several synthetic approaches for the synthesis of binary and ternary intermetallic compounds as nanocrystals. Many of these materials have functional properties which are important for scientific study as well as potential incorporation into numerous devices.

The first synthetic approach discussed is termed “Metallurgy in a Beaker.” In this approach, we utilize metal nanoparticles precipitated from solution as reactive precursors for the synthesis of multimetallic alloy and intermetallic nanoparticles. By precipitating multiple metal nanoparticles from solution, we obtain an intimately mixed nanocomposite which results in greatly reduced diffusion distances between the reacting metals, and subsequent annealing forms the intermetallic phase with greatly reduced annealing times compared to traditional methods. This method has successfully been demonstrated on several binary and ternary intermetallic phases, including known magnetic and superconducting compounds. Specifically, $FePt_3$, which displays room temperature ferromagnetism, was synthesized from a composite of Fe and Pt nanoparticles and annealed at 600 °C to nucleate the intermetallic phase. Additionally we were able to access ternary intermetallic nanocrystals by precipitating a mixture of Ag_2S and Pd. Annealing this nanocomposite formed Ag_2Pd_3S, which is known superconducting compound and measurements showed that the material made by this nanocomposite method was indeed superconducting. This work demonstrates a new approach to synthesizing intermetallics as nanocrystalline solids and has shown that the physical

properties of materials made by this method are equivalent or enhanced compared to materials made by traditional methods. Additionally, the nanoparticles created by this method are dispersible in solution, and can be processed using standard solution techniques to template the nanoparticles into morphologically diverse materials including thin films and colloidal crystal replicas.

The second synthetic method described here is the polyol process which involves the reduction of metal salts in solution using high boiling point polyalcohol solvents. This process was used to synthesize several known binary and ternary intermetallic compounds in the Au-Cu-Sn system. This system has previously been studied in-depth due to its application to microelectronics and solder applications. Identification of intermetallic phases is crucial to these applications as intermetallics are generally brittle, and can limit the lifetime of electronic devices. While studying this system, we discovered two new ternary intermetallic phases, $AuCuSn_2$ and $AuNiSn_2$. Both of these phases are atomically ordered and were isolated for the first time as nanocrystals using low temperature solution synthesis techniques. The structure of $AuCuSn_2$ was refined from powder diffraction data and found to have an ordered NiAs-type structure with Au and Cu in alternating layers with Sn. Other ternary systems were also explored using the polyol process including AuCoSn and several Pt-M-Sn systems (M= Co, Cu, Ni), and ternary alloy phases were synthesized in each system. These results demonstrate that the polyol process can access ternary intermetallic phases as nanocrystals and is an appropriate exploratory media for synthesizing new and possibly metastable intermetallic compounds. Additionally, the fact that we were able to discover new phases in well

studied ternary systems attests to the ability of this solution-based synthetic method to stabilize new structures that are difficult to access using traditional methods.

Using the polyol process, we also studied the formation of intermetallic $AuCuSn_2$. Because $AuCuSn_2$ is synthesized in solution, we were able to use solution-based techniques to monitor the reaction and determine the reaction pathway. We took aliquots at several points during the reaction and analyzed them using a number of complimentary techniques. Based on those results, we were able to determine that the reaction proceeds through a unique four step pathway: (1) galvanic reduction of Au(III) to Au(0) nanoparticles with concurrent oxidation of Sn(II) to Sn(IV) (as a SnO_2 shell), (2) formation of NiAs-type AuSn along with Cu and Sn nanoparticles using $NaBH_4$ reduction, (3) aggregation and thermal interdiffusion to form a ternary alloy, and (4) nucleation of the ordered intermetallic compound $AuCuSn_2$. The proposed pathway was also confirmed by forming $AuCuSn_2$ via reaction of AuSn nanoparticles with Cu nanoparticles formed ex-situ. This investigation provides a rare look at the steps involved in the formation of a new solid-state compound, and these mechanistic insights could provide valuable tools for the guided design of other new intermetallic solids. Furthermore, it demonstrates a novel strategy for studying mechanistic details of solid-state phase formation at the nanometer scale by combining data from multiple complementary techniques, including microscopy, spectroscopy, and diffraction.

Additional investigations into the reactivity and kinetics of chemical transformations involving metal nanoparticles have lead to the idea of orthogonal reactivity in multi-component nanoparticle systems, which would allow phase (or metal) specific reactions to take place sequentially within a system of multiple metal

nanoparticles. We established reaction conditions by which an extensive library of intermetallic compounds can be synthesized from single metal nanoparticles. These conditions can then be used to selectively react specific metal nanoparticles in solution of multiple metal particles. By exploiting differences in phase formation temperatures, we are able to individually react each metal in a multi-metal mixture to produce multiple binary intermetallic nanocrystalline products in a one pot reaction. This concept was demonstrated by reacting mixtures of Pt and Ni metal nanoparticles in solution with $Pb(C_2H_3O_2)_2$ and $SbCl_3$ to form PtPb and NiSb without any noticeable side products. Additionally we showed preliminary evidence that lithographically templated metal features can be selectively reacted to produce multimetallic features. While further optimization is needed for these reactions, it demonstrates that orthogonal reactivity can be realized in metal nanoparticle mixtures as well as patterned metal surfaces.

The techniques discussed in this dissertation provide several approaches to synthesizing intermetallic nanocrystals. We have shown that these strategies can be used to access a wide variety of binary and ternary intermetallic phases as nanocrystals, and they have the potential to greatly expand the availability of complex multimetallic nanomaterials for future studies and integration into nanotechnological devices. Furthermore, these studies demonstrate that low-temperature solution methods are an attractive medium for the exploratory synthesis of new and possibly metastable intermetallics. Additionally, it opens the door to studying phase formation of complex multimetallic solids at low temperatures. These techniques provide a different approach for synthesizing complex multimetallic materials and by studying the reaction pathways they could provide the tools necessary for rationally designing inorganic nanomaterials.

REFERENCES

1. Shevchenko, E. V.; Talapin, D. V.; Schnablegger, H.; Kornowski, A.; Festin, Ö.; Svedlindh, P.; Hasse, M.; Weller, H. *J. Am. Chem. Soc.* **2003**, *125*, 9090-9101.
2. (a) Burda, C.; Chen, X.; Narayanan, R.; El-Sayed, M. A. *Chem. Rev.* **2005**, *105*, 1025-1102. (b) Eustis, S.; El-Sayed, M. A. *Chem. Soc. Rev.* **2006**, *35*, 209-217. (c) Orendorff C. J.; Sau T. K.; Murphy C. J. *Small* **2006**, *2*, 636-639.
3. Hambrock, J.; Schröter, M. K.; Birkner, A.; Wöll, C.; Fischer, R. A. *Chem. Mater*. **2003**, *15*, 4217-4222.
4. Sun, S.; Murray, C. B.; Weller, D.; Folks, L.; Moser, A. *Science* **2000**, *287*, 1989-1992.
5. Sun, S.; Anders, S.; Thomson, T.; Baglin, J. E. E.; Toney, M. F.; Hamann, H. F.; Murray, C. B.; Terris, B. D. *J. Phys. Chem. B* **2003**, *107*, 5419-5425.
6. (a) Casado-Rivera, E.; Gal, Z.; Angelo, A. C. D.; Lind, C.; DiSalvo, F. J.; Abruna, H. D. *Chem. Phys. Chem.* **2003**, *4*, 193-199; (b) Casado-Rivera, E.; Volpe, D. J.; Alden, L.; Lind, C.; Downie, C.; Vazquez-Alvarez, T.; Angelo, A. C. D.; DiSalvo, F. J.; Abruna, H. D. *J. Am. Chem. Soc.* **2004**, *126*, 4043-4049; (c) Oana, M.; Hoffmann, R.; Abruna, H. D.; DiSalvo, F. J. *Surf. Sci.* **2005**, *574*, 1-16.
7. Sau, T.K.; Murphy, C.J. *Langmuir* **2004,** *20,* 6414-6420**.**
8. Liu, X.; He, T.J.; Liu, F.C.; Chen, D.M. *Chinese Journal Of Chemical Physics* **2005,** *18*, 81-86. (b) Slawinski, G.W.; Zamborini, F.P. *Langmuir* **2007**, *23*, 10357-10365.
9. Koch, C. C.; Whittenberger, J. D. *Intermetallics* **1996**, *4*, 339-355.

10. (a) Bai-Lin, Yu.; Xin-Feng, T.; Qiong, Q.; Qing-Jie, Z. *Acta Physica Sinica* **2004**, *53*, 3130-3135; (b) Xie, J.; Zhao, X.B.; Cao, G.S.; Zhao, M.J.; Su, S.F. *J. Power Sources* **2005**, *140*, 350–354.

11. (a) Ding, C.; Jihua, C.; Hongge, Y.; Zhenhua, C. *Mater. Sci. Eng. A* **2007**, *444*, 1-5; (b) Andrade-Gamboa, J.; Gennari, F. C.; Arneodo Larochette, P.; Neyertz, C.; Ahlers, M.; Pelegrina, J. L. *Mater. Sci. Eng. A* **2007**, *447*, 324-331.

12. Pithawalla, Y. B.; El-Shall, M. S.; Deevi, S. *Scripta Mater.* **2003**, *48*, 671-676.

13. Metal Salt Reduction nanoparticle synthesis

14. Cable, R. E.; Schaak, R. E. *Chem. Mater.* **2007**, *19*, 4098-4104.

15. (a) Heinrichs, B.; Delhez, P.; Schoebrechts, J. P.; Pirard, J. P. *J. Catal.* **1997**, *172*, 322-335. (b) Guczi, L.; Borko, L.; Schay, Z.; Bazin, D.; Mizukami, F. *Catal. Today* **2001**, *65*, 51-57. (c) Hutlova, A.; Niznansky, D.; Rehspringer, J. L.; Estournes, C.; Kurmoo, M. *Adv. Mater.* **2003**, *15*, 1622-1625.

16. Wright, J. D.; Sommerdijk, A. J. M. *Sol-Gel Materials: Chemistry and Applications*, Gordon and Breach: Amsterdam, 2001.

17. (a) Heibel, M.; Kumar, G.; Wyse, C.; Bukovec, P.; Bocarsly, A. B. *Chem. Mater.* **1996**, *8*, 1504-1511; (b) Vondrova, M.; Majsztrik, P. W.; Gould, S.; Bocarsly, A. *Chem. Mater.* **2005**, *17*, 4755-4757.

18. Rehbein, M.; Epple, M.; Fischer, R. D. *Solid State Sci.* **2000**, *2*, 473-488.

19. Stowell, C. A.; Korgel, B. A. *Nano Lett.* **2005**, *5*, 1203 -1207.

20. (a) Narayanan, R.; El-Sayed, M. A. *J. Am. Chem. Soc.* **2004**, *126*, 7194-7195. (b) Narayanan, R.; El-Sayed, M. A. *Nano Lett.* **2004**, *4*, 1343-1348.

21. (a) Kagan, C. R.; Murray, C. B.; Bawendi, M. G. *Science*, **1995**, *270*, 1335-1338. (b) Collier, C. P.; Saykally, R. J..; Shang, J. J.; Henrichs, S. E.; Heath, J. R. *Science* **1997**, *277*, 1978-1981. (c) Redi, F. X.; Cho, K.-S.; Murray, C. B.; O'Brien, S. *Nature* **2003**, *423*, 968-971.

22. Moison, J. M.; Houzay, F.; Barthe, F.; Leprince, L.; André, E.; Vatel, O. *Appl. Phys. Lett.* **1994**, *64*, 196-198.

23. Bahnemann, D. W.; Kormann, C.; Hoffman, M. R. *J. Phys. Chem.* **1987**, *91*, 3789-3798.

24. Wagner, R. S.; Ellis, W. C. *Appl. Phys. Lett.* **1964**, *4*, 89-90.

25. Muralidhar, G.; Massoth, F. E.; Shabtai, J. *J. Catal.* **1984**, *85*, 44-52.

26. Lopez, M. F.; Escudero, M. L. *Electrochim. Acta* **1998**, *43*, 671-678.

27. Liu, C. T. *Mater. Chem. Phys.* **1995**, *42*, 77-86.

28. (a) Morelli, D. T.; Caillat, T.; Fleurial, J.-P.; Borshchevsky, A.; Vandersande, J.; Chen, B.; and Uher, C. *Phys. Rev. B*, **1995**, *51*, 9622-9628; (b) Sharp, J.W.; Jones, E.C.; Williams, R. K.; Martin, P.M.; Sales, B.C. *J. Appl. Phys.*, **1995**, *78*, 1013-1018.

29. Ullakko, K.; Huang, J. K.; Kantner, C.; O'Handley, R. C.; Kokorin, V. V. *Appl. Phys. Lett.* **1996**, *69*, 1966-1968.

30. West, A. R. *Solid State Chemistry and Its Applications*; Wiley: Chichester, England, 1984.

31. (a) Onda, A.; Komatsu, T.; Yashima, T. *J. Catal.* **2001**, *201*, 13-21; (b) Komatsu, T.; Inaba, K.; Uezono, T.; Onda, A.; Yashima, T. *Appl. Cat. A* **2003**, *251*, 315-326; (c) Onda, A.; Komatsu, T.; Yashima, T. *J. Catal.* **2003**, *221*, 378-385.

32. (a) Novet, T.; Johnson, D. C. *J. Am. Chem. Soc.* **1991**, *113*, 3398-3403. (b) Noh, M.; Thiel, J.; Johnson, D. C. *Science* **1995**, *270*, 1181-1184. (c) Noh, M.; Johnson, C. D.; Hornbostel, M. D.; Thiel, J.; Johnson, D. C. *Chem. Mater.* **1996**, *8*, 1625-1635.

33. (a) Noh, M.; Thiel, J.; Johnson, D. C. *Science* **1995**, *270*, 1181-1184. (b) Noh, M.; Johnson, C. D.; Hornbostel, M. D.; Thiel, J.; Johnson, D. C. *Chem. Mater.* **1996**, *8*, 1625-1635.Sun, Y.; Mayers, B.; Herricks, T.; Xia, Y. *Nano Lett.* **2003**, *3*, 955-960.

34. Sun, Y; Mayers, B.; Herricks, T.; Xia, Y. *Nano Lett.* **2006**, 3, 955-960.

35. Seo, W. S.; Shim, J. H.; Oh, S. J.; Lee, E. K.; Hur, N. H.; Park, J. T. *J. Am. Chem. Soc.* **2005**, *127*, 6188-6189.

36. Park, J.; Lee, E.; Hwang, N.-M.; Kang, M.; Kim, S. C.; Hwang, Y.; Park, J.-G.; Noh, H.-J.; Kim, J.-Y.; Park, J.-H.; Hyeon, T. *Angew. Chem. Int. Ed.* **2005**, *44*, 2872-2877.

37. Wiley, B.; Sun, Y.; Mayers, B.; Xia, Y. *Chem. Eur. J.* **2005**, *11*, 454-463.

38. (a) Hoefelmeyer, J. D.; Niesz, K.; Somorjai, G.; Tilley, T. D. *Nano Lett.* **2005**, *5*, 435-438. (b) Kim, F.; Connor, S.; Song, H.; Kuykendall, T.; Yang, P. *Angew. Chem. Int. Ed.* **2004**, *43*, 3673-3677.

39. Sun, Y.; Wiley, B.; Li, Z.-Y.; Xia, Y. *J. Am. Chem. Soc.* **2004**, *126*, 9399-9406.

40. Chou, N. H.; Schaak, R. E. *J. Am. Chem. Soc.* **2007**, *129*, 7339-7345.

41. Dinega, D. P.; Bawendi, M. G. *Angew. Chem. Int. Ed.* **1999**, *38*, 1788-1791.

42. Zhao, Y.; Zhang, Y.; Zhu, H.; Hadjipanayis, G. C.; Xiao, J. Q. *J. Am. Chem. Soc.* **2004**, *126*, 6874-6875.

43. Greyson, E.C.; Barton, J.E.; Odom, T.W. *Small* **2006**, *2*, 368 – 371.

44. Schaak, R. E.; Sra, A. K.; Leonard, B. M.; Cable, R. E.; Bauer, J. C.; Han, Y.-F.; Means, J.; Teizer, W.; Vasquez, Y.; Funck, E. S. *J. Am. Chem. Soc.* **2005**, *127*, 3506-3515.

45. Sra, A. K.; Schaak, R. E. *J. Am. Chem. Soc.* **2004**, *126*, 6667-6672.

46. (a) Fievet, F.; Lagier, J.P.; Blin, B.; Beaudoin, B.; Figlarz, M. *Solid State Ionics* **1989**, *32/33*, 198-205; (b) Ducamp-Sanguesa, C.; Herrera-Urbina, R.; Figlarz, M. *Solid State Ionics* **1993**, *63-65*, 25-30.

47. (a) Toshima, N.; Kushihashi, K.; Yonezawa, T.; Hirai, H. *Chem. Lett*. **1989**, *10*, 1769-1772; (b) Toshima, N.; Harada, M.; Yamazaki, Y.; Asakura, K. J. *Phys. Chem.* **1992**, *96*, 9927-9933; (c) Toshima, N.; Yonezawa, T. *New J. Chem.* **1998**, 1179-1201.

48. (a) Murray, C. B.; Kagan, C. R.; Bawendi, M. G. *Annu. Rev. Mater. Sci.* **2000**, *30*, 545-610; (b) Murray, C. B.; Sun, S.; Gaschler, W.; Doyle, H.; Betley, T. A.; Kagan, C. R. *IBM. J. Res. Dev.* **2001**, *45*, 47-56.

49. Teng, X.; Yang, H. *Nano Lett.* **2005**, *5*, 885-891.

50. Leonard, B. M.; Bhuvanesh, N. S. P.; Schaak, R. E. *J. Am. Chem. Soc.* **2005**, *127*, 7326-7327.

51. Leonard, B. M.; Schaak, R. E. *J. Am. Chem. Soc*. **2006**, *128*, 11475-11482.

52. Leonard, B. M.; Schaak, R. E. In Preparation.

53. Cahn, R. W. *Contemp. Phys.* **2001**, *42*, 365-375.

54. (a) Goll, D.; Kronmuller, H. *Naturewissenschaften* **2000**, *87*, 423-438. (b) Paduani, C. *J. Appl. Phys.* **2001**, *90*, 6251.

55. (a) Gavaler, J. R.; Janocko, M. A.; Bradinski, A. I.; Rowland, G. W. *IEEE Trans. Magn.* **1975**, *2*, 192-196. (b) Cava, R. J.; Takagi, H.; Zandbergen, H. W.; Krajewski, J. J.; Peck, W. F.; Siegrist, T.; Batlogg, B.; Vandover, R. B.; Felder, R. J.; Mizuhashi, K.; Lee, J. O.; Eisaki, H.; Uchida, S. *Nature* **1994**, *367*, 252. (c) Cava, R. J.; Takagi, H.; Batlogg, B.; Zandbergen, H. W.; Krajewski, J. J.; Peck, W. F.; Vandover, R. B.; Felder, R. J.; Siegrist, T.; Mizuhashi, K.; Lee, J. O.; Eisaki, H.; Carter, S. A.; Uchida, S. *Nature* **1994**, *367*, 146. (d) Nagamatsu, J.; Makagawa, N.; Muranaka, T.; Zenitani, Y.; Akimitsu, J. *Nature* **2001**, *410*, 63-64. (e) He, T.; Huang, Q.; Ramirez, A. P.; Wang, Y.; Regan, K. A.; Rogado, N.; Hayward, M. A.; Haas, M. K.; Slusky, J. S.; Inumara, K.; Zandbergen, H. W.; Ong, N. P.; Cava, R. J. *Nature* **2001**, *411*, 54-56.

56. Stern, R. A.; Willoughby, S. D.; MacLaren, J. M.; Cui, J.; Pan, Q.; James, R. D. *J. Appl. Phys.* **2003**, *93*, 8644-8646.

57. Roucoux, A.; Schulz, J.; Patin, H. *Chem. Rev.* **2002**, *102*, 3757-3778.

58. (a) Zhang, C. J.; Baxter, R. J.; Hu, P.; Alavi, A.; Lee, M.-H. *J. Chem. Phys.* **2001**, *115*, 5272-5277. (b) Mathauser, A. T.; Teplyakov, A. V. *Catal. Lett.* **2001**, *73*, 207-210.

59. (a) Kirchheim, R.; Mutschele, T.; Keininger, W.; Gleiter, H.; Birringer, R.; Koble, T. D. *Mater. Sci. Eng.* **1988**, *99*, 457-462. (b) Kamakoti, P.; Sholl, D. S. *J. Membr. Sci.* **2003**, *225*, 145-154.

60. (a) Liu, C. T.; Stringer, J.; Mundy, J. N.; Horton, L. L.; Angelini, P. *Intermetallics* **1997**, *5*, 579-596. (b) Stoloff, N. S.; Liu, C. T.; Deevi, S. C. *Intermetallics* **2000**, *8*, 1313-1320.

61. (a) Gleiter, H. *Prog. Mater. Sci.* **1989**, *33*, 223-315. (b) Suryanarayana, C. *Prog. Mater. Sci.* **2001**, *46*, 1-184.

62. (a) Hahn, H. *Nanostruct. Mater.* **1997**, *9*, 3-12. (b) Koch, C. C. *Nanostruct. Mater.* **1997**, *9*, 13-22.

63. Blair, R. G.; Gillan, E. G.; Nguyen, N. K. B.; Daurio, D.; Kaner, R. B. *Chem. Mater.* **2003**, *15*, 3286-3293.

64. (a) Madou, M. J. *Fundamentals of Microfabrication: The Science of Miniaturization*, 2nd ed.; CRC Press: Boca Raton, FL, 2002. (b) Mitzi, D. B.; Kosbar, L. L.; Murray, C. E.; Copel, M.; Afzali, A. *Nature* **2004**, *428*, 299-303.

65. Gao, F.; Lu, Q.; Zhao, D. *Nano Lett.* **2003**, *3*, 85-88.

66. Lu, W.; Wang, B.; Wang, K.; Wang, X.; Hou, J. G. *Langmuir* **2003**, *9*, 5887-5891.

67. West, A. R. *Solid State Chemistry and its Applications*; Wiley: Chichester, England, 1984.

68. (a) Bidwell, L.R.; Schulz, W.J.; Saxer, R.K. *Acta Metallurgica* **1967,** *15*, 1143-1148. (b) Collings, E.W.; Smith,. R.D.; Ho, J.C. *Journal of the Less-Common Metals* 1976, *46*,189 – 195.

69. (a) Bonnemann, H.; Brijoux, W.; Brinkmann, R.; Fretzen, R.; Joussen, T.; Koppler, R.; Korall, B.; Neiteler, P.; Richter, J. *J. Mol. Catal.* **1994**, *86*, 129-177. (b) Glavee, G. N.; Klabunde, K. J.; Sorensen, C. M.; Hadjipanayis, G. C. *Langmuir* **1994**, *10*, 4726-4730.

70. (a) Raub, V. E.; Wullhorst, B.; Plate, W. *Z. Metallkd.* **1954**, *45*, 533-537. (b) El-Borady, M.; Schubert, K. *Z. Metallkd.* **1971**, *62*, 667-675.

71. Villars, P.; Prince, A.; Okamoto, H. *Handbook of Ternary Alloy Phase Diagrams*; ASM International: Materials Park, OH, 1995.

72. Khan, H. R.; Trunk, H.; Raub, Ch. J.; Fertig, W. A.; Lawson, A. C. *J Less-Common Met.* **1973**, *30*, 167-168.

73. Van Dover, R. B.; Gyorgy, E. M.; Cava, R. J.; Krajewski, J. J.; Felder, R. J.; Peck, W. F. *Phys. Rev. B* **1993**, *47*, 6134-6137.

74. (a) Perepezko, J. H. *Mater. Sci. Eng.* **1984**, *65*, 125-135. (b) Chen, X. Z.; Larson, P.; Sportouch, S.; Brazis, P.; Mahanti, S. D.; Kannenwurf, C. R.; Kanatzidis, M. G. *Chem. Mater.* **1999**, *11*, 75-83. (c) Latturner, S. E.; Kanatzidis, M. G. *Inorg. Chem.* **2004**, *43*, 2-4.

75. Sra, A. K.; Ewers, T. D.; Schaak, R. E. *Chem. Mater.* **2005**, *17*, 758-766.

76. Cable, R. E.; Schaak, R. E. *Chem. Mater.* **2005**, *17*, 6835-6841.

77. Cushing, B. L.; Kolesnichenko, V. L.; O'Connor, C. J. *Chem. Rev.* **2004**, *104*, 3893-3946.

78. Roeder, J. F.; Notis, M. R.; Goldstein, J. I. *Defect Diffus. Forum* **1988**, *59*, 271-278.

79. (a) Karlsen, O. B.; Kjekshus, A.; Rost, E. *Acta Chem. Scand.* **1990**, *44*, 197-198. (b) Peplinski, B.; Zakel, E. *Mater. Sci. Forum* **1994**, *166-169*, 443-448.

80. Karlsen, O. B.; Kjekshus, A.; Rost, E. *Acta Chem. Scand.* **1992**, *46*, 147-156.

81. *TOPAS*, version 2.0; General profile and structure analysis software for powder diffraction data; Bruker AXS: Karlsruhe, Germany.

82. Lange, S.; Nilges, T.; Hoffmann, R.; Pöttgen, R. *Z. Anorg. Allg. Chem.* **2006**, *632*, 1163-1166.

83. (a) Neumann, A.; Kjekshus, A.; Romming, C.; Rost, E. *J. Solid State Chem.* **1995**, *119*, 142-146. (b) Neumann, A.; Kjekshus, A.; Rost, E. *J. Solid State Chem.* **1996**, *123*, 203-207.

84. Van Noort, H.M.; De Mooij, D.B.; Buschow, K.H. *Phys. Stat. Sol (a)* **1984,** *86*, 655-662.

85. (a) Williams, J. R.; Johnson, M.; Johnson, D. C. *J. Am. Chem. Soc.* **2001**, *123*, 1645-1649. (b) Oyelaran, O.; Novet, T.; Johnson, C.D.; Johnson, D. C. *J. Am. Chem. Soc.* **1996**, *118*, 2422-2426. (c)Williams, J. R.; Johnson, M.; Johnson, D. C. *J. Am. Chem. Soc.* **2003**, *125*, 3489-3592. (d) Schneidmiller, R.; Bentley, A.; Hornbostel, M. D.; Johnson, D. C. *J. Am. Chem. Soc.* **1999**, *121*, 3142-3149.

86. (a) Sellinschegg, H.; Stuckmeyer, S. L.; Hornbostel, M. D.; Johnson, D. C. *Chem. Mater.* **1998,** *10*, 1096-1101. (b) Hornbostel, M. D.; Hyer, E. J.; Thiel, J.; Johnson, D. C. *J. Am. Chem. Soc.* **1997**, *119*, 2665-2668. (c) Schneidmiller, R.; Hornbostel, M. D.; Johnson, D. C. *Inorg. Chem.* **1997**, *36*, 5894-5899. (d) Hornbostel, M. D.; Hyer, E. J.; Edvalson, J. H.; Johnson, D. C. *Inorg. Chem.* **1997**, 36, 4270-4274.

87. (a) Stein, A.; Keller, S. W.; Mallouk, T. E. *Science* **1993**, *259*, 1558-1564; (b) Gopalakrishnan, J. *Chem. Mater.* **1995**, *7*, 1265-1275; (c) Schaak, R.E.; Mallouk, T. E. *Chem. Mater.* **2002**, *14*, 1455-1471.

88. (a) Livage, J.; Henry, M.; Sanchez, C. *Prog. Solid State Chem.* **1988**, *18*¸ 259. (b) Schwartz, R. W. *Chem. Mater.* **1997**, *9*, 2325-2340. (c) Cheetham, A. K.; Mellot, C. F. *Chem. Mater.* **1997**, *9*, 2269-2279. (d) Vioux, A. *Chem. Mater.* **1997**, *9*, 2292-2299.

89. (a) Feng, S.; Xu, R. *Acc. Chem. Res.* **2001**, *94*, 239. (b) Sheets, W. C.; Mugnier, E.; Barnabe, A.; Marks, T. J.; Poeppelmeier, K. R. *Chem. Mater.* **2006**, *18*, 7-20.

90. Vondrova, M.; Klimczuk, T.; Miller, V. L.; Kirby, B. W.; Yao, N.; Cava, R. J.; Bocarsly, A. B. *Chem. Mater*. **2005**, *17*, 6216-6218.

91. Cokoja, M.; Parala, H.; Schroter, M. K.; Birkner, A.; van den Berg, M. W. E.; Grunert, W.; Fischer, R. A. *Chem. Mater.* **2006**, *18*, 1634-1642.

92. Roychowdhury, C.; Matsumoto, F.; Mutolo, P. F.; Abruna, H. D.; DiSalvo, F. J. *Chem. Mater.* **2005**, *17*, 5871-5876.

93. Wiley, B.; Herricks, T.; Sun, Y.; Xia, Y. *Nano Lett.* **2004**, *4*¸1733-1739.

94. (a) Mulvaney, P. *Langmuir* **1996**, *12*, 788-800. (b) Link, S.; Wang, Z. L.; El-Sayed, M. A. *J. Phys. Chem. B* **1999**, *103*, 3529-3533.

95. Oldfield, G.; Ung, T.; Mulvaney, P. *Adv. Mater* **2000**, *12*, 1519-1522.

96. Lisiecki, I.; Pileni, M. P. *J. Phys. Chem.* **1995**, *99*, 5077-5082.

97. Henglein, A.; Giersig, M. *J. Phys. Chem.* **1994**, *98*, 6931-6935.

98. (a) Yin, Y.; Rioux, R. M.; Erdonmez, C. K.; Hughes, S.; Somorjai, G. A.; Alivisatos, A. P. *Science* **2004**, *304*, 711-714. (b) Son, D. H.; Hughes, S. M.; Yin, Y.; Alivisatos, A. P. *Science* **2004**, *306*, 1009-1012.

99. (a) Ely, T. O.; Amiens, C.; Chaudret, B.; Snoeck, E.; Verelst, M.; Respaud, M.; Broto, J.-M. *Chem. Mater.* **1999**, *11*, 526-529. (b) Hyeon, T. *Chem. Commun.* **2003**, 927-934. (c) Cushing, B. L.; Kolesnichenko, V. L.; O'Connor, C. J. *Chem. Rev.* **2004**, *104*, 3893-3946. (d) Green, M. *Chem. Commun.* **2005**, 3002-3011.

100. (a) Chen, S.; Wang, Z. L.; Ballato, J.; Foulger, S. H.; Carroll, D. L. *J. Am. Chem. Soc.* **2003**, *125*, 16186-16187. (b) Sau, T. K.; Murphy, C. J. *J. Am. Chem. Soc.*

2004, *126*, 8648-8649. (c) Hao, E.; Bailey, R. C.; Schatz, G. C.; Hupp, J. T.; Li, S. *Nano Lett.* **2004**, *4*, 327-330.

101. Sun, L.; Hao, Y.; Chien, C.L.; Searson, P.C. *IBM Journal Of Research And Development* **2005**, *49*, 79-102. (b) Lee, J.H.; Wu, J.H.; Liu, H.L.; Cho, J.U.; Cho, M.K.; An, B.H.; Min, J.H.;Noh, S.J.; Kim, Y.K. *Angew. Chem. Int. Ed.* **2007**, 46, 3663-3667.

102. (a) Nicewarner-Pena, S. R.; Freeman, R. G.; Reiss, B. D.; He, L.; Pena,D. J.; Walton, I. D.; Cromer, R.; Keating, C. D.; Natan, M. J. *Science***2001**, *294*, 137. (b) Mbindyo, J. K. N.; Reiss, B. D.; Martin, B. R.; Keating, C. D.; Natan, M. J.; Mallouk, T. E. *Adv. Mater.* **2001**, *13*, 249.

103. Ren, Q.; Zhao, Y.P.; Yue, J. C.; Cui, Y. B. *Biomedical Microdevices* **2006**, *8*, 201-208.

104. Mbindyo, J. K. N.; Reiss, B. D.; Martin, B. R.; Keating, C. D.; Natan, M. J.; Mallouk, T. E. *Adv. Mater.* **2001**, *13*, 249.

105. (a)Zeng, H.; Li, J.; Liu, J.P.; Wang, Z.; Sun, S. *Nature* **2002**, *420*, 395-398. (b) Skomski, R.; Coey, J. M. D. *Phys. Rev. B* 1993**,** *48*, 15812-15816.

106. Gu, H.; Zheng, R.; Zhang, X.; Xu, B. *J. Am. Chem. Soc.* **2004**, *126*, 5664-5665. (b) Gu, H.; Yang, Z.; Gao, J.; Chang, C. K.; Xu, B. *J. Am. Chem. Soc.* **2005**, *127*, 34-35. (c) Wang, L. Y.; Luo, J.; Fan, Q.; Suzuki, M.; Suzuki, I. S.; Engelhard, M. H.; Lin, Y.; Kim, N.; Wang, J. Q.; Zhong, C. J. *J. Phys. Chem. B.* **2005**, *109*, 21593-21601.

107. Yin, Y.D.; Erdonmez, C.K.; Cabot, A.; Hughes, S.; Alivisatos, A.P. *Adv. Func. Mater*. **2006**, *16*, 1389-1399.

108. Yin, M.; Wu, C.-K.; Lou, Y.; Burda, C.; Koberstein, J. T.; Zhu, Y.; O'Brien, S. *J. Am. Chem. Soc.* **2005**, *127,* 9506-9511.

109. (a) Henkes, A,E,; Schaak, R.E. *Chem. Mater.* **2007**,19, 4234-4242. (b) Henkes, A.E.; Vasquez, Y.; Schaak, R.E. *J. Am. Chem. Soc.* **2007,** 129, 1896.

110. Jeong, U.; Camargo, P.H.C.; Lee, Y.H.; Xia, Y. *J. Mater. Chem.,* **2006**, *16,* 3893-3897.

111. (a) Dawood, F.; Leonard, B.M.; Schaak; R.E. *Chem.f Mater.* **2007** ,*19,* 4545-4550. Henkes, A.E.; Bauer, J.C.; Sra, A.K.; Johnson, R,D.; Cable, R.E.; Schaak, R.E. *Chem. Mater.* **2006**,*18,* 567-571.

112. Shao, K.; Yao, J.N. *Materials Letters* **2006,** *60,* 3826-3829.

VITA

Brian M. Leonard

Chemistry Dept.
c/o Dr. Schaak or Dr. Dunbar
Texas A&M University M.S. 3255
College Station TX 77843
Leonard5_0@hotmail.com

EDUCATION

Ph.D., Inorganic Chemistry, Texas A&M University, May 2008

B.S., Chemistry, University of Nebraska at Kearney, May 2003

PUBLICATIONS

Dawood, F.; Leonard, B.M.; Schaak; R.E. *Chem. Mater.* **2007**, *19*, 4545-4550.

Leonard, B.M.; Schaak, R. E. *J. Am. Chem. Soc.* **2006**, *128*, 11475-11482.

Leonard, B.M.; Bhuvanesh, N.S.P.; Raymond Schaak, R.E. *J. Am. Chem. Soc.* **2005**, *127*, 7326-7327.
[Featured in C&EN "News of the Week," May 16, 2005]

Schaak, R. E.; Sra, A. K.; Leonard, B. M.; Cable, R. E.; Bauer, J. C.; Han, Y.-F.; Means, J.; Teizer, W.; Vasquez, Y.; Funck, E. S. *J. Am. Chem. Soc.* **2005**, *127*, 3506-3515.

Schaak, R. E.; Cable, R. E.; Leonard, B. M.; and Norris, B. C. *Langmuir*, **2004**, *20*, 7293-7297.

HONORS AND AWARDS

1st place, Student Research Week Competition, Texas A&M University

ACS Division of Inorganic Chemistry Travel Award, San Diego Meeting, 2005

Regents Fellowship Recipient, Texas A&M University Chemistry Dept.